VirginiaTech
Invent the Future®

Department of Biomedical
Engineering and Mechanics

Virginia Tech
Wake Forest
Biomedical Engineering

2015
STUDENT
SYMPOSIUM

ETHICON
a Johnson & Johnson company

Altair

BMES
BIOMEDICAL ENGINEERING SOCIETY™

COOK® MEDICAL

Medtronic

Wake Forest® Innovations

Virginia Tech
Wake Forest University
School of Biomedical Engineering and Sciences

VirginiaTech
College of Engineering
Department of Biomedical Engineering and Mechanics

A Letter From The Organizers

Dear Attendees,

Welcome to the 14th Annual School of Biomedical Engineering & Sciences Graduate Student Research Symposium hosted by the VT-WFU Biomedical Engineering Society Student Chapter!

The Virginia Tech-Wake Forest University School of Biomedical Engineering & Sciences (SBES) is a joint graduate program formed in 2003 to bring together three prestigious academic institutions: the College of Engineering at Virginia Tech, the Wake Forest University School of Medicine, and the Regional Virginia-Maryland College of Veterinary Medicine. Each university contributes diverse educational and research opportunities to the students, providing a unique graduate experience. On August 11, 2014, Virginia Tech announced a new collaboration between SBES and the Engineering Science and Mechanics department to form the new Department of Biomedical Engineering and Mechanics. This department fosters important networking opportunities across the Virginia Tech campus as well as provides the framework towards an undergraduate biomedical engineering degree and strong vision for the future.

The VT-WFU Biomedical Engineering Society (BMES) Student Chapter was founded to foster communication and collaboration among various research groups. Our mission is to encourage the development, dissemination, integration, and utilization of knowledge in biomedical engineering, as well as interact with the scientific community. The chapter offers unique ways for students to become involved in outreach projects, research collaborations, and social events with other students, faculty, and industry. We are involved in many service opportunities within our local communities, and participate annually in the BMES National meeting.

The SBES Graduate Student Research Symposium was developed to provide students and faculty the opportunity to interact and exchange research ideas with colleagues and industry personnel. The VT-WFU BMES Student Chapter would like to thank our sponsors Ethicon, Cook Medical, Altair, BMES, and Medtronic for their generous support. We greatly appreciate your participation and hope that this symposium will promote enhanced discussion and collaboration among researchers. Thank you for your attendance!

The VT-WFU BMES Executive Committee

Allison Pekkanen Matthew Davis *Presidents*	Brad Hubbard Samantha Schoell *Vice Presidents*	Alexandra Hyler Harleigh Warner *Treasurers*	Andrea Rolong Elie Zakhem *Secretaries*

Scott Verbridge
VT Faculty Advisor

Scott Gayzik and Ashley Weaver
WFU Faculty Advisors

Please visit our website for more information www.sbes.vt.edu/bmes/

8:00	**REGISTRATION, Latham Foyer** **POSTER SET UP, Latham B** **REFRESHMENTS, Latham Foyer**
8:00 - 5:00	**ADVISORY BOARD MEETING, Solitude**
9:00	**WELCOME, Latham A, Allison Pekkanen & Matthew Davis, VT-WFU BMES Presidents**
9:15-9:45	**Presenting Sponsor Highlight: Ethicon Presentation, Latham A**
9:15-11:30	**Altair Software Demonstration, Draper's Meadow**
9:45	**MORNING BREAK, Latham Foyer**

	Systems Modeling **10:15-11:30 am, Latham A**		**Cardiovascular and Perfusion Engineering** **10:15-11:30 am, Duckpond**		**Nanoengineering for Biomedical Applications** **10:15-11:30 am, Drillfield**	
		Page Number		*Page Number*		
10:15	**Quantification of Toy Sword Kinematics with Pediatric Volunteers** *Stephanie M. Beeman[1], Steven Rowson[1], and Stefan M. Duma[1]* *[1] School of Biomedical Engineering and Sciences, Center for Injury Biomechanics, Virginia Tech, Blacksburg, VA*	6	**Investigation and Analysis of Heart Failure with Preserved Ejection Fraction (HFPEF) with Magnetic Resonance** *Sourav Mishra[1], Philip J Brown[1], Robert A Kraft[1], Craig A Hamilton[1]. and Dalane W Kitzman[2]* *[1] School of Biomedical Engineering and Sciences, Wake Forest University, Winston-Salem, NC [2] Department of Cardiology, Wake Forest University School of Medicine, Winston-Salem, NC*	25	**Control Strategies to Achieve Consistent Particles' Characteristics in Atmospheric Plasma Spray Process** *Balachandar Guduri[1] and Romesh C. Batra[1]* *[1] Engineering Science and Mechanics, Virginia Tech, Blacksburg, VA*	20
10:30	**Optimal Parameter Analysis for Thermal Spray Process** *Unchalissa Taetragool[1], and Romesh C. Batra[1]* *[1] Engineering Science and Mechanics, Virginia Tech, Blacksburg, VA*	34	**Ephaptic Coupling as a First Line of Therapy During a Heart Attack** *Sharon George[1] and Steven Poelzing[1,2]* *[1] School of Biomedical Engineering and Sciences, Virginia Tech, Blacksburg, VA [2] Virginia Tech Carilion Research Institute, Roanoke, VA*	16	**Detection of Liver Organoid Biomarkers by SERS-Immunolabeled Gold Nanoparticles** *William M. Payne[1], Aaron M. Mohs[1,2], Adam R. Hall[1], Sneha S. Kelkar[3], and Anthony Atala[3]* *[1] School of Biomedical Engineering and Sciences, Wake Forest University, Winston Salem, NC, [2] University of Nebraska Medical Center, Pharmaceutical Sciences, Lincoln, NE, [3] Wake Forest Institute for Regenerative Medicine, Winston-Salem, NC*	29
10:45	**Evaluation of Vehicle-Based Crash Severity Metrics** *Ada H. Tsoi[1], and H. Clay Gabler[1]* *[1] School of Biomedical Engineering and Sciences, Center for Injury Biomechanics, Virginia Tech, Blacksburg, VA*	36	**The Development of a Thin-Filmed, Non-Invasive Tissue Perfusion Sensor to Quantify Pressure Ischemia of Explanted Organs** *Timothy J. O'Brien[1], Ali Roghanizad[1], Thomas E. Diller[1], and John L. Robertson[2]* *[1] Virginia Tech Mechanical Engineering, Blacksburg, VA, [2] School of Biomedical Engineering and Sciences, Virginia Tech, Blacksburg, VA*	28	**Indocyanine Green-Loaded Nanoparticles for Image Guided Tumor Surgery** *Tanner K. Hill[1,2], Sneha Kelkar[1,2], Frank C. Marini[2,3], and Aaron M. Mohs[1,2,3]* *[1] School of Biomedical Engineering and Sciences, Wake Forest University, Winston Salem, NC, [2] Wake Forest Institute for Regenerative Medicine, Winston-Salem, NC, [3] Wake Forest University Department of Cancer Biology, Winston-Salem, NC*	21
11:00	**Phenomenological Model for Unsteady Aerodynamics of Plunging Airfoils at High Frequencies and Angles of Attack** *Mohamed Y. Zakaria[1], and Muhammad R. Jahh[1]* *[1] Engineering Science and Mechanics, Virginia Tech, Blacksburg, VA*	42	**Wake Up Call: Sympathetic and Parasympathetic Stimulation Contribute to Arrhythmogenesis** *Amara Greer-Short[1,2] and Steven Poelzing[1,2]* *[1] School of Biomedical Engineering and Sciences, Virginia Tech, Blacksburg, VA [2] Virginia Tech Carilion Research Institute, Roanoke, VA*	19	**Carbon Nanotubes Attenuate Cancer and Improve Healing** *Elizabeth M. Wailes[1,2] and Nicole H. Levi-Polyachenko[1,2]* *[1] Wake Forest University, Department of Plastic and Reconstructive Surgery, Winston-Salem, NC [2] School of Biomedical Engineering and Sciences, Wake Forest University, Winston-Salem, NC*	39
11:15	**Reduction in Fatal Longitudinal Barrier Crash Rate Due to Electronic Stability Control** *Nicholas S. Johnson[1], and H. Clay Gabler[1]* *[1] School of Biomedical Engineering and Sciences, Center for Injury Biomechanics, Virginia Tech, Blacksburg, VA*	22	**A Test of Functional Compartmentalization in the Grasshopper *Schistocerca Americana* Using Internal Pressure Recordings** *Khaled Adjerid[1], Hodjat Pendar[1], Jon F. Harrison [2] and John J. Socha [1]* *[1] Engineering Science and Mechanics, Virginia Tech, Blacksburg, VA, [2] School of Life Sciences, Arizona State University, Phoenix, AZ*	1	**Tumor Engineering to Elucidate the Effect of Mild Hyperthermia on Transport of SWNHs in the Tumor Microenvironment** *Matthew R DeWitt[1], Allison Pekkanen[1], Rafael Davalos[1], and M. Nichole Rylander[2]* *[1] School of Biomedical Engineering and Sciences, Virginia Tech, Blacksburg, VA [2] Department of Mechanical Engineering, University of Texas at Austin, Austin, TX*	13

11:30	**LUNCH, Latham CDEF**	

Poster Session A
1:00 - 1:30, Latham B

Poster Session B
1:30 - 2:00, Latham B

	Microfluidic Devices and Applications **2:00-3:00 pm, Latham A**	Page Number	**Evaluation of Traumatic Head Injury** **2:00-3:00 pm, Duckpond**	Page Number	**Modeling at the Microscale** **2:00-3:00 pm, Drillfield**	Page Number
2:00	**A Microfluidic Chip for Screening Cell Biophysical Properties** *Hesam Babahosseini[1,2], Vaishnavi Srinivasaraghavan[2], and Masoud Agah[2]* *[1] Department of Mechanical Engineering, Virginia Tech, Blacksburg, VA, [2] Department of Electrical and Computer Engineering, Virginia Tech, Blacksburg, VA*	4	**Head Impact Exposure in Youth Football** *Bryan R. Cobb[1], Jillian E. Urban[2], Elizabeth M. Davenport[2], Steven Rowson[1], Stefan M. Duma[1], Joseph A. Maldjian[2], Christopher T. Whiltlow[2], Alexander K. Powers[2], and Joel D. Stitzel[2]* *[1] School of Biomedical Engineering and Sciences, Virginia Tech, Blacksburg, VA, [2] School of Biomedical Engineering and Sciences, Wake Forest University, Winston-Salem, NC*	12	**Biomechanical Analysis of Coaxial and Cortical Trajectory Pedicle Screws in Lumbar Spine Fusion Constructs** *Philip J. Brown[1], Greg J. Gillespie[1], James L. West[2], Joel D. Stitzel[1], and Wesley Hsu[2]* *[1] School of Biomedical Engineering and Sciences, Wake Forest University, Winston-Salem, NC, [2] Wake Forest Baptist Medical Center, Winston-Salem, NC*	8
2:15	**Slip Boundary Conditions and Fluid Structure Interaction in Microscale Gas Flow** *Krishnashis Chatterjee[1] and Anne Staples[1]* *[1] Engineering Science and Mechanics, Virginia Tech, Blacksburg, VA*	10	**Development and Validation of an Atlas-Based Finite Element Brain Model** *Logan E. Miller[1], Jillian E. Urban[1], Elizabeth M. Lillie[1], and Joel D. Stitzel[2]* *[1] Wake Forest University School of Medicine, Winston-Salem, NC, [2] School of Biomedical Engineering and Sciences, Wake Forest Universitv. Winston-Salem. NC*	24	**Computational Design of Carbon Nanotube Reinforced Polymeric Nanocomposites** *Priyal H. Shah[1] and Romesh C. Batra[1]* *[1] Engineering Science and Mechanics, Virginia Tech, Blacksburg, VA*	31
2:30	**A Microfluidic Device for Profiling Genome-Wide Histone Modifications Using 100 Cells** *Zhenning Cao[1], Changya Chen[2], Bin He[2], Kai Tan[2] and Chang Lu[1,3]* *[1] School of Biomedical Engineering and Sciences, Virginia Tech, Blacksburg, VA, [2] Department of Internal Medicine, Carver College of Medicine, University of Iowa, Iowa City, IA, [3] Department of Chemical Engineering, Virginia Tech, Blacksburg, VA*	9	**Laboratory Evaluation of Head Impact Sensors** *Abigail M. Zadnik[1], Bryan R. Cobb[1], Steven Rowson[1], and Stefan M. Duma[1]* *[1] School of Biomedical Engineering and Sciences, Virginia Tech, Blacksburg, VA*	41	**Primary Blast Overpressure as an Injury Mechanism for the Eye** *Vanessa D. Alphonse[1], Andrew R. Kemper[1], Craig McNally[1], Pamela J. VandeVord[1], and Stefan M. Duma[1]* *[1] School of Biomedical Engineering and Sciences, Center for Injury Biomechanics, Virginia Tech, Blacksburg, VA*	3
2:45	**Development of Blood-Brain Barrier-On-Chip for Studying Drug Delivery to the Brain by Pulsed Electric Fields** *Mohammad Bonakdar[1], and Rafael Davalos[1,2]* *[1] Department of Mechanical Engineering, Virginia Tech, Blacksburg, VA, [2] School of Biomedical Engineering and Sciences, Virginia Tech, Blacksburg, VA*	7	**Volumetric Analysis of Motor Vehicle Crash-Related Head Injuries from Real-World Head Impact Data** *Jillian E. Urban[1], Ervin L. Lowther, M.D.[2]; Christopher T. Whitlow[2,3], and Joel D. Stitzel[1]* *[1] School of Biomedical Engineering and Sciences, Center for Injury Biomechanics, Wake Forest University, Winston Salem, NC, [2] Wake Forest School of Medicine, Winston-Salem, NC, [3] Translational Science Institute, Wake Forest University, Winston-Salem, NC*	37	**Enhanced Immunomagnetic Separation by Embedded Ferromagnetic Pattern** *Chen Sun[1], and Chang Lu[1]* *[1] School of Biomedical Engineering and Sciences, Virginia Tech, Blacksburg, VA*	33

3:00	**AFTERNOON BREAK, Latham Foyer**

	Applications of Finite Element Modeling 3:15-4:30 pm, Latham A		Novel Materials: Design and Implementation 3:15-4:30 pm, Duckpond		Novel Utilization of Imaging Tools 3:15-4:30 pm, Drillfield	
		Page Number		*Page Number*		
3:15	**Driver Risk Variability in Finite Element Reconstruction of Ciren Motor Vehicle Crashes** *James P. Gaewsky[1], Ashley A. Weaver[1], Bharath Koya[1], and Joel D. Stitzel[1]* *[1] School of Biomedical Engineering and Sciences, Center for Injury Biomechanics, Wake Forest University, Winston-Salem, NC*	15	**Sparse Fiber-Collagen Composites for Ligament Tissue Engineering** *Patrick Thayer[1], Emily Tong[2], Linda Dahlgren[3], and Aaron Goldstein[1, 2]* *[1] School of Biomedical Engineering and Sciences, Virginia Tech, Blacksburg, VA, [2] Department of Chemical Engineering, Blacksburg, VA, [3] Department of Large Animal Clinical Sciences, Virginia-Maryland Regional College of Veterinary Medicine, Blacksburg, VA*	35	**Interior Micro-CT of Mouse Heart Using a Collimated Carbon-Nanotube Field Emission X-Ray Source** *Hao Gong[1] and Guohua Cao[1]* *[1] School of Biomedical Engineering and Sciences, Virginia Tech, Blacksburg, VA*	19
3:30	**Studying Finite Deformations of Nonlinear Elastic Plates Using Third Order Shear and Normal Deformable Theories** *Arka P. Chattopadhyay[1], and Romesh C. Batra[1]* *[1] Engineering Science and Mechanics, Virginia Tech, Blacksburg, VA*	11	**Theranostic Polymer Nanoparticles for Photothermal Ablation and Fluorescent Imaging of Cancer** *Elizabeth G. Graham[1,2] and Nicole H. Levi-Polyachenko[1,2]* *[1] Wake Forest University, Department of Plastic and Reconstructive Surgery, Winston-Salem, NC [2] School of Biomedical Engineering and Sciences, Wake Forest University, Winston-Salem, NC*	18	**Transcranial Focused Ultrasound Beam Profile Sensitivity for Neuromodulation** *Jerel K. Mueller[1], Wynn Legon[2], and William J. Tyler[3]* *[1] School of Biomedical Engineering and Sciences, Virginia Tech, Blacksburg, VA, [2] University of Minnesota, Department of Physical Medicine and Rehabilitation, Minneapolis, MN, [3] Arizona State University, School of Biological and Health Systems Engineering, Phoenix, AZ*	26
3:45	**Towards an Enhanced Railroad Safety, an Early Track-Defects Detection System** *Mohammad I. Albakri[1] and Pablo A. Tarazaga[2]* *[1] Engineering Science and Mechanics, Virginia Tech, Blacksburg, VA, [2] Department of Mechanical Engineering, Virginia Tech, Blacksburg, VA*	2	**Cell and Growth Factor Loaded Keratin Hydrogels for Treatment of Volumetric Muscle Loss (VML) Injuries** *Hannah B. Baker[1,] Juliana A. Passipieri[2], Seth Tomblyn[3], Luke Burnett[3], and George J. Christ[1,2]* *[1] School of Biomedical Engineering and Sciences, Wake Forest University, Winston Salem, NC, [2] University of Virginia, Charlottesville, VA, [3] KeraNetics LLC, Winston-Salem, NC*	5	**A Glimpse into BRCA1's Role During Transcription** *Carly E. Winton[1,2], Brian L. Gilmore[1], Andrew C. Demmert[1], Zhi Sheng[1], and Deborah F. Kelly[1,2]* *[1] Virginia Tech Carilion Research Institute, Roanoke, VA, [2] School of Biomedical Engineering and Sciences, Virginia Tech, Blacksburg, VA*	40
4:00	**Development of a Computationally Efficient Full Human Body Finite Element Model** *Doron Schwartz[1,2], Berkan Guleyupoglu[1,2], Joel D. Stitzel[1,2], and F. Scott Gayzik[1,2]* *[1] Wake Forest School of Medicine, Winston-Salem, NC, [2] School of Biomedical Engineering and Sciences, Center for Injury Biomechanics, Wake Forest University, Winston-Salem, NC*	30	**Effect of Alginate Microcapsule Stiffness on Encapsulated Ovarian Cell Viability** *Kevin Enck[1,2,] JP McQuilling[1,2], Sittadjody Sivanandane[1], and Emmanuel C. Opara[1,2]* *[1] School of Biomedical Engineering and Sciences, Center for Injury Biomechanics, Wake Forest University, Winston Salem, NC, [2] Wake Forest Institue for Regenerative Medicine, Winston-Salem. NC*	14	**Characterization of Rib Cortical Bone Thickness Changes with Age and Sex** *Sarah K. Lynch[1,2], Ashley A. Weaver[1,2], and Joel D. Stitzel[1,2]* *[1] School of Biomedical Engineering and Sciences, Wake Forest University, Winston-Salem, NC, [2] Wake Forest University School of Medicine, Winston-Salem, NC*	23
4:15	**The Application of Radial Basis Function Interpolation Methods in the Development of a 95th Percentile Male Seated FEA Model** *Nicholas A. Vavalle[1,2], Samantha L. Schoell[1,2], Ashley A. Weaver[1,2]. Joel D. Stitzel[1,2]. and F. Scott Gavzik[1,2]* *[1] Wake Forest School of Medicine, Winston-Salem, NC, [2] School of Biomedical Engineering and Sciences, Center for Injury Biomechanics, Wake Forest University, Winston-Salem, NC*	38	**Aligned and Suspended Nanofiber Networks for Studying Wound Closure Dynamics** *Puja Sharma[1], Colin Ng[2], Paige Szymanski[3], Bahareh Behkam[1,2]. and Amrinder S Nain[1, 2]* *[1] School of Biomedical Engineering and Sciences, Virginia Tech, Blacksburg, VA [2] Mechanical Engineering Department, Virginia Tech, Blacksburg, VA [3] Department of Bioengineering, University of Illinois at Urbana-Champaign, Urbana, IL*	32	**An Interface for Analysis of Medical Linear Accelerator Performance Parameters Using Process Behavior Charts** *Callistus M. Nguyen[1,2], Charles M. Able[2], Alan H. Baydush[2], Scott Isom[2], and Michael T. Munley[1,2]* *[1] School of Biomedical Engineering and Sciences, Wake Forest University, Winston-Salem, NC, [2] Wake Forest School of Medicine, Radiation Oncology, Winston-Salem, NC*	27
4:45	**ALL - AWARDS AND CLOSING REMARKS, Latham A**					

Thank you to Altair for their gracious sponsorship of the 2015 SBES Graduate Student Research Symposium. Visit Altair's website to discover how they are innovating in high-end software and consulting services.

A leading global provider of technology that strengthens client innovation, Altair empowers client innovation and decision-making through technology that optimizes the analysis, management and visualization of business and engineering information.

Privately held with more than 2,300 employees, Altair operates 48 offices throughout 20 countries.

With a 30-year-plus track record for product design, advanced engineering software, on-demand computing technologies and enterprise analytics solutions, Altair consistently delivers a competitive advantage to more than 5,000 corporate clients representing the automotive, aerospace, government and defense, heavy equipment and consumer products verticals. Altair also has a growing client presence in the electronics, architecture engineering and construction, and energy markets.

For more information, visit Altair's website at www.altair.com

World Headquarters
1820 East Big Beaver Rd
Troy, MI 48083
USA

ETHICON

PART OF THE Johnson & Johnson FAMILY OF COMPANIES

Better surgery for a better world

Our promise

Better surgery for a better world

At Ethicon, we're working to redefine surgery to change the world for the better. We share an enduring commitment to advance surgical care so more patients live longer, more fulfilling lives. And we are continuously evolving to better serve our customers.

Better Surgery

Creating value for healthcare systems

Ethicon in Australia and New Zealand responded to customers' needs by creating an easy-to-use inventory management solution. This innovative approach allows customers to save time and reduce costs by managing supply orders through an iPhone application.

Better Care

Advancing care around the world

Ethicon's solutions are changing lives around the world – including the life of a small boy in Argentina named Samuel. Using an innovative solution from Ethicon, surgeons in Argentina were able to perform for the first time a revolutionary, life-saving liver transplant on infant Samuel, who is now a healthy, thriving child.

Expanding access to care globally

By collaborating with key stakeholders, Ethicon was able to expand access to innovative surgical care in Brazil, which improved the quality of care, provided a solution with a shorter patient recovery, and helped patients live healthier lives.

Better World

People making a lasting difference

Ethicon associates raise money and volunteer for Operation Smile missions to heal the smiles of children around the world. Meet Armando, an eleven-year-old boy, who now has a new smile and a bright future.

Inspiring the next generation

Ethicon partners with iSPACE, an organization in Cincinnati, Ohio, that encourages children to get excited about science, technology, engineering, and mathematics. Ethicon engineers share real-world applications to instill curiosity in tomorrow's scientists and engineers.

A history of advancing surgery

It all started with a simple question: What if...?

What if there was a better way to help patients heal after surgery? What if we could improve their lives? What if we could change the way surgery was done forever? And in doing so, change the world for the better?

More than 80 years ago, the first group of Ethicon scientists and researchers started to think about healing in a new way. Their questions led to pioneering sutures that advanced surgeons' work and discoveries that enhanced patients' lives.

Today, we produce much more than sutures. Working with our customers and partners, we bring meaningful solutions to every area we touch. To wound closure and general surgery. To women's health and aesthetic medicine. To minimally invasive procedures and metabolic science.

While our world and the field of healthcare have changed, our passion to make a difference for patients remains. As we reach toward every corner of the globe, we remain committed to advancing surgical care and extending patients' access to health care across the globe.

At Ethicon, we continue to take pride in our heritage. We were founded on innovation and will continue exploring ways to improve surgical outcomes. Improving patient care continues to inspire us to work smarter, partner in more meaningful ways, and never be afraid to imagine a better world by asking the one simple question that started it all. What if…?

Our solutions

From leading-edge sutures and endocutters to comprehensive payor and provider solutions, our focus for almost a century has been to deliver innovations that matter to our customers and ultimately make a difference for patients. It means you can continue to depend on us for world-class educational offerings rooted in an unparalleled understanding of the science behind how tissue reacts in surgery. And it means a commitment to quality in all we do.

A career that counts

Want to join our team? We'd love to hear from you. We're always looking for bright, talented people who truly care about improving lives and making a difference. Discover if we have a career opportunity for you today.

Want to learn more? (http://careers.jnj.com/)

Thank you to Ethicon for their gracious sponsorship of the 2015 SBES Graduate Student Research Symposium. Visit Ethicon's website for more information on how they're revolutionizing surgery.

DSL 13-0309, DSL 12-9000

Thank you to the Biomedical Engineering Society for their gracious sponsorship of the 2015 SBES Graduate Student Research Symposium. Please visit their website to learn how they have become the leading society of professionals devoted to developing and using engineering to advance human health and well being.

The Biomedical Engineering Society (BMES) is the professional society for biomedical engineering and bioengineering. Founded in early 1968, the Society now boasts nearly 6,500 members and is growing, rapidly.

BMES serves as the lead society and professional home for biomedical engineering and bioengineering. Our leadership in accreditation, potential licensure, publications, scientific meetings, global programs, and diversity initiatives, as well as our commitment to ethics, all serve our mission to promote and enhance knowledge and education in biomedical engineering and bioengineering worldwide and its utilization for human health and well-being.

The Vision of BMES is to serve as the world's leading society of professionals devoted to developing and using engineering and technology to advance human health and well-being.

The Mission of BMES is to build and support the biomedical engineering community, locally, nationally and internationally, with activities designed to communicate recent advances, discoveries, and inventions; promote education and professional development; and integrate the perspectives of the academic, medical, governmental, and business sectors.

Leading and emerging researchers use BMES as a platform for sharing the latest information and research in the profession. BMES provides industry members exposure to an expanding market. Advertising and sponsorship opportunities can help increase your company's publicity year-round.

For more information, please visit the BMES website at www.bmes.org

BMES
8201 Corporate Drive, Suite 1125
Landover, MD 20785-2224
info@bmes.org

Special thanks to Cook Medical for their continued support of the 2015 SBES Graduate Student Research Symposium. We encourage you to visit their website to learn how they have impacted the medical world with their research.

Cook Endoscopy (formerly Wilson-Cook Medical Inc.) was established to provide innovative products for gastrointestinal endoscopy. By working closely with prominent gastroenterologists, Cook Endoscopy has become a worldwide leader in the design, development and production of endoscopic accessories. The company has been responsible for introducing numerous new devices to the endoscopy marketplace.

Cook Endoscopy continues to maintain close relationships with leading gastroenterologists worldwide, making new product development an ongoing process. The company focuses on designing and manufacturing devices used in gastrointestinal endoscopy, bronchoscopy, and surgery in the treatment of esophageal, stomach, pancreatic, liver and colon disorders. Key product lines include but are not limited to sphincterotomes, wire guides, stents, forceps, needles, cytology brushes, multi-band ligators, PEGs, and snares. Like other COOK companies, Cook Endoscopy's manufacturing technology emphasizes hand-craftsmanship of many products to ensure optimal quality and unmatched customer satisfaction.

The company’s dedication to advancing medical technology is further evidenced by educational and support programs. The company allocates grants and fellowships to a large number of organizations and facilities – including Wake Forest Baptist Medical Center – to enhance education and growth within the medical field.

Cook Medical Endoscopy Division’s parent company, Cook Medical – headquartered in Bloomington, Indiana – manufactures more than 16,000 different products across 10 divisions for 135 countries.

For more information, please visit Cook Medical’s website at www.cookmedical.com

Cook Medical
Endoscopy Division
4900 Bethania Station Rd.
Winston-Salem, NC 27105

Thank you to Medtronic for their gracious sponsorship of the 2015 SBES Graduate Student Research Symposium. Visit Medtronic's website to discover how they are creating life-changing therapies to help people with chronic diseases.

At Medtronic, we're committed to *Innovating for life* by pushing the boundaries of medical technology and changing the way the world treats chronic disease. Driven by our deep understanding of the human body and our collaboration with physicians, we're transforming technology to treat patients across the entire care continuum. Our innovations help physicians diagnose diseases earlier, treat patients with the least amount of disruption possible, and help alleviate symptoms throughout the patient's life. Today, we're improving the lives of millions of people worldwide each year across numerous conditions - including heart disease, diabetes, neurological disorders, spinal conditions, and vascular diseases. But it isn't enough. So we're innovating beyond products. We're breaking down barriers, challenging assumptions, and looking beyond the status quo - to continually find more ways to help people live better, longer.

Medtronic was founded in 1949 as a medical equipment repair company by Earl Bakken and his brother-in-law, Palmer Hermundslie. Today, we're the world's largest independent medical technology company. We employ more than 85,000 people worldwide - serving physicians, clinicians, and patients in more than 160 countries.

For more information, visit Medtronic's website at www.medtronic.com

Medtronic
Vascular Innovations
3576 Unocal Place
Santa Rosa, CA 95403-1774

Wake Forest® Innovations

Thank you to Wake Forest Innovations for their gracious sponsorship of the 2015 SBES Graduate Student Research Symposium.

Wake Forest Innovations accelerates the journey from discovery to commercialization so that important scientific discoveries can become life-improving realities.

- We help transform the ideas, discoveries and inventions of our scientists and clinicians into valuable proprietary technologies and license these to industry.
- We help industry to research and develop its own discoveries by providing open access to the intellectual, clinical and research capabilities of Wake Forest.

Through open innovation with industry we improve health by transforming ideas, discoveries and inventions into valuable health care products.

For more information, please visit WakeForestInnovations.com.

Wake Forest Innovations
575 North Patterson Avenue, Suite 550
Winston-Salem, NC 27101
innovation@wakehealth.edu
+1.336.713.1111

14th Annual Graduate Student Research Symposium
Oral and Poster Abstracts

Virginia Tech
Wake Forest University
School of Biomedical Engineering and Sciences
14th Annual Graduate Student Research Symposium, May 13, 2015

A TEST OF FUNCTIONAL COMPARTMENTALIZATION IN THE GRASSHOPPER *SCHISTOCERCA AMERICANA* USING INTERNAL PRESSURE RECORDINGS

Khaled Adjerid[1], Hodjat Pendar[1], Jon F. Harrison [2] and John J. Socha [1]
1. Virginia Tech, Engineering Science and Mechanics (ESM)
2. Arizona State University, School of Life Sciences (SLS)
Corresponding Author: Khaled Adjerid , Email: adjerid@vt.edu

INTRODUCTION

It is generally understood that hemocoel of insects is open. However, using synchrotron x-ray imaging, a study placed sedated specimens in a head up or head down orientation and the air sacs in the body compressed when at the bottom, and expanded when at the top. This was not present in non-sedated grasshoppers.

The over arching assumption is that the hemocoel of the American locust should act as a hydrostatic vessel of fluid, so this led us to pose the two hypotheses: 1) the static pressures of the hemocoel should change according to hydrostatic theory and 2) dynamic changes in any location throughout the hemocoel should be uniform.

Based on the height of the column of fluid above each of our measurement points in the head and the abdomen, we calculated the expected pressures in the hemolymph in three orientations. This represents the pressure in the absence of any dynamic changes in pressure, which are likely created by abdominal pumping or gut motion.

METHODOLOGY

We tested this hypothesis by comparing pressures with a pair of pressure sensors, inserted into the lateral body wall and data were collected at 100 Hz.

RESULTS

To test the first hypothesis, baseline pressure shifts in the two sensor locations for each change in position were analyzed. These shifts were then compared with the expected values determined by equation 1 for the length of the inect. For the thoracic pressure sensor, we found that in 3 out of the 4 position changes, the average measured value was significantly different from the expected value. The average measured pressure values for the abdominal sensor were not significantly different from the expected values within a 95% confidence interval. Additionally, the pressure change values were not significantly different from zero indicating that a) the pressures are not changing according to the hydrostatic vessel assumption and b) the pressures are being kept from changing very much at all.

Comparing the continuous dynamic pressure traces from the abdomen and thorax, using the slope coefficient from Dynamic Linear Regression model to compare similarity in thoracic pressures and abdominal pressures (0 being no correlation and 1 is perfect correlation of both shape and magnitude) we found that only 18.72±5.30% of the pressure traces were 80% or more similar while out of the 30 data sets, 86.66±5.30% were less than 50% correlated. Indicating a significant lack of correlation and similarity between the entirety of the two traces. This contrasts starkly with the expected value of ~100% similarity.

Lastly, we fit a simple linear model for individual pressure pulse magnitudes and durations where a slope of the linear fit line, m, would be expected to be ~1, indicating high similarity. However, when looking at the slopes of the linear fit lines, we find that the average slope for magnitude linear fit lines was 0.071±0.04 while the average slope of the duration linear fit was 0.011±0.06. Both of these values are significantly different from the expected value of ~1 within a 95% confidence interval.

This points to the fact that although several points do exist along the y = x line, (m = 1), the majority of the points exist in the regions outside of this area indicating either differing magnitudes in pulses occurring simultaneously or more interestingly, pressure pulses occurring in one region of the hemocoel that do not occur elsewhere.

CONCLUSIONS

The observation that the static pressures of the hemocoel don't change according to hydrostatic theory and dynamic changes in any location throughout the hemocoel are not uniform leads us to conclude that there is some form of compartmentalization and functional valving within the hemocoel and causing it not to like a hydrostatic vessel.

14th Annual Graduate Student Research Symposium, May 13, 2015

TOWARDS AN ENHANCED RAILROAD SAFETY, AN EARLY TRACK-DEFECTS DETECTION SYSTEM

Mohammad I. Albakri[1], Pablo A. Tarazaga[2]
1. Biomedical Engineering and Mechanics, Virginia Tech
2. Mechanical Engineering Department, Virginia Tech
Corresponding Author: Mohammad Albakri, Email: malbakri@vt.edu

INTRODUCTION

Track defects are a major safety concern for the railroad industry. Such defects occur as a result of mechanical failure of track components or due to excessive loading induced by extreme temperatures. Current track inspection techniques rely on either visual inspection, or specially equipped carts, making them costly and time consuming. Furthermore, a practical, nondestructive technique for monitoring thermal loads on rails is yet to be developed. This work addresses these challenges in a novel way by combining impedance-based structural health monitoring (SHM) and wave propagation techniques. Both mechanical defects and thermal loads can be monitored with the proposed approach, which in turn enhances railroad safety.

METHODOLOGY

Impedance-based SHM utilizes piezoelectric wafers to excite the structure and capture its local dynamic response. By comparing the measured impedance signature to a base-line measurement taken at the pristine state, structural defects, such as cracks and loose joints, can be detected [1-2].
Thermal loads, on the other hand, can be monitored by comparing rail's current temperature to its Neutral Temperature (NT); the temperature at which rails experience no thermal stresses. The developed approach combines semi-analytical FEM, acoustoelastic theory, dispersion compensation, and numerical optimization to achieve reference-free NT measurements. Figure 1 outlines the underlying principle of this approach.

RESULTS

Four types of damages related to insulated rail joints have been investigated and successfully detected with impedance-based SHM. These are rail damage, insulation failure, bolt loosening, and joint bar damage.

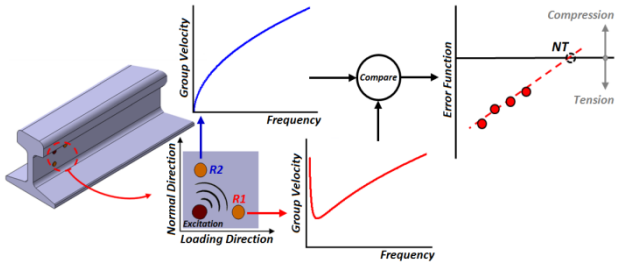

Figure 1: Reference-free rail NT measurement approach.

Numerical simulations are conducted to assess the effects of uncertainties in material and geometric characteristics on stress calculations and NT estimates. The results are summarized in Table 1 for the modulus of elasticity case.

Table 1: Effects of uncertainties in Young's Modulus.

E/E_0	Estimated Stress (MPa)				Linear Fit	RNT
	50°F	55°F	60°F	65°F		
125%	26.5	22.1	17.7	13.4	$\sigma = -0.874T + 70.18$	80.3
110%	26.9	22.4	18	13.5	$\sigma = -0.892T + 71.49$	80.15
90%	27.8	23.2	18.5	13.8	$\sigma = -0.934T + 74.53$	79.8
75%	28.5	24	19.2	14.4	$\sigma = -0.942T + 75.69$	80.35

CONCLUSIONS

Impedance-based SHM and wave propagation techniques are utilized to detect mechanical defects and thermal loads affecting track components. Different track defects have been successfully detected. Numerical simulations also showed that the developed NT measurement technique is robust against material and geometric uncertainties.

REFERENCES

[1] M. Albakri and P. Tarazaga, SHM, Ed. Springer Int. Publishing, V 5, 2014, pp. 19–27.
[2] M. Albakri and P. Tarazaga, J. Smart Mat. Str., under review.

Virginia Tech
Wake Forest University
School of Biomedical Engineering and Sciences
14th Annual Graduate Student Research Symposium, May 13, 2015

PRIMARY BLAST OVERPRESSURE AS AN INJURY MECHANISM FOR THE EYE

Vanessa D. Alphonse[1], Andrew R. Kemper[1], Craig McNally[1], Pamela J. VandeVord[1], Stefan M. Duma[1]
1. Virginia Tech – Wake Forest Center for Injury Biomechanics, SBES
Corresponding Author: Vanessa D. Alphonse, Email: vda@vt.edu

INTRODUCTION

The increased use of improvised explosive devices (IEDs) in current military conflicts motivates the need to understand how primary blast (i.e., the pressure wave) affects the body. This work comprises a two-prong approach to evaluate the response of the eye to blast:

1. *Experimentally quantify injury risk for porcine eyes exposed to survivable blast.*
2. *Develop an area-sensitive physical model of the eye for blunt and blast trauma.*

METHODOLOGY

An Advanced Blast Simulator was used to mimic free-field blast profiles at 3 pressure levels (10psi, 20psi, 30psi). The 30psi test represents the threshold for lung injury [1]. A custom MATLAB® script was used to quantify magnitude, duration, and impulse of each trace.

Porcine Eye Testing. Porcine eyes were placed in one of three boundary conditions (Figure 1) and exposed to a single blast. A total of 98 eyes were used; 58 were exposed to blast, 24 served as shams, and 16 served as controls. Pressure sensors were placed inside the eye, within the orbit, and around the face. Peak pressure inside the eye was used to quantify eye injury risk [2].

Synthetic Eye Testing. An array of 9 pressure sensors were placed in an existing biofidelic synthetic eye (Figure 2). This instrumented eye was placed in the isolated eye boundary condition. A total of 9 blast tests (3 at each pressure level) and 18 blunt tests were conducted.

Figure 1: Boundary conditions. Left to right; isolated eye, synthetic orbit with eye, and 3D

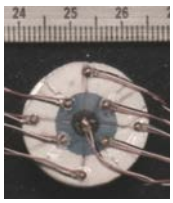

Figure 2: Pressure sensor array.

RESULTS

Porcine Eye Testing. Eye injury risk was calculated to be less than 5% for all porcine eye blast tests. No damage beyond postmortem degradation was observed during dissection of the tested eyes. The lack of observed injuries was consistent with the low predicted injury risk.

Synthetic Eye Testing. Blast tests resulted in a more consistent loading pattern among the sensors in the array compared to the blunt tests, where the central sensor measured the highest pressures (Figure 3).

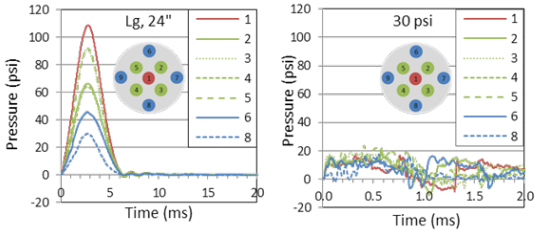

Figure 3: Synthetic eye response to blunt impact (left), and blast exposure (right).

CONCLUSIONS

The novel pressure data collected in this study using the synthetic and 3D orbits serves as a stepping stone to assessing the ability of shock waves to enter the skull through the ocular cavity. Furthermore, data were collected for an unprotected eye and can be used as a baseline for comparison with personal protective equipment to assess the efficacy of military goggles, spectacles, and helmets. Lastly, this work provides the first experimental data that can be used to validate the response of computational models of the eye for blast exposure.

REFERENCES

[1] Stuhmiller JH, *J Biomech*, 1996;29(2):227-234.
[2] Duma SM, *Curr Eye Res*, 2012;37(1): 43-49.

A MICROFLUIDIC CHIP FOR SCREENING CELL BIOPHYSICAL PROPERTIES

Hesam Babahosseini[1,2], Vaishnavi Srinivasaraghavan[2], and Masoud Agah[2]
1. Department of Mechanical Engineering
2. VT MEMS Lab, Department of Electrical and Computer Engineering
Corresponding Author: Hesam Babahosseini, Email: hbabahosseini@vt.edu

INTRODUCTION

Biophysical properties of single cells are associated with their disease status [1]. Thus, cell biophysics can serve as a reliable biomarker to distinguish cancerous cells from normal ones. Previously, it has been shown that the average deformability of cancerous cells is significantly larger than that of normal cells. In this study, we designed a microfluidic chip to screen the biophysical properties of benign and tumor cells.

METHODOLOGY

The microfluidic device was fabricated from PDMS using the standard lithography techniques and is shown in Figure 1. The device consists of a narrow (6µm-wide) and shallow (12µm-deep) constriction channel which is straight and 300µm-long. The constriction channel was designed with a rectangular cross section (6µmx12µm) to enable deformation of the cells when they are pulled through the channel. Non-invasive MCF10A and highly invasive MDA-MB-231 breast cells were used in this work.

RESULTS

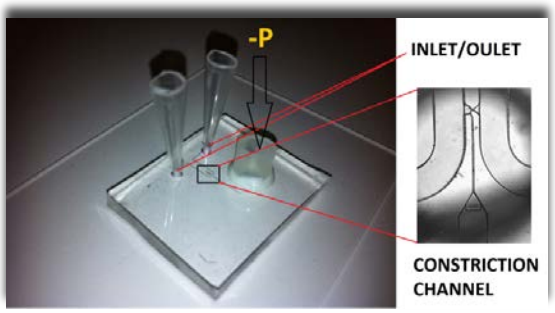

Figure 1: Optical image of the fabricated microfluidic chip with a zoomed in view of the constriction channel.

The measured transit times for breast cells are shown in Table 1. As shown in Table 1, the average, standard deviation values of transit times for MCF10A cells are larger than that for MDA-MB-231 cells. The transit time reduces from 0.203±0.226 s (n=120) for MCF-10A to 0.115±0.0747 s (n=100) for cancerous MDA-MB-231 breast cells. The above result indicates that MCF-10A cells are less deformable than MDA-MB-231 cells. This is consistent with our results found previously using AFM in [1].

Table 1: Elasticity and transit time characteristics of normal and cancerous breast cells.

Cell Type	Elasticity (kPa)	Transit time (sec.)
	mean±std.	***mean±std.***
MDA-MB-231	0.51±0.35	0.115±0.0747
MCF10A	1.13±0.84	0.203±0.226

CONCLUSIONS

A microfluidic chip with a narrow constriction channel was designed and the transit time of suspended cells through the channel was measured. The transit times of aggressive cells of breast cancer were lesser than the benign cells. This work demonstrates that the presented microfluidic platform can be a high-throughput alternative providing information regarding cell biophysics, and consequently the health status of the cells.

REFERENCES

1. H. Babahosseini, A. K. Ketene, E. M. Schmelz, P. C. Roberts, and M. Agah, "Biomechanical profile of cancer stem-like/tumor-initiating cells derived from a progressive ovarian cancer model," Nanomedicine: Nanotechnology, Biology and Medicine, vol. 10, no. 5, January 2014, pp. 1013–1019.

CELL AND GROWTH FACTOR LOADED KERATIN HYDROGELS FOR TREATMENT OF VOLUMETRIC MUSCLE LOSS (VML) INJURIES

Hannah B. Baker[1,], Juliana A. Passipieri, Ph.D.[2], Seth Tomblyn, Ph.D.[3], Luke Burnett, Ph.D.[3], George J. Christ, Ph.D.[1,2]
1. Wake Forest-Virginia Tech School of Biomedical Engineering and Sciences, Winston-Salem, NC
2. University of Virginia, Charlottesville, VA 3. KeraNetics LLC, Winston-Salem, NC
Corresponding Author: Hannah B. Baker, Email: hbaker@wakehealth.edu

INTRODUCTION

Our overall goal is to develop a platform of biomaterials technologies aimed at treating the spectrum of volumetric muscle loss (VML) injuries. To pursue this goal we have investigated cell and growth factor loaded keratin hydrogels in a mouse model of VML. At two months post injury, functional recovery was significantly improved for muscles treated with a combination of keratin, IGF-1, and bFGF. This study indicates keratin hydrogels as a promising treatment for VML injuries.

METHODOLOGY

Human hair keratin was purified using a patented process by KeraNetics, LLC. Keratose and kerateine hydrogels were mixed in a 70:30 ratio. Growth factors were added to kerateine and primary isolated mouse muscle cells were added to keratose. VML injury in the mouse latissimus dorsi (LD) was created by surgically resecting ~50% of the LD muscle from 2 month old female C57BL/6 mice. At 8 weeks post-surgery, the LD muscles were resected for *ex vivo* functional testing via electrical stimulation. Tissues for histological analysis were formalin fixed and either frozen or paraffin embedded.

RESULTS

At 8 weeks post-injury, muscles treated with a combination of keratin, IGF-1, and bFGF contracted with a significantly greater force than all treatment groups besides keratin alone and keratin combined with cells and IGF-1 (Figure 1). Histological results (not shown) show new tissue formation with the defect site for muscles treated with keratin, IGF-1, and bFGF, while muscles treated with bladder acellular matrix (BAM) and left untreated (NR) showed little to no new tissue formation.

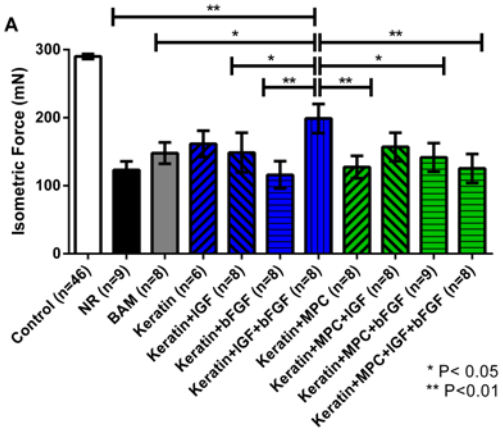

Figure 1: Functional recovery at 8 weeks

CONCLUSIONS

Keratin + IGF-1 and bFGF showed the greatest improvement in muscle function and form, these results were not significantly different from keratin alone and keratin with cells and IGF-1. These results evidence the potential for keratin hydrogels as a VML treatment.

ACKNOWLEDGMENTS

NIBIB T32 Fellowship and D.o.D. for Funding.
Chris Bergman, Manasi Vadhavkar, Cathy Mathis, and Daniel Lovell for technical support and assistance.

REFERENCES

1. Hill P, Brantley H, Van Dyke M. Biomaterials. 2010;31:585-93.
2. de Guzman RC, Merrill MR, Richter JR, Hamzi RI, Greengauz-Roberts OK, Van Dyke, ME. Biomaterials. 2011;32:8205-17.

QUANTIFICATION OF TOY SWORD KINEMATICS WITH PEDIATRIC VOLUNTEERS

Stephanie M. Beeman[1], Steven Rowson[1], and Stefan M. Duma[1]
1. Virginia Tech – Wake Forest, Center for Injury Biomechanics, Biomedical Engineering and Mechanics
Corresponding Author: Stephanie M. Beeman, Email: smbeeman@vt.edu

INTRODUCTION

Injuries present a major threat to the health and welfare of children and adolescents. Play, recreational activities, and organized sports pose a risk of unintentional physical injuries, particularly since children are still gaining motor and cognitive skills. Toy swords may be categorized as war toys which have a controversial, widely debated role in child play [1]. Even while playing without intent to harm, children playing with war toys may sustain injuries due to the nature of play [1]. Toy safety research data is unavailable with regard to toy swords. Understanding the physical capacity of children of different ages is important for the evaluation of injury risk and the design of new toys. Therefore, the purpose of this study was to quantify the linear and angular toy sword velocities generated by children swinging toy swords.

METHODOLOGY

A total of 36 male subjects, ages 4-14 years old, each participated in one trial. Approval to perform this study was obtained from the Virginia Tech IRB and informed consent and assent were obtained prior to testing. Subjects were instructed to swing a toy sword as fast and hard as possible for ~10 seconds. An 18-camera Vicon motion analysis system was used to capture subject and toy sword kinematics (Figure 1). Peak linear and angular toy sword velocities were calculated.

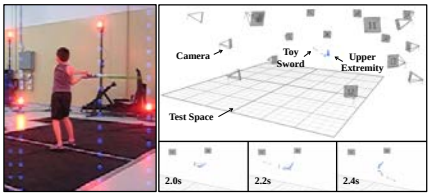

Figure 1: Subject swinging a toy sword and a sequence of swing reconstruction images.

RESULTS

A strong linear correlation was identified between age and velocity (Figure 2). The 8-14 year old males were not significantly different from each other. The 4 year old males generated significantly lower velocities than the 8-14 year old males. The 6 year old males produced significantly lower velocities than the 10- 14 year old males.

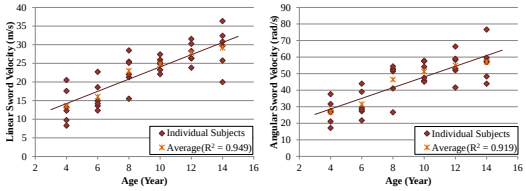

Figure 2: Linear and angular toy sword velocities.

CONCLUSIONS

It was concluded that age had a significant effect on the linear and angular velocities generated by children. The trends observed within this study likely result from typical pediatric and adolescent development. By accounting for the physical capabilities of a specific population, toys can be designed with decreased inherent risks of injury.

ACKNOWLEDGMENTS

The authors would like to thank Hasbro for providing support for this study as well as Melissa Hulse, Brock Strom III, and Ryan Field for their contributions.

REFERENCES

[1] Hart, JL and MT Tannock, Encyclopedia on Early Childhood Development, 1-6, 2013.

Virginia Tech
Wake Forest University
School of Biomedical Engineering and Sciences
14th Annual Graduate Student Research Symposium, May 13, 2015

DEVELOPMENT OF BLOOD-BRAIN BARRIER-ON-CHIP FOR STUDYING DRUG DELIVERY TO THE BRAIN BY PULSED ELECTRIC FIELDS

Mohammad Bonakdar[1], Rafael V. Davalos[12]
1. Mechanical Engineering, Virginia Tech
2. Biomedical Engineering and Mechanics, Virginia Tech
Corresponding Author: Mohammad Bonakdar, Email: Mohammad@vt.edu

INTRODUCTION

The blood-brain barrier (BBB) is the wall of the microvascular network of the brain. This wall is comprised of tightly packed endothelial cells which restrict the transport of substances from blood to the brain tissue. This barrier also restricts the transport of drugs which target the brain tissue. Hence, methods are sought to temporarily permeabilize the BBB for drug delivery. One of the methods that has been introduced is the application of pulsed electric fields (PEFs). However it is still unclear how the PEFs would affect different pathways across the BBB which will be used for the delivery of different types of molecules. In this study we developed a microfluidic model of the BBB as an in vitro model, to study the transport mechanisms in a quantitative manner. We used fluorescent microscopy and electrical impedance spectroscopy to quantify the permeability of paracellular and transcellular pathways across the BBB.

METHODOLOGY

Several microfluidic platforms (Fig1) are designed and fabricated using advanced microfabrication techniques to study the uptake and transport of molecules into and across the BBB. Brain endothelial cells are cultured as a monolayer in these devices. Upon confluence the cells are exposed to PEFs while in contact with a solution of naturally impermeable molecules (FITC Dextran). The uptake of molecules into the endothelial cells is measured by fluorescent microscopy and quantified using proper calibration curves. The cell morphology inside the channel is obtained by confocal microscopy. For transport analysis a double layer microfluidic device is fabricated. The cells in the top channel are exposed to the drug and after applying the PEFs, the amount of molecules transported to the bottom channel is quantified. A third platform is fabricated with embedded impedance sensors which enables measuring the electrical impedance spectrum across the cell layer. By proper electrical modeling, the impedance data is further transformed into the permeability of different pathways across the BBB.

Figure 1: Microfluidic platforms for BBB.

RESULTS

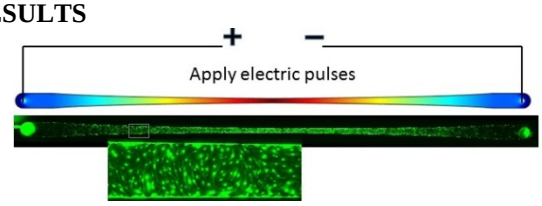

Figure 2: Distribution of electric field and absorption of Dextran in the microchannel .

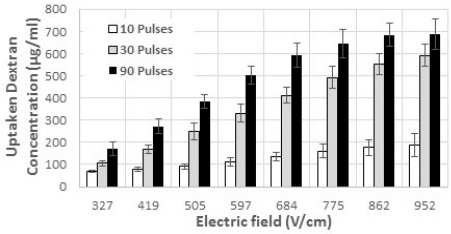

Figure 3: Concentration of absorbed dextran.

CONCLUSIONS

We used advanced microfabrication techniques to make several platforms for BBB-on-Chip. We used these platforms to study BBB permeabilization due to PEFs.

ACKNOWLEDGMENTS

This work has been supported by NSF and ICTAS.

BIOMECHANICAL ANALYSIS OF COAXIAL AND CORTICAL TRAJECTORY PEDICLE SCREWS IN LUMBAR SPINE FUSION CONSTRUCTS

Philip J. Brown[1], Greg J. Gillespie[1], James L. West[2], Joel D. Stitzel[1], Wesley Hsu[2]
1. VT-WFU School of Biomedical Engineering and Sciences, Winston Salem, NC, USA
2. Wake Forest Baptist Medical Center, Winston Salem, NC, USA
Corresponding Author: Philip Brown, Email: phibrown@wakehealth.edu

INTRODUCTION

Lower back pain is known to be associated with the degeneration of the functional spinal unit (FSU) [1,2]. Intervertebral fusion is considered the standard of care for the treatment of lumbar segmental instability, degenerative intervertebral disks, and pain management [3]. Pedicle screw fixation with interconnected rigid rods is the current gold standard in fusion techniques [4]. Current pedicle screws use a transpedicular path following the coaxial trajectory (CaT) [5]. An alternate approach is the cortical bone trajectory (CBT) which follows a caudocephalad path to engage the cortex of the pedicle [5]. We aim to characterize the stiffness and range of motion of the lumbar spine with multi-level fusions of coaxial, cortical bone, and hybrid trajectory techniques.

METHODOLOGY

Using the hybrid method of compliance testing, 12 cadaveric lumbar spines with fusion hardware were tested for stiffness and range of motion in flexion/extension, lateral bending, and axial rotation to 8Nm. Specimens were tested using a force/moment controlled six axis robot [Kuka KR-300ultra]. Relative functional spinal unit (FSU) motion was tracked using active optical markers with a motion tracking camera [NDI 3D Investigator]. Three surgical conditions of three surgical groups (1) CaT, (2) CBT, and (3) a hybrid of the two will be studied to determine the feasibility of cortical bone trajectory pedicle screws in surgery.

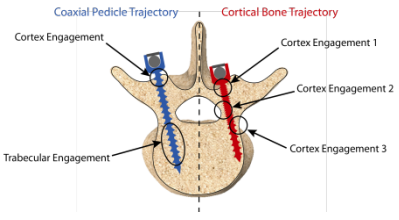

Figure 1: Pedicle Screw Installation.

RESULTS

In Table 1, I have divided the fusions by level and by fusion technique. Data is presented as a ratio of fused range of motion over normal physiological range of motion. No statistical differences have been observed. This data includes 7 of the intended 12 samples and does not include bone mineral density normalization.

Table 1: Relative Range of Motion [% of Normal]

Fusion	Direction	Mean	Std Dev
Axial Trajectory	Axial Rotation	57%	13%
	Extension	23%	25%
	Flexion	32%	20%
	Lateral Bending	27%	13%
Cortical Trajectory	Axial Rotation	73%	15%
	Extension	17%	18%
	Flexion	25%	11%
	Lateral Bending	41%	17%

CONCLUSIONS

Our data shows that both techniques are equivalent in the ability to maintain temporary relative fusion. Clinician may prefer CBT as a means to lessen the severity of fusion particularly in adjacent level secondary fusions.

ACKNOWLEDGMENTS

The authors would like to thank Greg Gillispie, Jared Mitchell, and Dr. James West for their combined efforts.

REFERENCES

1. Phillips, F.M., et al., Spine 2013. 38(7):E409-22.
2. Andersson,G., The Lancet, 1999. 354(9178):581-585.
3. Mageswaran, P., et al., J Neurosurg Spine, 2012. 17(3):232-42.
4. Perez-Orribo, L., Spine, 1976, 2013. 38(8):635-41.
5. Santoni, B.G., et al., Spine J, 2009. 9(5): p. 366-73

A MICROFLUIDIC DEVICE FOR PROFILING GENOME-WIDE HISTONE MODIFICATION USING 100 CELLS

Zhenning Cao[1], Changya Chen[2], Bin He[2], Kai Tan[2] and Chang Lu[1,3]
1. School of Biomedical Engineering and Sciences, VT-WFU, Blacksburg, VA 24061, USA
2. Department of Internal Medicine, Carver College of Medicine, University of Iowa, Iowa City, IA 52242, USA
3. Department of Chemical Engineering, Virginia Tech, Blacksburg, VA 24061, USA
Corresponding Author: Zhenning Cao, Email: caozn@vt.edu

INTRODUCTION

All biological processes rely on expression of genes under coordinated transcriptional and epigenetic regulations. Understanding these regulations is essential for our comprehension of development and diseases. Chromatin immunoprecipitation (ChIP) assay has become the technique of choice for examining in vivo DNA-protein interactions in cells or tissues. However conventional ChIP protocols have some serious limitations. They require millions of cells for a genome-wide analysis (i.e. ChIP-Seq) and 3-4 days to generate ChIPed DNA for sequencing. The requirement of a large number of cells poses a serious challenge when using scarce sources, such as stem cells and clinical samples. Conventional ChIP assays involve extensive manual handling of samples. These cumbersome procedures require a long assay time and lead to loss of materials and noise in the data.

METHODOLOGY

Microfluidics provides the platform for conducting molecular assays with drastic reduction in the volume, high level of integration and automation, and effective manipulation of cells and particles. Here we introduce a simple microfluidics-based protocol, microfluidic oscillatory washing-based ChIP-Seq (MOWChIP-Seq), which increases the collection efficiency of ChIPed DNA by 2-3 orders of magnitude compared to the state-of-the-art and allows genome-wide analysis of histone modifications using as few as 100 cells (which, to the best of our knowledge, represents the highest sensitivity ever reported). The combined use of a packed bed of beads for ChIP and effective microfluidic oscillatory washing for removing nonspecific adsorption/trapping is the key to extremely high yield of highly-enriched DNA. Our technology is fundamentally different from other high-sensitivity ChIP technologies which rely on superior amplification (e.g. Nano-ChIP-seq)[1,2] and indexing/pooling (e.g. iChIP)[3] schemes, thus may potentially complement other methods.

RESULTS

We validated the technology by examining two histone modifications (H3K4me3 and H3K27Ac) in a human B cell line and benchmarked our technology against Nano-ChIP-Seq and iChIP. MOWChIP-Seq with 100-600 cells achieved data quality that was comparable to that of iChIP using 5K cells (i.e. the smallest sample size used in their published data) and substantially superior to that of nano-ChIP-Seq using 20K cells. Using scarce hematopoietic stem and progenitor cells (HSPCs) isolated from mouse fetal liver, we uncovered a large number of novel enhancers and super enhancers, suggesting that enhancer activity is highly dynamic during early hematopoiesis.

CONCLUSIONS

Our microfluidic device has a simple structure and is easy to operate. We envision that our technology will dramatically revolutionize the studies of epigenomes based on scarce primary cell samples.

REFERENCES

1. Adli, M., Zhu, J. & Bernstein, B. E. Genome-wide chromatin maps derived from limited numbers of hematopoietic progenitors. *Nat Methods* **7**, 615-618, doi:10.1038/nmeth.1478 (2010).
2. Shankaranarayanan, P. *et al.* Single-tube linear DNA amplification (LinDA) for robust ChIP-seq. *Nat Methods* **8**, 565-U565, doi:Doi 10.1038/Nmeth.1626 (2011).
3. Lara-Astiaso, D. *et al.* Immunogenetics. Chromatin state dynamics during blood formation. *Science* **345**, 943-949, doi:10.1126/science.1256271 (2014).

SLIP BOUNDARY CONDITIONS AND FLUID STRUCTURE INTERACTION IN MICROSCALE GAS FLOW

Krishnashis Chatterjee[1] and Anne Staples[1]
1. Department of Biomedical Engineering and Mechanics, Virginia Tech, Blacksburg, VA, USA
Corresponding Author: Krishnashis Chatterjee, Email: krisc83@vt.edu

INTRODUCTION

Current engineered microfluidic devices mostly involve the actuation of an arrangement of valves and pumps for flow of liquids in a complex network of channels. However, for gas transport, a more simplified and efficient less widely acknowledged mode is by rhythmic contractions of highly inelastic, but locally collapsible, micro tubes. This study analytically investigates the effects of slip boundary conditions and fluid structure interactions on volumetric flow rate, velocities and wall shear stress.

METHODOLOGY

Two dimensional, non-dimensionalized Navier Stokes equations for Stokes flow at the microscale are solved with appropriate lubrication theory assumptions and slip boundary conditions. Subsequently an interaction between the material properties of the micro tube and fluid flow parameters is also investigated.

RESULTS

Final expressions for velocities, mass flow rate, stream functions, shear stresses and other fluid flow parameters are obtained. Graphs showing the variation of these parameters in time and both vertical and horizontal directions are also examined. The relationship between the mass flow rate and the phase lag between the contractions are plotted in order to arrive at the optimum value of the mass flow rate.

CONCLUSIONS

The results provide an idea about the efficiency of this valveless mode of gas transport at the microscale, as well as the optimum phase lag for the maximum volume flow rate when rarefaction effects and fluid structure interactions are taken into account.

ACKNOWLEDGMENTS

NSF Grant Number: 1437387

STUDYING FINITE DEFORMATIONS OF NONLINEAR ELASTIC PLATES USING THIRD ORDER SHEAR AND NORMAL DEFORMABLE THEORIES

Arka P. Chattopadhyay[1] and Romesh C. Batra[1]
1. Department of Biomedical Engineering and Mechanics, Virginia Tech
Corresponding Author: Arka P. Chattopadhyay, Email: arka@vt.edu

INTRODUCTION

We study the transient finite deformations of rectangular plates loaded under a spatially distributed time varying load to simulate a shock wave on the plate. We analyze a St. Venant Kirchhoff plate using the third order shear and normal deformable theory (TSNDT). The TSNDT accounts for transverse normal and shear strains and the six stress components are computed from the constitutive relation rather than a stress recovery method. In our analysis, we consider all geometric nonlinearities. For St. Venant-Kirchhoff material, the 1st Piola-Kirchhoff stress tensor and the Cauchy stress are nonlinear functions of the corresponding strain measures thus introducing material nonlinearity into the model.
The numerical solution of the nonlinear problem is obtained from the finite element method (FEM) using the conditionally stable central difference time integration algorithm and 4-node quadrilateral elements on the plate midsurface. In our finite element model, each node has 12 degrees of freedom - 3 displacements and their 1st, 2nd and 3rd order derivatives with respect to the thickness coordinate. The stresses from the TSNDT are found to agree with those from the solutions of the nonlinear problem using the 3-D elasticity theory and the software Abaqus. It is found that the linear theory over-predicts deflections and stresses in the plate.

METHODOLOGY

For analyzing the deformations of a plate, we express the displacements of any point in the volume domain of the plate as a Taylor series expansion about the mid-surface.

$$u_i = \sum_{j=0}^{3} X_3^j u_{ij},\ u_{ij} = \frac{1}{j!}\frac{\partial^j u_i}{\partial X_3^j}\bigg|_{X_3=0} \qquad (1)$$

In Eqn. (1), i takes the values of 1 - 3 and j of 0 - 3 thus giving 12 unknowns on the midsurface, using which the displacements of any point in the plate can be computed.
We formulate the equations of motion in Lagrangian description and develop the FEM model of these using the Galerkin formulation. We solve the system of nonlinear ODEs using a numerical solver developed in FORTRAN. The solver is verified and validated by studying certain example problems and comparing the results with the corresponding results from 3D elasticity solver Abaqus and results from literature.

RESULTS

Figure 1 shows the in-plane normal stress σ_{11} at the center of the top surface of the plate for different peak loads. It is observed that for a nonlinear problem, the time history changes qualitatively unlike the linear problem in which the displacements are scaled with increase in the load.

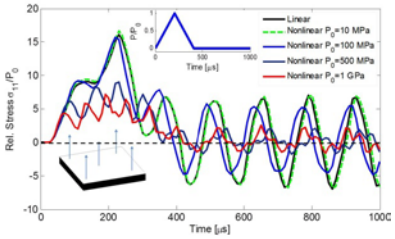

Figure 1: Time histories of the in-plane normal stress at the center of the top surface for different peak loads.

CONCLUSIONS

We have developed a mathematical model to study the finite deformations of a plate using the TSNDT and solved the problem using the FEM. The results of example problems using the TSNDT were compared with 3D elasticity FEM solutions from Abaqus and good agreement of results were observed. We also delineated the effects of nonlinearity in the model by comparing the results from the linear and nonlinear formulations.

HEAD IMPACT EXPOSURE IN YOUTH FOOTBALL

Bryan R. Cobb[1], Jillian E. Urban[2], Elizabeth M. Davenport[2], Steven Rowson[1], Stefan M. Duma[1], Joseph A. Maldjian[2], Christopher T. Whiltlow[2], Alexander K. Powers[2], and Joel D. Stitzel[2]
1. Virginia Tech, Department of Biomedical Engineering and Mechanics,
2. Wake Forest University, School of Biomedical Engineering & Sciences
Corresponding Author: Bryan R. Cobb, Email: cobb84@vt.edu

INTRODUCTION

Concussions in youth football have garnered substantial public interest in recent years. Among team sports, football is the number one contributor to the estimated 1.6 to 3.8 million sports related concussions sustained each year.[1] Youth players, age 6 to 13 years, account for roughly 70% of participants in organized football, yet few studies have focused on the head impact exposure these players experience. The objective of this study was to quantify the head impact exposure of youth football players, aged 9 to 12 years, for all practices and games over the course of single season.

METHODOLOGY

On-field head impact data were collected from 50 players, age 9 to 12 years, on three youth tackle football teams. Players were equipped with helmet-mounted accelerometer arrays for practices and games during a single fall football season. The data were analyzed to assess the impact frequency and acceleration magnitudes players experienced. Comparisons were made between session types and among the three teams. Furthermore, uncertainty were assessed using random measurement error estimates from a previously published study.[2]

RESULTS

During the season, 11,978 impacts were recorded for this age group. Players averaged 240 ± 147 impacts for the season with linear and rotational 95th percentile magnitudes of 43 ± 7 g and 2034 ± 361 rad/s^2. Overall, practice and game sessions involved similar impact frequencies and magnitudes. Team A had substantially fewer impacts per practice and lower 95th percentile magnitudes in practices compared to the other two teams due to a efforts to limit contact in practices (Fig. 1).

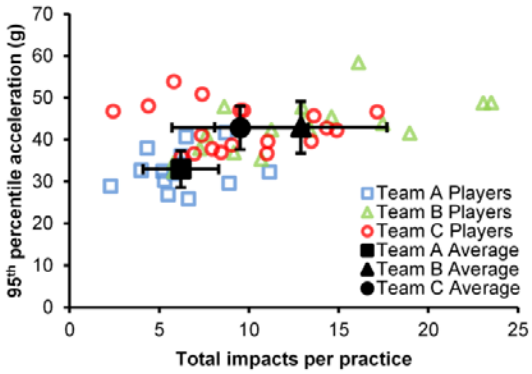

Figure 1: Summary of head impact exposure in practice.

CONCLUSIONS

While the acceleration magnitudes among 9 to 12 year old players tended to be lower than those reported for older players, some recorded high magnitude impacts that were similar to those seen at the high school and college level. Overall, players experienced similar levels of head impact exposure in practices and games on a per-session basis. For one team however, lower head impact exposure was observed in practices compared to games. The reduced exposure was due to newly implemented rules designed to restrict player contact in practice suggesting that such rules can reduce head impact exposure in youth football.

REFERENCES

1. Langlois JA, Rutland-Brown W and Wald MM. The epidemiology and impact of traumatic brain injury: a brief overview. *The Journal of head trauma rehabilitation*. 2006; 21: 375-8.

2. Beckwith JG, Greenwald RM and Chu JJ. Measuring Head Kinematics in Football: Correlation Between the Head Impact Telemetry System and Hybrid III Headform. *Ann Biomed Eng*. 2012; 40: 237-48

Virginia Tech
Wake Forest University
School of Biomedical Engineering and Sciences
14th Annual Graduate Student Research Symposium, May 13, 2015

TUMOR ENGINEERING TO ELUCIDATE THE EFFECT OF MILD HYPERTHERMIA ON TRANSPORT OF SWNHS IN THE TUMOR MICROENVIRONMENT

Matthew R DeWitt[1], Allison Pekkanen[1], Rafael Davalos[1], and M. Nichole Rylander[2]
1. Virginia Tech-Wake Forest School of Biomedical Engineering and Sciences
2. University of Texas at Austin – Mechanical Engineering
Corresponding Author: Matthew DeWitt, Email: mttdwtt@vt.edu

INTRODUCTION

Therapeutic use of mild hyperthermia(41-43°C) has extensively been studied for enhancement of a wide range of chemotherapeutic drugs. While in vitro and in vivo studies have shown enhancement with mild hyperthermia, the practicality of simultaneous application of the two modalities in the tumor environment can be difficult to achieve, limiting the overall utility of the combination.
Single-walled Carbon Nanohorns (SWNHs) are a promising nanoparticle choice for multimodal therapies for the delivery of heat and chemotherapeutic agent to produce this desired synergistic effect. Current studies to evaluate nanoparticle mediated thermal enhancement therapies are primarily executed in a traditional 2D cell culture system in which the particles are applied directly over seeded cells resulting in possibly exaggerated effects of synergy.
In this study we have developed a novel perfusable tissue engineered model of the tumor microenvironment of collagen tissue containing human breast cancer cells and vessels with endothelial cells and we validated and characterized nanoparticle transport within and determined the effect of mild hyperthermia in the tissue level transport of SWNHs.

METHODOLOGY

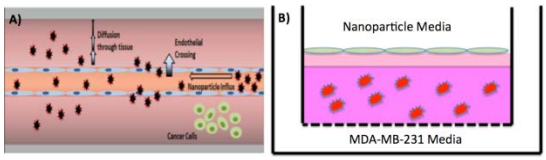

Figure 1: A) Flow setup B) Static setup

The 3D culture system described in Figure 1B was utilized to study uptake by the MDA-MB-231 cells in a co-culture setup with a monolayer of TIME cells, elucidating the effect of mild hyperthermia on diffusion and uptake by the cells. The temperature was varied between 42°C and 37°C and a nanoparticle solution was administered in the endothelial media cavity for up to 6h. FACs was used to quantify uptake by cells located within tumor matrix and fluorescent tracking was accomplished.

RESULTS

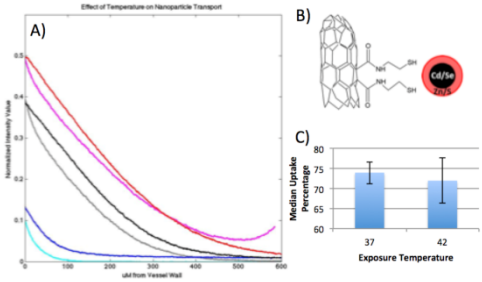

Figure 3: A) Radial intensity values of QD-SWNH fluorescence at 37 and 42°C at 30m, 3h, and 6h. B) Depiction of SWNH-QD C) FACS median uptake of MDA-MB-231 within matrix at 37 and 42°C

Following characterization of the 3D microfluidic model, SWNH-QD (Figure 2B) were created and tested in the system under normothermia and mild hyperthermia (Figure 2A). Radial fluorescent intensity from the vessel wall is plotted. A significant change in fluorescent intensity can be seen for the approximately 100nm particles at the 3 h time point, highlighting the effect of mild hyperthermia on extravasation and diffusion within the matrix.

CONCLUSIONS

We have demonstrated that tumor engineering models can be utilized to study the transport of SWNHs within the tumor microenvironment. Two tissue engineered models, were developed and validated to understand the effect of hyperthermia on nanoparticle transport which is crucial when developing novel photothermal therapies.

ACKNOWLEDGMENTS

Funding: NSF Early CAREER Award and the NSF-GRFP

EFFECT OF ALGINATE MICROCAPSULE STIFFNESS ON ENCAPSULATED OVARIAN CELL VIABILITY

Kevin Enck[1,2], JP McQuilling[1,2], Sittadjody Sivanandane[1], and Emmanuel C Opara[1,2]
1. SBES (Wake Forest University Campus)
2. Wake Forest Institute for Regenerative Medicine
Corresponding Author: Kevin Enck, Email: kenck@wakehealth.edu

INTRODUCTION

Cell encapsulation techniques have been widely used as delivery methods for molecules secreted by cells protected from immune destruction. Hydrogels are known to be great matrix platforms for cell encapsulation because of their durability and ability to change many of their physical characteristics. In particular, the alginate hydrogel is the most used matrix because alginate is abundant, biocompatible, and has tunable characteristics. Matrix stiffness has also been widely known to regulate various cellular activities, because cells that are surrounded by an ECM can sense their environment and adapt to it. Alginate hydrogels are given their rigidity by crosslinkers that bind the alginate together. Our laboratory is interested in ovarian tissue engineering based on alginate hydrogel, and currently there is no report on the effect of hydrogel stiffness on the behavior of encapsulated ovarian cells.

METHODOLOGY

Divalent cations, Ca^{2+} and $Sr^{2+,}$ link the linear copolymers together after suspending the alginate in $CaCl_2$ and $SrCl_2$ separately. This forms a wide range of hydrogel porosity, due to binding affinities, which directly relates to hydrogel stiffness. Following microcapsule fabrication with either Ca^{2+} or Sr^{2+} crosslinker, an induction of mechanical stress using soda lime bead agitation was used to test the stiffness of the capsules. An ELISA was used in a preceding study to analyze the 17 β-estradiol secretion, a key hormone in ovarian cell functionality, from each type of microcapsules along with live/dead staining to assess cell viability.

RESULTS

Our previous work illustrated in Figure 1, shows that 17 β-estradiol secretion from Ca^{2+} crosslinked microbeads was not sustained over time, in contrast to the Sr^{2+} crosslinked microbeads as shown in figure 1. We therefore hypothesized that a higher hydrogel matrix stiffness was required for maintenance of ovarian cell phenotype and sustained hormone secretion. Figure 2 shows the differences in the mechanical strength of microbeads made with each crosslinker. This clearly supports our hypothesis that Sr^{2+} crosslinked alginate microbeads have a greater stiffness and are much more durable since most of the beads were intact while all of the Ca^{2+} beads were ruptured.

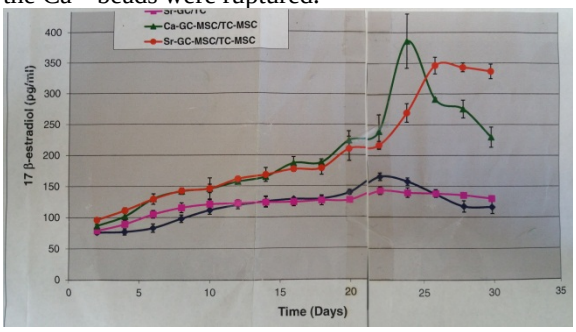

Figure 1: ELISA of 17 β-estradiol secretion between Ca (green) and Sr (orange) over 30 day study.

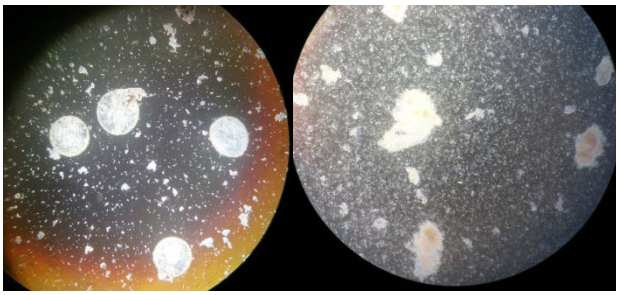

Figure 2: Strontium (left) and Calcium (right) alginate microbeads after agitation.

CONCLUSIONS

This preliminary study illustrates the importance of hydrogel stiffness in the function of encapsulated cells.

Virginia Tech
Wake Forest University
School of Biomedical Engineering and Sciences
14th Annual Graduate Student Research Symposium, May 13, 2015

DRIVER RISK VARIABILITY IN FINITE ELEMENT RECONSTRUCTION OF CIREN MOTOR VEHICLE CRASHES

James P. Gaewsky[1], Ashley A. Weaver[1], Bharath Koya[1], and Joel D. Stitzel[1]
1. Virginia Tech-Wake Forest Center for Injury Biomechanics (Wake Forest University, Biomedical Engineering)
Corresponding Author: James P. Gaewsky, Email: jgaewsky@wakehealth.edu

INTRODUCTION

The Crash Injury Research and Engineering Network (CIREN) surveys hundreds of motor vehicle crashes (MVCs) each year to assess occupant injury outcomes in real world crash events across the United States. Although the CIREN database contains a wealth of crash injury information, relatively few studies have computationally modeled MVCs studied by CIREN to assess occupant injuries. This study developed a method to reconstruct a wide range of full frontal CIREN MVCs using dynamic finite element model (FEM) simulations in a three step process and assessed the variability in injury risk and severity for common frontal crash injury patterns.

METHODOLOGY

Step 1: A simplified vehicle model (SVM) was developed and tuned to mimic the frontal crash response of the CIREN case vehicle for each reconstruction. Frontal NCAP crash test vehicle kinematics for each case were implemented into crash test reconstructions with a Hybrid III anthropomorphic test device (ATD) FEM. Ten vehicle restraint parameters (e.g. airbag inflation rate) were varied across 200 simulations using Latin Hypercube Design (LHD) of experiments to find an optimal set of vehicle parameters resulting in simulated ATD responses closely matching test data. **Step 2:** THUMS v4.01 was implemented into the tuned SVM using CIREN occupant positioning information (baseline simulation), as well as a range of occupant positions by varying seatback angle, longitudinal seat track position, D-ring height, and steering position/angle using a 120 simulation LHD. **Step 3:** The CIREN case's event data recorder (EDR) velocity pulse was applied to the tuned SVM for each of the 120 THUMS occupant positions. Simulated instrumentation was implemented and used to measure injury metrics in THUMS correlated to common frontal crash injuries. AIS-based risks were estimated from the injury metrics using published injury risk curves.

RESULTS

The SVM was successfully tuned for all frontal CIREN reconstructions. Sprague and Geers magnitude (M) and phase (P) error factors validated the FEM against the crash test ATD head, chest and pelvis accelerations ($|M| < 0.23$, $P < 0.12$) and femur and belt force ($|M| < 0.12$, $P < 0.13$) signals. One reconstructed 2010 Camry occupant had no reported head injuries or knee-thigh-hip (KTH) injuries and injury risks calculated for the CIREN-reported occupant position versus the range of positions simulated were: AIS 1+, 2+, 3+ head (42%, 22-100%; 7.4%, 0-99%; 1.0%, 0-55%); AIS 2+, 3+ KTH (2.8%, 2-4%, 2.8%, 2-4%). In a 2006 Chevrolet Cobalt reconstruction, the occupant's AIS 3 lung contusion (49% of lung contused) was predicted because over 49% of the THUMS lung elements exceeded a 32.5% first principal strain threshold, consistent with previous literature.

CONCLUSIONS

Head, chest, pelvis, and femur injury risks predicted with FEMs were well correlated with documented CIREN injuries, and this methodology can be extended to reconstruct more CIREN/NASS frontal crashes. The reconstruction process allows for quantification of the sensitivity and uncertainty of injury risk predictions based on occupant position which is often uncertain in real-world crashes. THUMS injury metrics assessed include strain-based metrics for assessing organ injuries (i.e. lung) that are not easily assessed in post-mortem human subjects (PMHS) or ATDs. This information is potentially valuable to assess the effectiveness of restraint systems to prevent or mitigate injuries that are not easily studied using PMHS and ATDs.

ACKNOWLEDGMENTS

Funding has been provided by Toyota's Collaborative Safety Research Center.

EPHAPTIC COUPLING AS A FIRST LINE OF THERAPY DURING A HEART ATTACK

Sharon A George[1], Steven Poelzing[1,2]
1. Virginia Tech, Department of Biomedical Engineering and Mechanics
2. Virginia Tech, Carilion Research Institute
Corresponding Author: Sharon A George, Email: sharonag@vt.edu

INTRODUCTION

About a million people in the US suffer a heart attack each year. Heart attacks occur when a coronary vessel is blocked and blood supply to a region of the heart stops resulting in myocardial ischemia (MI).
MI produces structural changes in the heart such as gap junctional (GJ) uncoupling which can have functional consequences like conduction slowing. Expensive peptide therapy that prevent GJ uncoupling have been demonstrated to attenuate the effects of MI on conduction.[1]
Recently we demonstrated that Ephaptic Coupling (EpC) can mask the dependence of conduction on GJ coupling.[2] Therefore, we hypothesized that promoting EpC by modulating extracellular ion composition can attenuate the effects of MI on conduction.

METHODOLOGY

Two solutions – Solution A (promoted EpC) and Solution B (weakened EpC) were identified. Adult male guinea pig hearts were perfused with these solutions for 20 mins followed by MI for 30 mins and finally 20 mins of reperfusion. MI was simulated by oxygen and glucose depravation and acidosis (pH 6.5) in Solution A and B. Conduction velocity (CV) was determined by optical mapping. CV in the longitudinal (CV_L – parallel to the cell fibers) and transverse (CV_T – perpendicular to the cell fibers) directions were calculated. Anisotropic ratio (AR = CV_L/CV_T) was calculated as an index of arrhythmogenic risk.

RESULTS

No differences in CV were measured between solutions (A or B) and over time (15 mins). MI slowed CV_L and CV_T but only CV_T demonstrated solution dependence. Specifically, MI slowed CV_T more in hearts perfused with Solution B (gray curve, Figure1) relative to Solution A (black curve, Figure1). CV_L and AR were not significantly different between solutions.

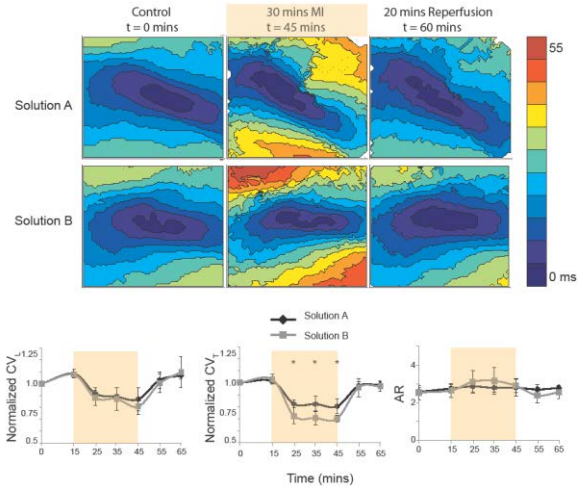

Figure 1: Solution modulates effect of MI on conduction. Activation maps (Upper Panel) demonstrate conduction spread over the epicardium. Crowding of isochrones lines during MI suggest CV slowing which was greater with Solution B relative to Solution A. CV_L, CV_T and AR are summarized below.

CONCLUSIONS

Ephaptic coupling could be a cost-effective therapy to attenuate the detrimental effects of MI on cardiac conduction.

REFERENCES

1. Kjolbye et al. 2008. Maintenance of intercellular coupling by the antiarrhythmic peptide rotigaptide suppresses arrhythmogenic discordant alternans.
2. George et al. 2015. Extracellular sodium and potassium levels modulate cardiac conduction in mice heterozygous null for the Connexin43 gene.

Virginia Tech
Wake Forest University
School of Biomedical Engineering and Sciences
14th Annual Graduate Student Research Symposium, May 13, 2015

INTERIOR MICRO-CT OF MOUSE HEART USING A COLLIMATED CARBON-NANOTUBE FIELD EMISSION X-RAY SOURCE

Hao Gong[1] and Guohua Cao[1*]
1. Virginia Tech, School of Biomedical Engineering and Sciences
Corresponding Author: Guohua Cao, Email: ghcao@vt.edu

INTRODUCTION

Micro computed tomography (micro-CT) provides the biomedical researchers with non-invasive evaluation of anatomical structure and physiological function of mouse hearts. However, mouse cardiac micro-CT is still limited by cumulative ionizing radiation, which can perturb pathophysiology of interest. Interior tomography has been proposed to reduce dose by guiding the irradiation only through an internal region-of-interest (ROI) within the sample. Moreover, mouse ultra-fast heart rate (<600 bpm) induces severe motion-blurring to micro-CT images. Recently, we developed a mouse cardiac micro-CT using carbon-nanotube (CNT) based x-ray source, and minimized the motion-blurring. Therefore, we combine the strengths of interior tomography and CNT source based micro-CT (i.e. interior micro-CT) to provide low-dose and high-quality mouse cardiac imaging.

METHODOLOGY

A micro-CT platform was built based on an in-house-developed CNT x-ray source. Interior tomography was implemented by using an aperture collimator at source side. Interior micro-CT scans were conducted by using micro-CT phantoms and a mouse specimen. Image reconstruction was conducted by using our recently published iterative algorithm. Radiation dose was measured for both interior and global micro-CT. More details of the methods can be found in [1].

RESULTS

Overall, the imaging results from interior micro-CT were comparable to those from conventional global micro-CT (Fig.1). For water phantom, interior micro-CT image presented higher contrast-noise-ratio (> 2.2 increment factor) than global micro-CT image. For multi-feature phantom, interior micro-CT image presented very similar quality to global micro-CT image with a high structural similarity index of 0.9102. For mouse specimen, interior micro-CT image yielded largely suppressed shading artifacts than global micro-CT image (marked by arrows). The radiation dose measurement demonstrated up to 84% reduction from global micro-CT to interior micro-CT.

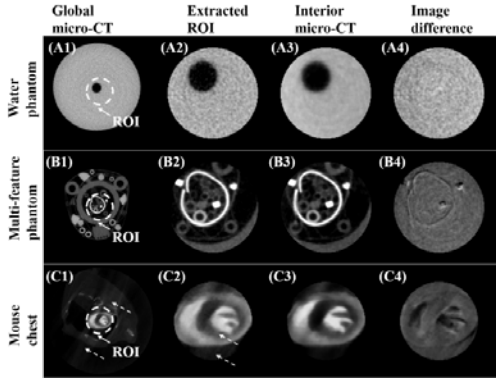

Figure 1: Imaging results of global and interior micro-CT

CONCLUSIONS

The high-quality imaging results and significantly reduced radiation dose make the CNT x-ray source based interior micro-CT attractive for mouse cardiac imaging.

ACKNOWLEDGMENTS

This work was partially supported by Dr.Cao's new faculty startup package at Virginia Tech, a seed grant from ICTAS and Dr.Cao's CAREER support from NSF.

REFERENCES

[1]H. Gong, J. Lu, O. Zhou, and G. Cao, "Implementation of interior micro-CT on a carbon nanotube dynamic micro-CT scanner for lower radiation dose," 2015, pp. 94124N-94124N-9.

THERANOSTIC POLYMER NANOPARTICLES FOR PHOTOTHERMAL ABLATION AND FLUORESCENT IMAGING OF CANCER

Elizabeth G. Graham[1,2] and Nicole H. Levi-Polyachenko, PhD[1,2]
1. Wake Forest University, Department of Plastic and Reconstructive Surgery
2. Virginia Tech - Wake Forest University, School of Biomedical Engineering and Sciences
Corresponding Author: Elizabeth Graham, Email: elgraham@wakehealth.edu

INTRODUCTION

Nanoparticle (NP) mediated photothermal ablation of cancer is a promising technique that utilizes light energy to destroy cancer cells. Specifically, NPs that absorb in the near infrared (NIR) region, 700 - 900 nm, are optimal as these wavelengths are where tissues are most transparent, NIR photothermal therapies allow for efficacious localized hyperthermia. Our lab has recently used poly[4,4-bis(2-ethylhexyl)-cyclopenta[2,1-b;3,4-b']dithiophene-2,6-diyl-alt−2,1,3-benzoselenadiazole-4,7-diyl] (PCPDTBSe), a donor-acceptor electrically conductive polymer, to form NPs capable of generating heat when stimulated by 800 nm light. [1]

Non-invasive visualization of NPs is invaluable for better understanding NP behavior *in vitro* and *in vivo*. Conjugated polymer-based probes are attracting significant attention as a fluorescent moiety. One such conjugated polymer is poly(9,9-dihexylfluorene)-co-2,1,3-benzothiadiazole-co-4,7-dithiophen-2-yl)-2,1,3-benzothiadiazole (PFBTDBT10) which absorbs at 464 nm and fluoresces at 700 nm. [2]

METHODOLOGY

PCPDTBSe and PFBTDBT10 were used to form a hybrid NP and were collected by centrifugation. NPs were characterized by ultraviolet visible spectroscopy, fluorimeter, transmission electron microscopy, and dynamic light scattering. NPs were evaluated *in vitro* by cytotoxicity assay, clonogenic assay, and photothermal ablation assay in murine breast cancer cell lines 4T1 and EO771 and murine non-cancerous fibroblast cell line Tib80. Fluorescent microscopy was also performed after 24 hour incubation with NPs to investigate *in vitro* uptake. *In vivo* photothermal efficacy and fluorescent imaging was investigated in Balb/c mice with luciferase transfected 4T1 tumors.

RESULTS

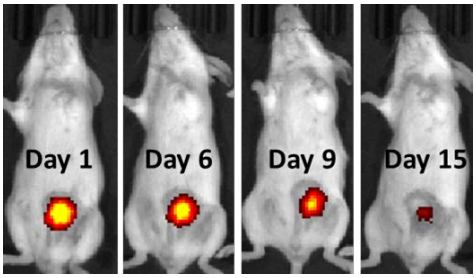

Figure 1: Fluorescence of NPs injected intratumorally.

PFBTDBT10 and PCPDTBSe polymers were combined to generate an optimal theranostic NP capable of both NIR photothermal ablation and NIR fluorescent imaging. This NP was found to be non-cytotoxic and capable of generating efficient photothermal ablation *in vitro*. Additionally, it is visible *in vivo* (Figure 1).

CONCLUSIONS

We have been able to synthesize a non-cytotoxic hybrid NP capable of both thermal ablation and fluorescence *in vitro* and *in vivo* that has long term optical stability and solubility in aqueous media.

ACKNOWLEDGMENTS

I would like to thank the Wake Forest Department of Plastic Surgery for the generous funding and resources.

REFERENCES

1. C. M. Macneill, et al., Macromol Biosci, Oct 2012.
2. Ding, et al., Small, vol.9, no. 18, pp.3093-3102, 2013.

WAKE UP CALL: SYMPATHETIC AND PARASYMPATHETIC STIMULATION CONTRIBUTE TO ARRHYTHMOGENESIS

Amara Greer-Short[1,2] and Steven Poelzing Ph.D[1,2]
1. Virginia Tech Carilion Research Institute
2. Virginia Tech – Wake Forest University School of Biomedical Engineering and Sciences
Corresponding Author: Steven Poelzing, Email: poelzing@vtc.vt.edu

INTRODUCTION

There is an increased risk for sudden cardiac death around the time of awakening, possibly due to sympathetic stimulation[1], which accompanies the upright posture and initiation of daytime activities. Sympathetic stimulation has previously been associated with calcium-mediated arrhythmias, but also has a time-dependent β agonist induced desensitization effect.[2] Parasympathetic activity, which is augmented during sleep, has opposing effects on calcium handling in the cell, but has also been associated with aggravated arrhythmogenesis.[3] We hypothesize that the time course and synergy of sympathetic and parasympathetic activity modulates arrhythmogenesis

METHODOLOGY

Retired breeder guinea pig hearts were excised and Langendorff-perfused. Isoproterenol (Iso, 0.6μM) was used as the sympathetic agonist and acetylcholine (ACh, 10μM) for parasympathetic. Overdrive excited (OE) beats were produced using a 15 second rapid pacing protocol every minute up to 20 minutes and the ECG continuously recorded.

RESULTS

Iso significantly increased total OE incidence relative to control from 0% to 7% (n=6). Total ACh OE incidence did not significantly change relative to control (2%, n=4). Pre-perfusing Iso for 20 min followed by ACh did not significantly change total OE incidence (9%, n=7) relative to Iso. In contrast, pre-perfusing ACh followed by Iso significantly increased total incidence (37%, n=5) relative to Iso (7%). OE incidence for Iso peaked at 2 minutes, which is when Iso reached its maximal change in heart rate relative (57%) to control. After the peak, OE incidence decreased to a steady state value of 0%, which paralleled the decrease in heart rate. However, when Iso followed ACh, peak OE incidence and heart rate were reached by 2 minutes and remained elevated. Therefore, ACh pre-treatment modified heart sensitivity to Iso by blunting β agonist induced desensitization.

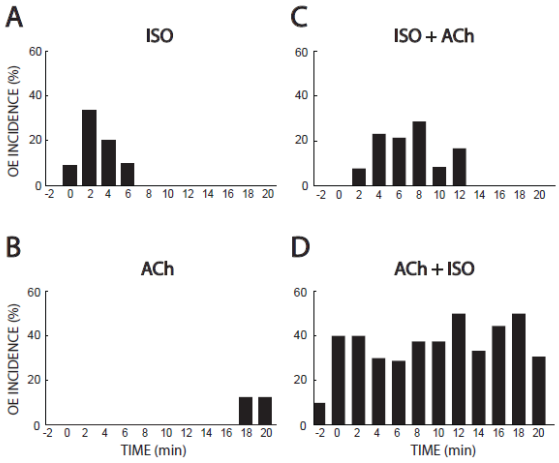

Figure 1: OE incidence over time under different sympathetic and/or parasympathetic stimulation conditions.

CONCLUSIONS

Sympathetic agonism, either alone or joint with parasympathetic, increases arrhythmogenesis. However, parasympathetic pre-treatment, followed by a sympathetic agonist, creates a substrate for prolonged arrhythmogenesis when compared to sympathetic activity alone. The temporal response of arrhythmogenesis and heart rate to Iso and ACh suggests that acute β adrenergic desensitization is prevented by when parasympathetic precedes sympathetic activation.

REFERENCES

1. Muller JE et al. Circulation. 1987; 75(1): 131-8.
2. Limas CJ and Limas C. Circ Res. 1984; 55(4): 524-31.
3. He W et al. Clin Res Cardiol. 2013; 102(5): 361-70.

CONTROL STRATEGIES TO ACHIEVE CONSISTENT PARTICLES' CHARACTERISTICS IN ATMOSPHERIC PLASMA SPRAY PROCESS

Balachandar Guduri[1], Romesh C. Batra[1]
1. Department of Biomedical Engineering and Mechanics
Corresponding Author: Balachandar Guduri, Email: gbalu@vt.edu

INTRODUCTION

Over the last two decades, atmospheric plasma spray (APS) process has become a well-established coating technology to produce different types of coatings for applications in aerospace, automotive, agricultural, and bio-medical industries. The quality of these coatings is crucial for the performance of coated components. It has been reported in the literature that up to 200 process parameters may influence the quality of the coatings, a large part of them being unquantifiable. Till to date, the effects of all process parameters on coating properties have not been studied. Additionally, frequent parametric drifts and fluctuations during spray process primarily due to the electrode wear and intrinsic plasma jet instabilities may also affect the coating quality. In order to achieve desired consistent quality and repeatability the operating parameters have to be controlled appropriately.

METHODOLOGY

Obtaining consistent particles' mean temperature and mean axial velocity is crucial in achieving consistent coating quality. Initially, significant input and output parameters and their effects in APS have been identified and quantified. Finally, a model reference adaptive control (MRAC) algorithm is developed based on Lyapunov stability theory [1] and is implemented in FORTRAN using developed adaptive and control laws to achieve the desired response of mean particles' characteristics.

RESULTS

The control algorithm is tested using LAVA-P, which simulates the plasma jet and particle injection, to study the effects of control process on mean temperature and mean axial velocity of the particles. Figure 1 shows control response of particles' mean axial velocity and mean temperature in the presence of disturbance of arc voltage. The developed MRAC algorithm is forced the LAVA-P system to follow the desired reference model by changing the argon flow rate and hydrogen flow rate.

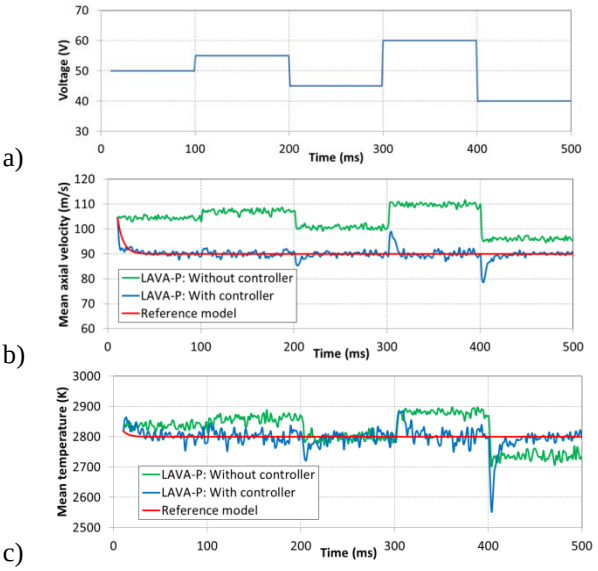

Figure 1: Control response of b) mean axial velocity and c) mean temperature for given disturbance of a) voltage

CONCLUSIONS

The interdependence between the significant operating parameters and output parameters such as mean temperature and mean axial velocity based on the physical model of APS has been identified and quantified. Based on quantified interdependence, model reference adaptive control is developed to obtain desired consistency in particle characteristics during the presence of parametric drifts and fluctuations. The control algorithm is tested using LAVA-P software.

REFERENCES

1. P. A. Ioannou, and J. Sun. Courier Corporation, 2012.

INDOCYANINE GREEN-LOADED NANOPARTICLES FOR IMAGE GUIDED TUMOR SURGERY

Tanner K. Hill[1,2], Sneha Kelkar[1,2], Frank C. Marini[2,3], and Aaron M. Mohs[1,2,3]
1. Virginia Tech-Wake Forest University School of Biomedical Engineering and Sciences
2. Wake Forest Institute for Regenerative Medicine
3. Wake Forest University Department of Cancer Biology
Corresponding Author: Tanner K. Hill, Email: tahill@wakehealth.edu

INTRODUCTION

Surgical removal of solid tumors in patients is one of the most common methodologies for the treatment of many major cancer types, and also the most curative. Currently, a combination of pre-operative imaging is used in conjunction with visual and tactile identification to identify tumors and tumor boundaries. Unfortunately, these lack the requisite resolution to identify all the diseased tissue present, as the presence of positive margins and local tumor recurrence occur in a large fraction of patients[1].

Numerous NP formulations have been effectively used to target solid tumors and improve delivery of therapeutics and contrast agents. This work examines the synthesis, characterization, and *in vivo* efficacy of indocyanine green (ICG) loaded hyaluronic acid (HLA) derived nanoparticles (NPs) for the purpose of near infrared (NIR) fluorescence image guided surgery (IGS)[2].

METHODOLOGY

NP formation was driven by self-assembly after conjugation of hydrophobic groups to HLA. Hydrophobic conjugates 1-pyrenebutanamide (PBA) and 5β-cholanamide (5βCA) were synthesized from their precursor carboxylic acids. Octadecylamine (ODA) was also used. Final products were confirmed with mass spec and NMR. NPs were loaded with ICG and tested for physical and optical properties using DLS, absorbance, and fluorescence spectroscopy. *In vivo* analysis of NanoICG was examined in two experiments using MDA-MB-231 xenograft tumors in female nude mice. NanoICG or ICG was administered systemically by tail vein injection at a dose of 10 nmol/mouse. Mice were sacrificed at 24 hours and examined using a combination of a LI-COR Pearl Impulse small animal imaging system, and a dedicated IGS system[3].

RESULTS

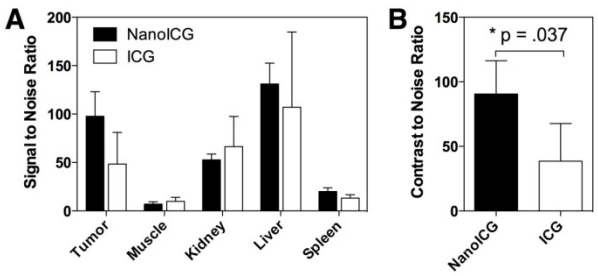

Figure 1: NanoICG improves both total signal and contrast of tumors in xenograft mice.

CONCLUSIONS

Novel HLA-derived NPs were synthesized and improved tumor signal and contrast in xenograft mice. These NPs could potentially serve as contrast agents for other types of solid tumors and merit further examination in larger animal models.

ACKNOWLEDGMENTS

NIH (R00 CA153916, R01 EB019449 to A.M.M), VT-WFU SBES, and Wake Forest Institute for Regenerative Medicine.

REFERENCES

1. Pleijhuis, R. G. et al.. *Annals of Surgical Oncology* **2009,** *16*, (10).
2. Hill, T. K. et al.. *Bioconjugate chemistry* **2015**, 26 (2).
3. Mohs, A. M. et al.. *Biomedical Engineering, IEEE Transactions on* **2015,** *PP*, (99).

Virginia Tech
Wake Forest University
School of Biomedical Engineering and Sciences
14th Annual Graduate Student Research Symposium, May 13, 2015

REDUCTION IN FATAL LONGITUDINAL BARRIER CRASH RATE DUE TO ELECTRONIC STABILITY CONTROL

Nicholas S. Johnson[1], H. Clay Gabler[1]
1. Virginia Tech / Wake Forest Center for Injury Biomechanics
Corresponding Author: Nicholas S. Johnson, Email: johnso5a@vt.edu

INTRODUCTION

Electronic stability control (ESC) is a vehicle safety system designed to keep vehicles moving in the direction commanded by the driver, and thereby prevent loss-of-control crashes. Prior research has shown that ESC is highly effective at reducing road departures related to loss-of-control. ESC is mandatory in all U.S. passenger vehicles manufactured from model year 2012 onward, and by 2014 it is estimated that approximately one third of passenger vehicles on the road were equipped with ESC. The proliferation of ESC may therefore alter benefit-to-cost ratios for roadside barriers. The objective of this analysis is to determine the effect of ESC on fatal crashes with roadside barriers. This objective is a first step towards determining if ESC reduces the overall rate of crashes with roadside barriers, and if ESC has any effect on impact conditions or injury outcomes in barrier crashes.

METHODOLOGY

First, vehicle models were identified that changed from having no ESC in one model year to being completely equipped with ESC in the next model year, without other significant changes. Fatal crashes involving these vehicle models were then drawn from the FARS (Fatality Analysis Reporting System) database, which is a census of all U.S. road fatalities each year. The number of fatal crashes involving guardrail was compared to the number of fatal crashes where ESC would have had little if any effect on the outcome of the crash, for vehicles with and without ESC. This provided an estimate of the effectiveness of ESC at preventing fatality in guardrail crashes which controlled for factors such as changes in exposure and improvements to vehicle safety not related to ESC.

RESULTS

For cars, ESC reduces odds of fatal crashes with roadside barriers by about 50 percent and reduces odds of fatal rollovers occurring in association with roadside barriers by about 45 percent. Both findings are statistically significant. For light trucks and vans (LTVs), ESC reduces barrier fatality odds by about 40 percent and barrier-associated rollover fatality odds by about 55 percent. The latter finding is statistically significant, and the former is very nearly significant. Based on the effectiveness levels observed in this study, it is expected that ESC could prevent about 410 out of 1180 possible barrier-related fatalities per year by 2028, when 75 percent of the fleet is estimated to be equipped with ESC.

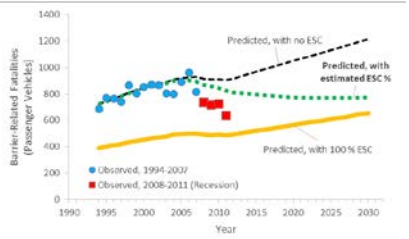

Figure 1: Predicted yearly barrier-related fatalities, with 0 % and 100 % ESC presence in the fleet.

CONCLUSIONS

For cars and LTVs, ESC reduces the odds of fatal crashes with roadside barrier, and the odds of fatal rollover involving barrier, by about half. LTVs benefit slightly more in fatal barrier-associated rollovers, and cars benefit slightly more in fatal non-rollover barrier crashes. ESC has the potential to prevent close to half of all barrier-related fatalities per year. The study findings suggest that ESC significantly reduces road departures into roadside barriers, and/or that ESC changes departure conditions so that barrier crashes have less severe outcomes.

CHARACTERIZATION OF RIB CORTICAL BONE THICKNESS CHANGES WITH AGE AND SEX

Sarah K. Lynch[1,2], Ashley A. Weaver[1,2], and Joel D. Stitzel[1,2]
1. Virginia Tech-Wake Forest University Center for Injury Biomechanics
2. Wake Forest University School of Medicine
Corresponding Author: Sarah K. Lynch, Email: Salynch@wakehealth.edu

INTRODUCTION

In motor vehicle crashes (MVCs), thoracic injuries are only surpassed by head injuries in relation to fatalities, number of serious injuries, and overall economic cost [1]. Characterization of thoracic anatomy can help mitigate thoracic injuries, especially as changes in anatomy occur based on age and sex of occupants.

METHODOLOGY

Rib cortical thickness data from 222 subjects were collected using a validated algorithm [2,3]. The algorithm calculates a reasonable cortical density that represents cortical bone from a subject's computed tomography (CT) scan. The calculated cortical density is used in the algorithm to estimate the cortical thickness at thousands of locations on a rib surface model. The cortical thickness measurements on surface point clouds for the entire rib cage were sub-sectioned for regional analysis. Average thickness measurements within the sub sections were estimated, and then regressed for each individual sub-section across ages 10-100 and separately for the sexes.

RESULTS

In total, cortical thickness measurements have been collected at 38,640 locations per sex, so that age and sex-related comparisons can be made. The regressions showed increasing cortex thickness until approximately 45 years of age for women and 55 years of age for men, then steady cortical thinning into the elderly ages (Figure 1).

CONCLUSIONS

A cortical density based thickness estimation algorithm was applied to 222 subjects. The resulting thicknesses were grouped by location and regressed with age (from 0-100) and sex. Regressions showed cortex thickening until a maximum thickness reached in the middle ages, and gradual cortex thinning into the elderly ages for both sexes.

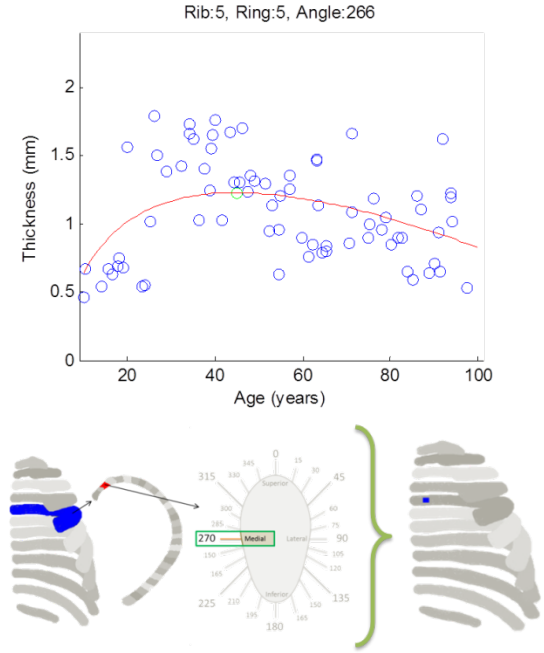

Figure 1: Sample regression plot for a single sub-section for males shows cortical thickening through the younger ages, a maximum thickness reached in the middle ages, and a steady thinning into the elderly ages.

ACKNOWLEDGMENTS

Funding: National Highway Traffic Safety Administration

REFERENCES

[1] Cavanaugh, J.M., Accidental Injury: Biomechanics and Prevention, 2002.
[2] Treece et al. Med Image Anal, 2010. 14(3): p. 276-90.
[3] Treece et al. Med Image Anal, 2012. 16(5): p. 952-65.

DEVELOPMENT AND VALIDATION OF AN ATLAS-BASED FINITE ELEMENT BRAIN MODEL

Logan E. Miller[1], Jillian E. Urban[1], Elizabeth M. Lillie[1], and Joel D. Stitzel[2]
1. Wake Forest University School of Medicine, Biomedical Engineering
2. Virginia Tech – Wake Forest Center for Injury Biomechanics
Corresponding Author: Logan Miller, Email: logmille@wakehealth.edu

INTRODUCTION

TBI is a leading cause of disability and injury-related death, accounting for nearly one third of all injury-related deaths (1). To prevent these types of injuries, the injury mechanisms need to be well characterized and understood. In the current study, a high-resolution, anatomically accurate finite element (FE) model will be developed and validated against experimental data to provide a tool to predict and prevent brain injury.

METHODOLOGY

The atlas-based brain model (ABM) was developed from the International Consortium for Brain Mapping (ICBM) brain atlas. A finite element model was created from this image set by converting voxel into an element using a custom code developed in MATLAB. The current model consists of 6 parts: brain, CSF, ventricles, falx, tentorium, and a rigid skull. The material properties used are similar to those used in the SIMon model (Table 1), excluding the brain material model, which will be optimized in the current study (2). To optimize the brain properties, five brain material parameters were varied using the Latin Hypercube Design (LHD) method to generate 100 combinations of the parameters. The ABM was subjected to the boundary conditions from three experimental cadaver tests (C755-T2, C383-T1, and C291-T1) with each of the all 100 variations of material parameters as the brain material model (3). Brain displacements at various locations throughout the model were compared to the experimental results obtained by Hardy et al. (2001) and response was quantified using CORA (CORrelation and Analysis), a method that evaluates the correlation of two curves. CORA scores were computed for each variation to identify the optimal combination of material properties.

Table 1: Material Properties

Part	LS-DYNA Material Type	Material Properties
CSF/Ventricles	Elastic fluid	ρ=1000 kg/m3, E=0 MPa, v=0.5, K=2100 MPa
Falx/Tentorium	Elastic	ρ=1130 kg/m3, E=31.5 MPa, v=0.45, K=2100 MPa
Skull	Rigid	ρ=35200 kg/m3, E=6900 MPa, v=0.3

RESULTS

Relationships between CORA score and material parameters were investigated and are shown in Figure 1.

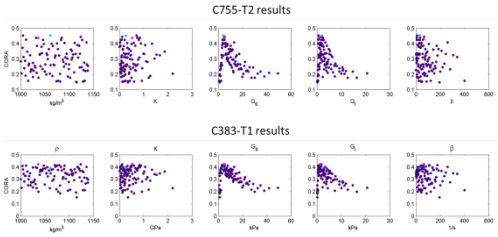

Figure 1: Relationships between CORA score and material parameters for C755-T2 and C383-T1 optimizations.

CONCLUSIONS

The material optimization process demonstrates a strong relationship between brain shear properties and model response, and is able to identify an optimal value for these parameters. Additionally, the ABM has been validated in three distinct impact configurations and shows good agreement with experimental data and competitive results when compared with existing models.

REFERENCES

1. Coronado V.G., et al., *CDC Surveill Summaries*, 2011.
2. Takhounts E.G., et al., *Stapp Car Crash Journal*, 2008.
3. Hardy W.N., et al., *Stapp Car Crash Journal*, 2001.

INVESTIGATION AND ANALYSIS OF HEART FAILURE WITH PRESERVED EJECTION FRACTION (HFPEF) WITH MAGNETIC RESONANCE

Sourav Mishra[1], Philip J Brown[1], Robert A Kraft[1], Craig A Hamilton[1], and Dalane W Kitzman[2]
1. VT-WFU School of Biomedical Engineering & Sciences
2. Department of Cardiology, Wake Forest University School of Medicine
Corresponding Author: Sourav Mishra, Email: somishra@wakehealth.edu

INTRODUCTION

Heart Failure with preserved Ejection fraction (HFpEF) is a cardiovascular condition steadily on the rise. It has higher incidence in elderly, especially female and obese. Exercise intolerance is the primary clinical symptom of HFpEF. Recent studies have suggested its determinants in peripheral vasculature & skeletal muscles [1]. Our group is proposing a Magnetic Resonance Imaging (MRI) protocol which can address this problem.

METHODOLOGY

The subjects to this protocol have to undergo a 3-minute exercise test followed by MR acquisitions. Work and power shall be measured while participants are exercising. Perfusion images will be acquired at the calf immediately thereafter with pseudo-Continuous Arterial Spin Labeling (pCASL). Fat and Water content in region of interest (ROI) shall be obtained by a newly introduced Siemens MR software. High resolution T2-weighted images will help register and segment all quantitative images to a common space. The clinical information obtained via patterns in exercise, perfusion and fat content shall be useful in understanding skeletal muscle's role in HFpEF.

RESULTS

Post exercise perfusion computed in terms of peak measures is observed to be in close correspondence with previous literature involving more direct means [2].

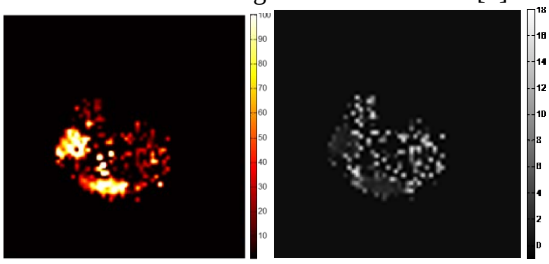

Figure 1: Computed perfusion peak & decay maps.

Fat quantification accuracy has been verified from both in-vivo and phantom studies to be linear and reproducible.

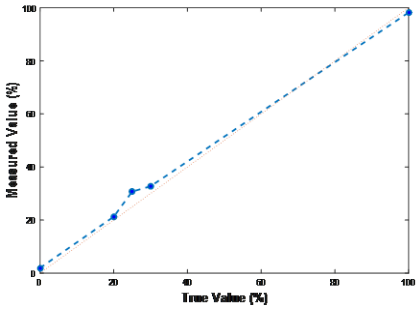

Figure 2: Linearity of fat percentage calculation.

CONCLUSIONS

These MRI methods will provide a means of non-invasively understanding skeletal muscles role in HFpEF by making several critical measurements concurrently.

ACKNOWLEDGMENTS

The study is supported by NIH grants R01AG045551-01A1 and R01HL107257-04. We are indebted to Philip Brown for ergometer fabrication and Dr. Youngkyoo Jung for the pCASL sequence.

REFERENCES

1. Haykowsky, M.J., et al., *Determinants of exercise intolerance in elderly heart failure patients with preserved ejection fraction.* Journal of the American College of Cardiology, 2011. **58**(3): p. 265-274.
2. Proctor, D.N., et al., *Leg blood flow and VO2 during peak cycle exercise in younger and older women.* Med Sci Sports Exerc, 2004. **36**(4): p. 623-31.

TRANSCRANIAL FOCUSED ULTRASOUND BEAM PROFILE SENSITIVITY FOR NEUROMODULATION

Jerel K. Mueller[1], Wynn Legon[2], and William J. Tyler[3]
1. Virginia Tech, School of Biomedical Engineering and Sciences
2. University of Minnesota, Department of Physical Medicine and Rehabilitation
3. Arizona State University, School of Biological and Health Systems Engineering
Corresponding Author: Jerel Mueller, Email: jerel.mueller@vt.edu

INTRODUCTION

While ultrasound is largely established for use in diagnostic imaging and heating therapies, its application for neuromodulation is relatively new and not well understood. The objective of the present study was to investigate issues related to interactions between focused acoustic beams and tissues to better understand the possible limitations of transcranial ultrasound for neuromodulation. Utilizing computational models, the insertion behavior of ultrasound across various tissues and geometries was explored.

METHODOLOGY

A computational model of transcranial focused ultrasound was constructed and validated against bench top experimental data. The models were then incrementally extended to address and investigate a number of issues related to the use of ultrasound for neuromodulation. These included the effect of variations in skull geometry and gyral anatomy, as well as the effect of transmission across multiple tissue and media layers, such as scalp, skull, CSF, and gray/white matter on ultrasound insertion behavior. In addition, a sensitivity analysis was run to characterize the influence of acoustic properties of intracranial tissues.

To quantify the model response to ultrasound, we characterized the ultrasound beam using half maximum intensity contours and their corresponding area moments of inertia. While the relationship between ultrasound intensity and stimulation of neural tissue is not established, the half maximum intensity contours provided a quantitative measure of the model response to estimate the influence of tissues and geometry on the region of effects by ultrasound. Finally, the heating associated with ultrasonic stimulation waveforms designed for neuromodulation was modeled.

RESULTS

Depending on factors such as acoustic frequency, the insertion behavior of a transcranially focused ultrasound beam is subtly influenced by the geometry and acoustic properties of the underlying tissues.

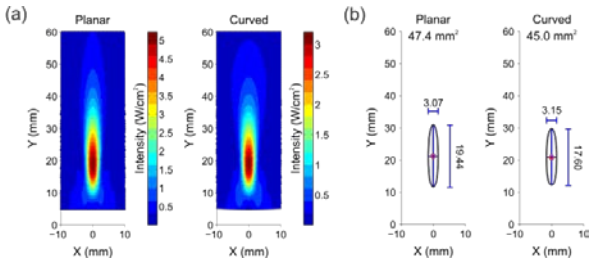

Figure 1: Comparison of intensity profiles between planar and curved skull layers. (a) Intensity contours of focused ultrasound. (b) Half maximum intensity contours.

CONCLUSIONS

As ultrasound offers the advantages of finer spatial resolution and variable depths of stimulation compared to more established noninvasive electromagnetic methods, it is an appealing alternative to electromagnetic methods for a number of possible applications. However, it is still not clear how the neuronal response couples to the exertions of ultrasound on tissue. Using a computational model to systematically investigate parameters of interest, we found that the profiles of intensity produced by focused ultrasound is relatively insensitive to the geometry of intracranial tissue, that the material properties of the intracranial tissue can influence the intensity profile more substantially, and that the skull is a major source of influence on the ultrasound beam profile. An understanding of both the insertion behavior of ultrasound across the skull and the coupled neuronal response is key to the continued advancement of ultrasound stimulation methods.

AN INTERFACE FOR ANALYSIS OF MEDICAL LINEAR ACCELERATOR PERFORMANCE PARAMETERS USING PROCESS BEHAVIOR CHARTS

Callistus M. Nguyen[1,2], Charles M. Able[2], Alan H. Baydush[2], Scott Isom[2], and Michael T. Munley[1,2]
1. Virginia Tech – Wake Forest School of Biomedical Engineering and Sciences, Biomedical Engineering
2. Wake Forest School of Medicine, Radiation Oncology
Corresponding Author: Callistus M. Nguyen, Email: canguyen@wakehealth.edu

INTRODUCTION

The purpose of this work was to develop an effective process for detecting unexpected deviations in the medical linear accelerator system operating parameters and/or performance that predicts component failure or system dysfunction.

METHODOLOGY

Seven linear accelerators were monitored by delivering daily robust quality assurance (QA) treatments. Each QA treatment generated trajectory and text log files that were used to monitor various operational components and subsystem performance. Statistical process control (SPC) is an analytical measure of normal and abnormal variation of a process. Its success rests upon the fact that any process can be mapped by a series of inputs and outputs. Thus, a modified SPC analysis of the log files was used to evaluate the performance of medical linear accelerators. A total of 525 performance parameters were monitored using process behavior charts (PBCs), specifically individual and moving range (I/MR) charts. A graphical user interface (GUI) developed in MATLAB then presented the results in a graphical display allowing the user to easily analyze and interpret the operation of the components.

RESULTS

The Predictive Maintenance Dashboard (PMD) has shown its effectiveness as a user friendly interface displaying the modified SPC analysis of system functions (Figure 1). The dashboard is modeled after traditional SPC charts that include the PBCs, a horizontal frequency distribution of data samples and a statistical summary of PBC parameters The PMD offers other features that allow for rapid assessment of performance parameters. These features range from the status lights next to each parameter pushbutton to coded colors to alert the user of system dysfunction. All of these features enhance the SPC analytics; thus, the PMD transforms the SPC model into a powerful and investigative tool in predicting component failure.

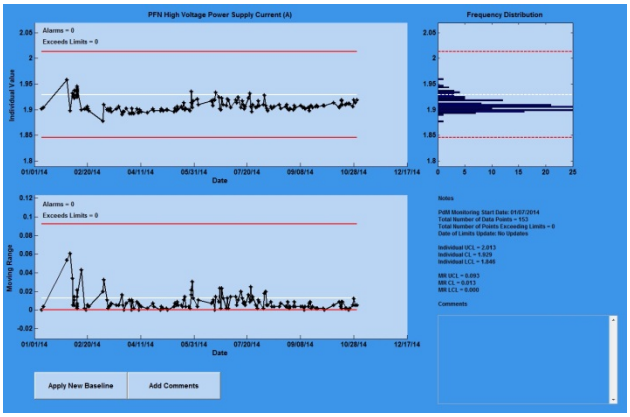

Figure 1: The PMD displaying the status of the categories and I/MR charts of a specific component of a linear accelerator.

CONCLUSIONS

The PMD has shown its effectiveness as a user friendly interface displaying the SPC analysis of medical linear accelerator functions. The interface contains features that build an integral system for assessing degradation in performance. Modified SPC analytics has also shown promise in identifying early detection of performance degradation in medical linear accelerators. The PMD is a powerful predictive maintenance tool and extensive analysis over time will better determine its overall utility.

ACKNOWLEDGMENTS

This project is being funded by Varian Medical Systems, Inc. (Palo Alto, CA).

THE DEVELOPMENT OF A THIN-FILMED, NON-INVASIVE TISSUE PERFUSION SENSOR TO QUANTIFY PRESSURE ISCHEMIA OF EXPLANTED ORGANS

Timothy J. O'Brien[1], Ali Roghanizad[1], Dr. Thomas E. Diller[1], and Dr. John L. Robertson[1,2]
1. Virginia Tech Mechanical Engineering
2. Virginia Tech – Wake Forest School of Biomedical Engineering and Sciences
Corresponding Author: Timothy J. O'Brien, Email: tjobrien@vt.edu

INTRODUCTION

According to the Organ Procurement and Transplant Network (OPTN), there are approximately 123,298 people in need of a life-saving organ transplant. Every 10 minutes, another name is added to that wait list. Unfortunately, approximately 21 people die each day while waiting. While the demand for organs increases every year, the consistent shortage in supply is disconcerting. The development of machine perfusion organ preservation systems (hypothermic machine perfusion and normothermic machine perfusion) has affected the future of organ preservation, yet many of these systems are still overlooking one key feature, pressure ischemia. Pressure ischemia is simply the restriction of blood flow to tissue due to some applied pressure. The study of pressure ischemia becomes critical to the transport of explanted organs when considering the manner of which said organ is resting throughout the transition.

In the work reported here, a novel, non-invasive, thin-filmed sensor (CHFT+) was designed for measuring tissue perfusion on the underside of an explanted organ. Smart Perfusion's Vasowave™ (VW) was utilized as the platform to support organ viability and collect vital data of explanted organs. The goal of this effort was to illustrate the need for future organ preservation systems to consider the effects of pressure ischemia during preservation.

METHODOLOGY

The CHFT+ sensor is applied to the tissue and given approximately 10 seconds to acquire steady-state values. Then a thermal event is initiated and a steady rise in temperature is applied to the back side of the CHFT+ sensor for approximately 60 seconds. The resulting temperature and heat flux signals are collected and applied to a mathematical model based off the Penne's Bioheat Equation. The measured temperature and heat flux values are sent through a parameter estimation routine to calculate the perfusion, core temperature, and contact resistance.

RESULTS

This work illustrated the manufacture of a novel perfusion sensing technology and exploited its unique qualities to measure and evaluate the perfusion of an explanted porcine kidney from its underside for the first time. Figure 1 illustrates a CHFT+ sensor and both the topside and underside perfusion measurements of an explanted porcine kidney.

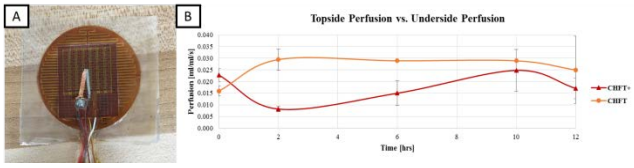

Figure 1: (A) CHFT+ sensor **(B)** Top-side and underside perfusion of an explanted porcine kidney over a 12 hour

CONCLUSIONS

The performance of the CHFT+ sensor was effectively shown in a controlled phantom tissue setting, where the sensor displayed good repeatability and sensitivity. Preliminary results from a live tissue test indicate that the perfusion on the underside of an explanted organ could be hindered by the occurrence of pressure ischemia. The implication that underside perfusion of an explanted organ is lesser than that of the topside is substantial and could effectively change the way the organ preservation technologies are designed.

ACKNOWLEDGMENTS

Smart Perfusion, LLC.

DETECTION OF LIVER ORGANOID BIOMARKERS BY SERS-IMMUNOLABELED GOLD NANOPARTICLES

William M. Payne[1], Aaron M. Mohs[1,2], Adam R. Hall[1], Sneha S. Kelkar[3], Anthony Atala[3]
1. Virginia Tech-Wake Forest School of Biomedical Engineering and Sciences
2. University of Nebraska Medical Center, Pharmaceutical Sciences
3. Wake Forest Institute for Regenerative Medicine
Corresponding Author: William Payne, Email: wpayne@wakehealth.edu

INTRODUCTION

Lab-on-a-chip technology has the potential to rapidly change the way experiments are conducted in a variety of fields ranging from medicine to environmental science. Specifically, sensors, detectors, and monitoring devices are increasingly being miniaturised to perform many experiments or measurements on a single chip. In this research, we develop an immunolabeled gold nanoparticle complex capable of detecting liver organoid biomarkers intended for use in a microfluidic device. Human Serum Albumin (HSA) and α-Glutathione S-Transferase (α-GST) are liver biomarkers that indicate liver health and damage respectively. Herein we demonstrate detection of the liver organoid biomarkers at nanomolar concentrations.

METHODOLOGY

Gold nanoparticles (40 nm) were labelled with the Raman reporter 5,5′-Dithiobis(succinimidyl-2-nitrobenzoate) (DSNB) and antibody for either HSA or α-GST. DSNB was synthesized by the procedure presented by Grubisha, et al. DSNB was conjugated to the gold nanoparticles via disulfide reduction, and antibody was then added to the gold nanoparticle-DSNB complex by click chemistry. Detection of analytes in solution was performed by surface-enhanced Raman spectroscopy (SERS).

RESULTS

Synthesis of DSNB was confirmed by Thin Layer Chromatography (TLC) and Raman spectroscopy. Antibody conjugation was confirmed by fluorescence spectroscopy. Detection of organoid biomarkers was shown by SERS. The addition of the analyte increases SERS signal obtained from the nanoparticles, providing the basis for quantitative detection of biomarkers in solution.

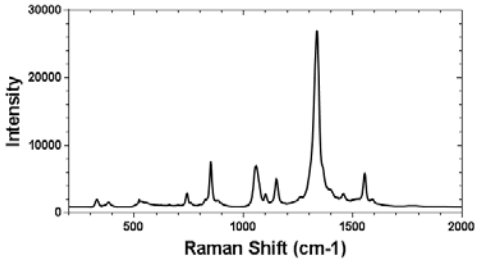

Figure 1: Raman Spectrum of DSNB.

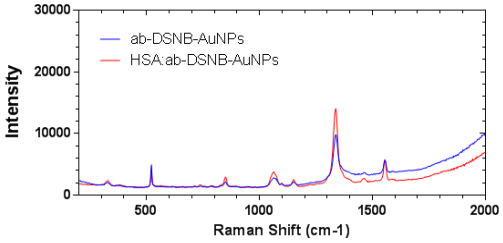

Figure 2: Detection of HSA by SERS-nanoparticles.

CONCLUSIONS

A novel immunolabeled gold nanoparticle was produced to detect liver organoid biomarkers in solution. This research is the first example of solution-based use of SERS nanoparticles for detection of biomarkers and the first detection of liver organoid biomarkers by SERS immunoassay.

ACKNOWLEDGMENTS

The authors acknowledge funding from VT- WFU SBES and WF Institute for Regenerative Medicine.

REFERENCES

Grubisha, et al. *Analytical Chemistry* 2003 *75* (21), 5936-5943

DEVELOPMENT OF A COMPUTATIONALLY EFFICIENT FULL HUMAN BODY FINITE ELEMENT MODEL

Doron Schwartz[1,2], Berkan Guleyupoglu[1,2], Joel D. Stitzel[1,2], and F. Scott Gayzik[1,2]
1. Wake Forest School of Medicine
2. Virginia Tech – Wake Forest University Center for Injury Biomechanics
Corresponding Author: Doron Schwartz, Email: dschwart@wakehealth.edu

INTRODUCTION

Computer simulations using Finite Element Analysis (FEA) are becoming a more prominent tool in the study of motor vehicle crash safety. The current GHBMC detailed 50th percentile occupant (M50-O) is an anatomically detailed finite element model with 1.3 million nodes and 2.2 million elements [1, 2]. While this complexity provides the ability to investigate the biomechanics of specific injuries, it results in a computationally expensive model. Therefore, the goal of this study is to develop a simplified and computationally efficient human body finite element model.

METHODOLOGY

The simplified occupant model (M50-OS) was developed using the same source geometry as the M50-O. While some meshed components were preserved, the total element count was reduced by re-meshing, homogenizing, or in some cases omitting structures that are explicitly contained in the M50-O, shown in Figure 1.

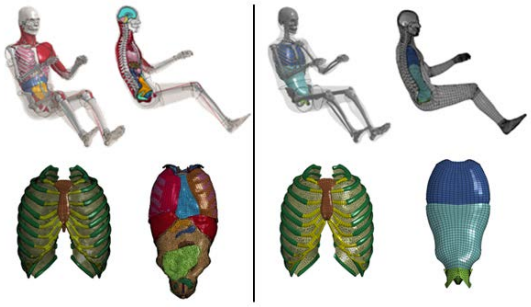

Figure 1: Visual comparison of the M50-O (left) and M50-OS (right).

RESULTS

The M50-OS model has 11 contacts and 354 thousand elements, by contrast the M50-O model has 447 contacts and 2.2 million elements. The model can be repositioned without requiring simulation. In total 13 validation and robustness simulations were completed. This included denuded rib compression at 7 discrete sites [3], five rigid body impacts, and one sled simulation. The frontal rigid chest impact simulation produced a peak force and deflection within the corridor of 4.63 kN and 31.2% respectively [4]. Two rigid tests showed similar results and run times with peak forces of 4.4 kN, 7.7 kN for the abdominal bar impact [5] and lateral sled impact [6]. The lateral plate impact at 12 m/s exhibited two peaks of roughly 20 kN but a more biofidelic response immediately afterward, plateauing at 9 kN at 12 ms [7]. Results from a frontal sled simulation showed that reaction forces and kinematic trends matched experimental results well [8]. Use of the detailed model brain within the simplified model demonstrated a paradigm for using the M50-OS to leverage aspects of the M50-O. The rigid impacts demonstrated a runtime reduction of 35 times on average, the sled impact was reduced by 23 times and the M50-OS with the deformable skull and brain exhibited a runtime 4.75 faster.

CONCLUSIONS

A simplified model with the same body habitus as the GHBMC 50th percentile seated occupant model was developed for computational efficiency and ease of positioning. The results demonstrate that the model compares favorably with the detailed model and cadaveric studies while substantially reducing computational cost.

REFERENCES

[1] Gayzik, FS, Ann Biomed Eng, 39(10):2568-83, 2011.
[2] Vavalle, N, Ann Biomed Eng, 41(3): 497-512, 2013.
[3] Kindig, M, Comp Biomech and Biomed, 1-15, 2013.
[4] Kroell, C, SAE Tech Paper, No. 741187, 1974.
[5] Hardy, W, Stapp Car Crash, 45:1-32, 2001.
[6] Cavanaugh, J, SAE Tech Paper, No. 902305, 1990.
[7] Kemper, A, Stapp Car Crash, 52:379-420, 2008.
[8] Shaw, G, Stapp Car Crash, 53:1-48, 2009.

14th Annual Graduate Student Research Symposium, May 13, 2015

COMPUTATIONAL DESIGN OF CARBON NANOTUBE REINFORCED POLYMERIC NANOCOMPOSITES

Priyal H. Shah[1], and Romesh C. Batra[1]
1. Department of Biomedical Engineering and Mechanics, Virginia Tech
Corresponding Author: Priyal H. Shah, Email: spriyal@vt.edu

INTRODUCTION

Single wall carbon nanotubes (SWCNTs) due to their high specific properties are suitable for designing nanocomposites with polymeric matrices, which can be candidate materials for applications requiring high specific strength. However, their full potential as reinforcements in a composite is limited due to their poor interfacial binding with the surrounding matrix. The covalent functionalization of SWCNTs is an effective technique to enhance this binding (Liu, P., 2005. Eur. Polym. J., 41). However, introduction of covalent bonds to the carbon atoms of SWCNTs may damage their pristine structures and degrade their mechanical properties. Thus our objective is to find covalent functional groups that are most effective in enhancing the binding of the SWCNT with a given matrix while causing least damage to its properties. We hypothesize that these groups will maximize the effective elastic properties of functionalized SWCNT reinforced nanocomposites. We will validate this hypothesis by testing these nanocomposites to derive their elastic properties.

METHODOLOGY

We consider four groups of different polarities, namely, hydrogen, amine, hydroxyl, and carboxyl as model functional groups and using molecular mechanics and dynamics simulations determine their effects on (i) elastic moduli of the SWCNT and (ii) interfacial binding energy (IBE) of the SWCNT with high density polyethylene (HDPE) which is considered as a sample matrix material. We first deform SWCNTs in pure tension and simple shear and from curves of the strain energy of deformation versus the applied strain, deduce the values of their elastic moduli. Next, we study interaction between the SWCNTs and the HDPE in the composite and compute the IBE from the potential energy of the composite, E_{comp} and those of the SWCNT, E_{SWCNT} and the matrix, E_{HDPE} in their isolated states as: IBE = E_{comp}-(E_{SWCNT}+E_{HDPE}).

RESULTS

It is found that functionalization reduces Young's moduli (E) and shear moduli (G) of the SWCNT, the reduction increases with an increase in the amount of functionalization and is independent of the type of functionalizing agent. With 20% of carbon atoms functionalized, E and G of the SWCNT are found to decrease by about 34% and 43%, respectively. Next, it is observed that (Fig. 1) the IBE increases with an increase in the amount of functionalization and depends inversely on the polarity of the functional group. Hydrogen and carboxyl are found to be the most and the least significant in enhancing the IBE. Around 220% increase in the IBE is obtained when 20% carbon atoms of the SWCNT are functionalized with hydrogen.

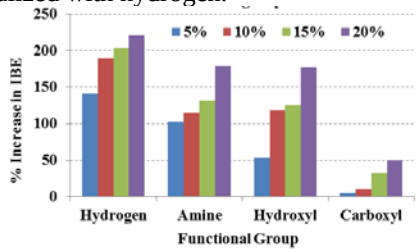

Figure 1: Effect of functionalization on IBE.

CONCLUSIONS

The reduction in elastic moduli is found to be independent of type of the functional group. Hydrogen is found to maximize the IBE of the SWCNT/HDPE interface and hence it is hypothesized to maximize the effective properties of the SWCNT/HDPE nanocomposites.

ACKNOWLEDGMENTS

The work is partially supported by the Army Research Laboratory.

ALIGNED AND SUSPENDED NANOFIBER NETWORKS FOR STUDYING WOUND CLOSURE DYNAMICS

Puja Sharma[1], Colin Ng[2], Paige Szymanski[3], Bahareh Behkam[2, 1], Amrinder S Nain[2, 1]
1. School of Biomedical Engineering and Sciences, Virginia Tech, Blacksburg, VA
2. Mechanical Engineering Department, Virginia Tech, Blacksburg, VA
3. Department of Bioengineering, University of Illinois at Urbana-Champaign, Urbana, IL
Corresponding Author: Puja Sharma, Email: pujas@vt.edu

INTRODUCTION

Collective cell migration as suspended sheets is physiologically relevant to conditions involving poorly developed or absent extracellular matrix (ECM) including burn wounds and colonization of tissue engineered scaffolds[1]. However, traditional would healing assays are unable to capture collective cell migration in suspended sheets. We present a novel wound closure model with cell monolayers on raised platforms bridged by suspended and aligned nanofibers having diameters comparable to collagen fibers. Cells move outwards and formed suspended sheets. Merging of these sheets formed gaps with closures depending upon fiber topography, spacing, shape and size of gaps. The results obtained from the study can be instrumental in design of wound closure scaffolds and also in studying collective cell migration observed in metastasis.

METHODOLOGY

NIH 3T3s were cultured on raised plastic cover slips bridged with suspended and aligned polystyrene (PS). STEP technique[2] was used to manufacture the fibers. Time lapse images of the cells were taken in a microscope with incubating capacity. AxioVision and ImageJ were used to analyze the data.

RESULTS

Fibroblasts sensed the aligned fibers and started migrating away from the monolayer, thus bridging the gap between the two monolayers (Fig. 1 A-E). Tightly packed cell streams bundled fibers forming suspended cell sheets (SCS) of different sizes (Fig. 1F (i-ii), shown by dotted rectangle). Interestingly, we found the migration of SCS to be oscillatory with migration rates inversely related to cell stream separation. SCS migration was severely compromised when cell stream separation exceeded 375µm. Eventually, cell streams from two directions of

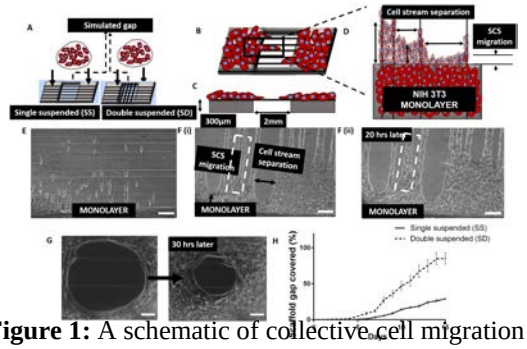

Figure 1: A schematic of collective cell migration on suspended nanofibers (A-D) accompanied by time lapse images (E-F). Time lapse images of local gap closure (G), and closure% of simulated gap for parallel (SS) and crosshatch (SD) fibers (H). Scale bars are 100µm for E-F and 50µm for G.

the monolayer merged to form gaps, whose closure was dependent on the size and shape (Fig. 1G). In particular, local gaps <85,000µm^2 closed regardless of shape, 85-140,000µm^2 closure was dependent on its shape, and >140,000µm^2 were unable to close. We then investigated the role of fiber network configuration (parallel vs. crosshatch) on gap closure and found crosshatch networks to significantly enhance closure dynamics compared to parallel (Fig.1H).

CONCLUSIONS

Collective cell migration on aligned and suspended fiber networks is different from that on flat substrates. For the first time, we have demonstrated that gap closure is influenced by fiber topography, cell stream separation, shape and size.

REFERENCES

1. Vedula, SR., *Physiology (Bethesda).* **28,** 370–9 (2013).
2. Nain, A. S. *et al. Small* **4,** 1153–9 (2008).

ENHANCED IMMUNOMAGNETIC SEPARATION BY EMBEDDED FERROMAGNETIC PATTERN

Chen Sun[1], Chang Lu[1]
1. School of Biomedical Engineering and Sciences, Virginia Tech
Corresponding Author: Chen Sun, Email: chensun@vt.edu

INTRODUCTION

Identification, isolation and enrichment of specific cells from complex biological samples have been of growing interest in cellular studies, disease and medicine researches. Immunomagnetic separation (IMS) is the use of antibody functionalized magnetic beads to bind specific proteins on target cells and separate cells by external magnetic field. Microfluidic chip based IMS combines the benefits of microfluidics and immunomagnetic cell sorting, so that it is a potentially optimized method for small sample cell isolation. However, low magnetic force generated by limited external magnetic field gradient has always been a big obstacle for enhancement of current cell sorters.
Here, we proposed a simple microfluidic device containing ferromagnetic structure for cell capture based on IMS. Embedding a pattern of magnetic material on the bottom of a microfluidic channel would concentrate field lines from an external magnetic field source, and thus improve local magnetic field inside the channel. We tested the ability of our microfluidic channels in capturing magnetic beads coated RAW 264.7 cells, and found that ferromagnetic embedded channel showed up to over 4 times higher capture rate compared to no patterned channel. Mathematical models were built to simulate the magnetic field distribution inside channels, which matched the experimental data very well.

METHODOLOGY

A reversible bonded microfluidic channel was first fabricated by soft lithography without plasma treatment. The magnetic pattern was formed by flowing ferrofluid into this mold followed by baking. RAW 264.7 cells were coated with magnetic beads by antibody-antigen recognition, and flowed into microfluidic channel with syringe pump. A magnetic block was placed above the channel to provide an external magnetic field source.

RESULTS

Cell capture in microfluidic channel containing magnetic pattern was studied as a function of flow rate and compared with the one without the pattern. Both channels had the same dimension, and in same external electric fields. As shown in Figure 1, fewer cells were captured as the flow velocity increased in both channels, and the cell capture rates in magnetic pattern coated channel were higher than those in "bare" channel at all investigated flow velocities. We also noticed that as the cell flow velocity increased, the capture rate decreased slowly in the channel with magnetic patter, while the ability of trapping cell in channel without pattern reduced rapidly. Finally, the cell capture rate reached to a plateau at around 12-14% when the flow velocity faster than 10mm/s in the "bare" channel and 24-26% in magnetic patterned channel.

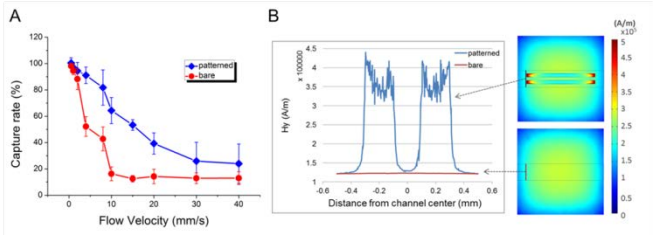

Figure 1: (A) Cell capture rate as a function of flow rate in ferromagnetic patterned channel (blue diamonds) and the one without the pattern (red circles). (B) Magnetic field intensity in channels modeled by COMSOL.

CONCLUSIONS

We have developed a novel ferromagnetic patterned microfluidic channel for immunomagnetic separation. Magnetic field in the microfluidic channel was largely increased by the micromagnetic structure, resulting in an enhanced target cell capture.

14th Annual Graduate Student Research Symposium, May 13, 2015

OPTIMAL PARAMETER ANALYSIS FOR THERMAL SPRAY PROCESS

Unchalissa Taetragool[1], Romesh C. Batra[1]
1. Department of Biomedical Engineering and Mechanics, Virginia Tech
Corresponding Author: Unchalissa Taetragool, Email: tunchali@vt.edu

INTRODUCTION

The mean particle temperature and velocity are in-flight particle behaviors that can affect the coating properties in the thermal plasma spray process, which are normally controlled by the operating process parameters. In this work, argon and hydrogen flow rates, powder feed rate, and current are considered. The objective of this work is to determine the correct values of the operating input parameters in order to reach desirable output behaviors values. The design of experiments is applied to the framework. First, the factorial experiments are performed to identify the factors that are significant to the mean particle temperature and velocity. Then, the relationships between significant factors and responses are determined by the regression model and the response surface methodology and used as the objective functions in the optimization algorithm. Finally, a set of optimal values of the operating factors is given from the best-so-far artificial bee colony optimization algorithm.

METHODOLOGY

The model begins with a screening process using the factorial experiments. Factors are determined whether they have an effect on the outputs of interest. All effects of interactions between factors are also investigated. A relationships between the significant effects and the responses are then determined. In this work, the quadratic least square regression method and the response surface methodology are used to model the quadratic functions for the mean particle temperature and velocity. The results from the two methods are compared. After that, the mathematical functions of the responses are applied to the best-so-far Artificial Bee Colony optimization algorithm as objective functions. The optimization algorithm lastly find an optimal solution, which is a set of values of all four factors, for the desirable responses.

RESULTS

The main effects of the input parameters as well as the effects of the interactions between each parameter were investigated by the factorial experiments. Results showed that that all four factors and their interactions have significant effects on the mean particle temperature and velocity. The quadratic models of the mean particle temperature and velocity from the quadratic least square regression method and the response surface methodology were given and used as the objective functions in the optimization algorithm. The best-so-far artificial bee colony optimization algorithm finally delivered the sets of values of the four input parameters that can reach the desirable mean particle temperature and velocity. The results from different objective functions, which were obtained from the quadratic least square regression method and the response surface methodology, agree that the ranges of hydrogen flow rate and the powder feed rate can be varied. However, the range of the argon flow rates should be in between 46.58 – 48.70 slm while the currents can be range from 478 – 600 A.

CONCLUSIONS

This work presented the optimal parameter analysis for a thermal spray process. The set of values of the input parameters was suggested in order to reach the desirable responses are the mean particle temperature and particle velocity. Argon flow rate, hydrogen flow rate, current, and powder feed rate were four input parameters studied in this research. We also validated the sets of input parameters from the optimization algorithm by simulating them in the LAVA-P-3D software. The average percentage errors from the simulated results were less than 9%. We believe that our framework can be applied to a thermal spray process and can suggest a set of input variables for the desirable responses.

SPARSE FIBER-COLLAGEN COMPOSITES FOR LIGAMENT TISSUE ENGINEERING

Patrick Thayer[1], Emily Tong[2], Linda Dahlgren[3], and Aaron Goldstein[1, 2]
1. School of Biomedical Engineering and Sciences
2. Department of Chemical Engineering
3. Department of Large Animal Clinical Sciences, Virginia-Maryland Regional College of Veterinary Medicine
Corresponding Author: Patrick Thayer, Email: pthayer3@vt.edu

INTRODUCTION

Ligament ruptures are common in sports such as football, afflicting thousands of Americans annually, and often requiring surgical replacement with autologous or allogeneic grafts. However, healing of the reconstructed tissue can be slow and the subsequent biomechanics remain impaired, leading to eventual joint degeneration and osteoarthritis. Tissue engineering holds promise in overcoming these limitations through the fabrication of scaffold materials that can support cell proliferation, infiltration, and differentiation into an organized tissue.
A scaffold that supports ligament healing must possess several properties including supporting the deposition of an anisotropic extracellular matrix, be mechanically robust under repeated loading, and support the organization and differentiation of mesenchymal stem cells. For these reasons, aligned electrospun fibers were utilized due to their micro-scale size and the ability to present diverse stimuli (topographical, mechanical, chemical, biological) to the cells. Furthermore, these electrospun fibers were included sparsely within collagen gels, permitting cells to freely remodel their environment without interference from the fiber component.

METHODOLOGY

Sparse fiber-hydrogel composites were fabricated through the incorporation of electrospun fibers of varying elastic moduli within a collagen gel and cultured for up to 14 days.

RESULTS

Aligned fiber networks with elastic moduli ranging from 5.6 to 31 MPa were incorporated in collagen gels and cultured for up to 14 days. In contrast to the relative unorganized cells found within a fiber-less collagen gel, cells within the composites exhibited alignment to the underlying fiber network (whether proximal or distant) and greater elongation after just 2 days of culture. Expression of early ligament markers scleraxis and late fibroblastic marker tenomodulin, along with a marker of a regenerative phenotype, α-SMA, was increased on the 5.6 MPa fibers, while on the 31 MPa fibers, collagen I expression was increased. Confocal imaging revealed on the 5.6 MPa fiber meshes, the presence of a dense monolayer of oriented spindle shaped cells on the fibers, with oriented cells throughout the collagen bulk (Figure 1). In contrast, in composites composed of 31 MPa fibers, the cells were either localized to the fibers or on the collagen gel surface with minimal cells in the bulk.

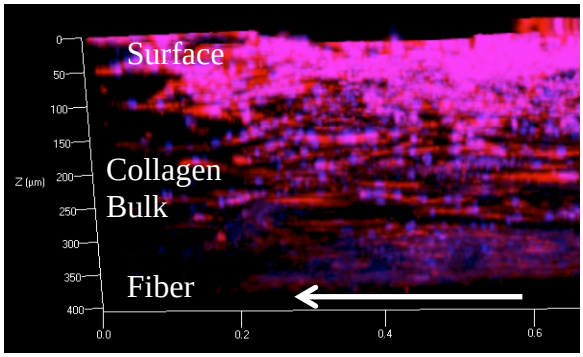

Figure 1: Reconstruction of cells distributed through the composites. Cells found in a monolayer on the surface, dispersed in the bulk, and confluent the fibers. Arrow: Fiber orientation.

CONCLUSIONS

Included cells were sensitive to the mechanical properties of the underlying fiber network. While these studies focused on the generation of composites for a ligament graft, this sparse-fiber/hydrogel platform can be applied toward diverse tissue targets such as nerve, bone, muscle, and cartilage.

Virginia Tech
Wake Forest University
School of Biomedical Engineering and Sciences
14th Annual Graduate Student Research Symposium, May 13, 2015

EVALUATION OF VEHICLE-BASED CRASH SEVERITY METRICS

Ada H. Tsoi[1] and H. Clay Gabler[1]
1. School of Biomedical Engineering and Sciences, Virginia Tech, Blacksburg, VA
Corresponding Author: Ada Tsoi, Email: atsoi@vt.edu

INTRODUCTION

Vehicle change in velocity (ΔV) is a widely used crash severity metric for estimation of occupant injury risk.[1] Despite its widespread use, ΔV is a vehicle-based metric which does not consider the crash pulse or the performance of occupant restraints. Such criticisms have prompted the search for alternative metrics. The purpose of this study was to assess the ability of the occupant impact velocity (OIV), acceleration severity index (ASI), vehicle pulse index (VPI), and maximum ΔV to predict serious injury in real world crashes.

METHODOLOGY

The study was based on data downloaded from 2000-2013 National Automotive Sampling System - Crashworthiness Data System (NASS-CDS) event data recorders (EDRs). NASS-CDS is an annually tabulated, probability sample of nationally representative crashes from which crash investigators collect data. Vehicles in our study were required to be GM vehicles involved in a frontal collision, excluding those that involved rollover. Cases were restricted to single-event crashes that caused an airbag deployment. All EDR data were checked for a successful, completed recording of the event and that the crash pulse was complete, before extracting the vehicle longitudinal velocity. The maximum abbreviated injury scale was used to describe occupant injury outcome and occupants were categorized into non-serious and serious injury outcomes. ASI and OIV were calculated according to MASH.[2] VPI was calculated according to ISO/TR 12353-3[3], with vehicle-specific parameters derived from New Car Assessment Program crash tests with Structural Impact Simulation and Model Extraction (SISAME; Washington, D.C.). Using binary logistic regression, the cumulative probability of injury risk was determined for each metric and assessed for statistical significance, goodness-of-fit, and prediction accuracy.

RESULTS

The real world dataset included 303 vehicles. A Wald chi-square test showed each vehicle-based crash severity metric estimate to be a significant predictor in the model ($p<0.0001$). Among the belted drivers, the goodness-of-fit statistics (Hosmer-Lemeshow, Nagelkerke maximized R^2, Akaike information criterion, area under receiver operator curve) showed that ASI was the best predictor, followed by VPI, OIV, and ΔV. Among the unbelted drivers, there was no clear hierarchy of metrics.

CONCLUSIONS

VPI outperformed the traditional vehicle-based crash severity metric, ΔV, in distinguishing severe injuries among belted occupants. The findings of this study suggest that regulatory agencies should consider crash severity metrics other than just ΔV in their in-depth crash databases, e.g. NASS-CDS. Beyond just a greater ability to discriminate severe injuries, improved crash severity metrics could be used in advanced automatic crash notification, i.e. OnStar, to offer a more cost effective and timely method of triaging occupants. Moreover, this study has established vehicle-specific parameters for VPI and shown the potential of EDR data to replace traditional strategies used in the automotive safety community.

REFERENCES

1. Kononen DW, et al. *Accid Anal Prev.* 2011; 43(1): 112-122.
2. Manual for Assessing Safety Hardware. Washington, DC: AASHTO; 2009.
3. Road vehicles - Traffic accident analysis - Part 3: Guidelines for the Interpretation of Recorded Crash Pulse Data to Determine Impact Severity. ISO; 2013. ISO/TR 12353-3.

VOLUMETRIC ANALYSIS OF MOTOR VEHICLE CRASH-RELATED HEAD INJURIES FROM REAL-WORLD HEAD IMPACT DATA

Jillian E. Urban[1], Ervin L. Lowther, M.D.[2]; Christopher T. Whitlow[2,3], Joel D. Stitzel[1]
1. Center for Injury Biomechanics (Wake Forest University, SBES)
2. Wake Forest School of Medicine (Wake Forest University, Radiology, Neuroradiology)
3. Translational Science Institute (Wake Forest University)
Corresponding Author: Jillian Urban, Email: jurban@wakehealth.edu

INTRODUCTION

Traumatic intracranial injuries are acceleration-based injuries, often resulting from direct contact or loading to the head in combination with rotational forces.[1-4] An important research question is the relative importance of linear and rotational accelerations, and skull deformation for particular intracranial injuries. In this study, we evaluate the volume of each component of intracranial hemorrhage, as well as the total volume of intracranial hemorrhage that results from MVCs and how these volumes relate to crash and occupant parameters including contact location and contact surface stiffness.

METHODOLOGY

Head computed tomography (CT) demonstrating subarachnoid hemorrhage (SAH), subdural hematoma (SDH), epidural hematoma (EDH,), cerebral contusion or intraparenchymal hemorrhage (IPH/C), intraventricular hemorrhage (IVH), and diffuse axonal injury (DAI) were selected from the Crash Injury Research and Engineering Network (CIREN) database. Detailed data regarding the occupant, injury, vehicle, and crash were collected. Semi-automated methods were used to quantify volume of injury and approximate head contact location identified from a soft tissue scalp contusion. Linear regression was performed between injury characteristics, as well as crash and occupant parameters. A non-parametric Wilcoxon test of multiple comparisons was performed to assess differences in injury volume by contact stiffness type.

RESULTS

There were 164 cases identified from occupants in the CIREN database. The injuries evaluated include SAH (n=85), SDH (n=77), EDH (n=10), cerebral contusion or IPH (n=64), IVH (n=35), and DAI (n=13).

Table 1: P-values and r^2 values of the linear regression.

Log (Inj.Vol)	Crash Type	Variable	Dir.	P-value	r^2
SDH	Far-Side	Delta-V	(+)	0.0473*	0.4707
SDH	Far-Side	Cmax	(+)	0.0494*	0.3641
SDH	All Crash Types	Delta-V	(+)	0.0408*	0.0668
IPH/C	Frontal	Delta-V	(+)	0.0330*	0.2285
IVH	Far-Side	Cmax	(-)	0.0202*	0.6925
IVH	Frontal	Delta-V	(+)	0.0193*	0.4365
IVH	Frontal	Cmax	(+)	0.0454*	0.3163

SAH volume resulting from "hard" contacts was significantly greater than those from "compliant" contacts (p=0.0361).

CONCLUSIONS

SAH was most significantly correlated with impact surface, while SDH, IPH/C and IVH were most significantly correlated with crash severity metrics. Injury-specific volume distributions were observed with and without skull fracture by contact type.

ACKNOWLEDGMENTS

The authors would like to thank NHTSA for funding.

REFERENCES

[1] Nirula et al, Accid Anal Prev, 2003. [2] Nuscholtz et al, STAPP, 1984. [3] Ommaya, J Neurosurg, 1971. [4] Yoganandan et al, Accid Anal Prev, 2010.

THE APPLICATION OF RADIAL BASIS FUNCTION INTERPOLATION METHODS IN THE DEVELOPMENT OF A 95TH PERCENTILE MALE SEATED FEA MODEL

Nicholas A. Vavalle[1,2], Samantha L. Schoell[1,2], Ashley A. Weaver[1,2], Joel D. Stitzel[1,2], and F. Scott Gayzik[1,2]
1. Wake Forest School of Medicine, 575 N Patterson Ave., Winston-Salem, NC 27101
2. Virginia Tech – Wake Forest University Center for Injury Biomechanics
Corresponding Author: Nicholas A. Vavalle, Email: nvavalle@wakehealth.edu

INTRODUCTION

Human body finite element models are a valuable tool in the study of injury biomechanics. However, the traditional model development process can be time consuming, requiring image segmentation, meshing, and other modeling considerations. Scaling and morphing existing models provides an alternative for generating morphologically distinct models. The objective of this work was to use radial basis function interpolation to morph the Global Human Body Models Consortium (GHBMC) average male model (M50) to the body habitus of a 95th percentile male (M95).

METHODOLOGY

The GHBMC M50 model was created using imaging data from a living subject representing a 50th percentile male. A similar dataset was collected from a living 95th percentile male (height 189.5 cm, weight 102.5 kg, age 26 years), consisting of MRI, upright MRI, CT, an external anthropometry. This data was used in the morphing process. Homologous landmarks on the reference (M50) and target (M95) geometries, in conjunction with the FE node locations of the M50 model, were used as inputs to the morphing algorithm. To create the homologous landmarks, imaging data of the 50th percentile male was registered to the 95th percentile male set using symmetric diffeomorphic registration. Radial basis function interpolation was applied with a thin-plate spline as the basis function and a relaxation algorithm. The mesh is morphed without reducing element quality by smoothly interpolating points between the landmarks. Simulations of the M95 in seven loading scenarios are presented ranging from hub-type impacts to full sled tests.

RESULTS

The model represented a mass of 103.3 kg and contained 2.2 million elements with 1.3 million nodes. The morphed model matched anthropometric data to within a root-mean square difference of 4.4% while maintaining element quality commensurate to the M50 model and matching other anatomical ranges and targets. The simulation validation data matched experimental data well in most cases, with an average objective rating score of 0.76 (out of 1).

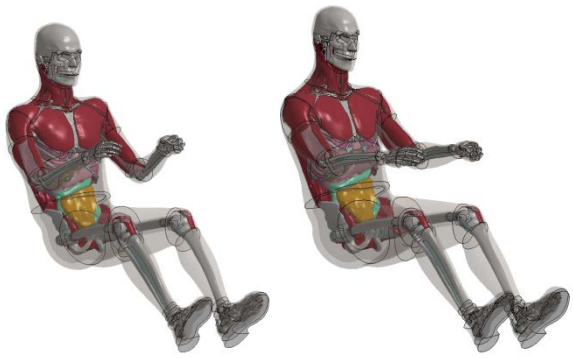

Figure 2: GHBMC M50 and M95 models, showing the effects of morphing.

CONCLUSIONS

The methods used in this study provide a framework for expedited model development, and address a need within the modeling community to decrease the time required for HBFEM development. This approach inherently facilitates comparisons of the morphed body habitus to the reference body type, and may ultimately be extended to study how body shape and size variance affects injury prediction using human body model simulation.

ACKNOWLEDGMENTS

This work was funded by the Global Human Body Models Consortium project number WFU-005.

CARBON NANOTUBES ATTENUATE CANCER AND IMPROVE HEALING

Elizabeth M. Wailes[1,2] and Nicole H. Levi-Polyachenko[1,2]
1. Virginia Tech-Wake Forest University School of Biomedical Engineering and Sciences
2. Wake Forest University School of Medicine Department of Plastic and Reconstructive Surgery
Corresponding Author: Elizabeth M. Wailes, Email: ewailes@wakehealth.edu

INTRODUCTION

When cancer occurs, there is a stromal reaction to the cancer cells which generates a fibrotic response like the kind seen in wound healing: the surrounding fibroblasts upregulate into myofibroblasts to secrete more collagen.[1] Because fibroblasts create and maintain the connective tissue layer that instructs epithelial cell behavior via stromal-epithelial interactions, perhaps multi-walled nanotubes (MWNT) could again inhibit the fibrotic reaction as it has in my previous research in wound healing, but with a new application to cancer.

METHODOLOGY

Co-culture models were generated using collagen gels, HEPM fibroblasts, and dsRed-expressing MDA-MB-231 breast cancer cells. Gels were made with or without fibroblasts, fibroblasts treated with transforming growth factor beta (TGF-β), and 1% MWNT. TGF-β is known to promote the stromal reaction and cancer cell invasion. Movement of the cancer cells was measured with an invasion assay and cell tracking. Gel contraction, matrix metalloproteinase (MMP) expression, and the viability of each cell type were also assessed to gauge overall cell behavior and activity.

RESULTS

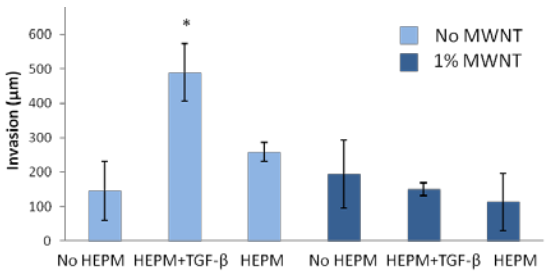

Figure 1: Invasion distance of cancer cells seeded on top of gels containing various cells with or without MWNT.

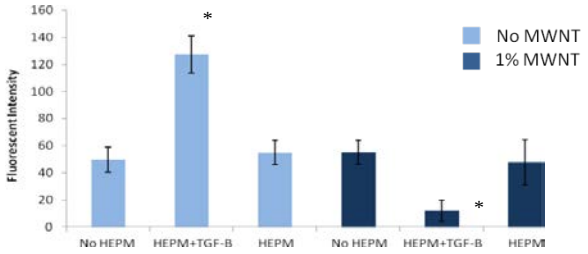

Figure 2: Cancer cell viability after one week in culture.

The MWNT were able to prevent cancer cell movement in both the z (invasion) and x/y directions (cell tracking) with significance on at least a $p \leq 0.001$ level. MMPs are known to aid cancer cell invasion by breaking down the matrix surrounding the cells to ease their path through it. MWNT were also able to decrease the expression of one of the main MMPs responsible for this behavior in breast cancer, MMP-9, on a $p \leq 0.005$ level. In addition, MWNT reduced the number of cancer cells present after one week of culture while strongly *increasing* the number of fibroblasts present after the same time. These differences were significant on a $p \leq 0.0001$ level.

CONCLUSIONS

MWNT are able to inhibit cancer cell movement, aggression, and growth while promoting fibroblast health. These properties make MWNT very advantageous as a potential secondary cancer treatment after tumor resection to prevent recurrence and encourage healing.

ACKNOWLEDGEMENTS

We would like to thank the Department of Plastic and Reconstructive Surgery for funding.

REFERENCES

1. Kalluri R, Zeisberg M. Nat Rev Cancer. 6, 392-401 **(2006)**

A GLIMPSE INTO BRCA1'S ROLE DURING TRANSCRIPTION

Carly E. Winton[1,2], Brian L. Gilmore[1], Andrew C. Demmert[1], Zhi Sheng[1], and Deborah F. Kelly[1,2]
1. Virginia Tech Carilion School of Medicine and Research Institute, Roanoke, VA 24016, USA.
2. School of Biomedical Engineering and Science, Virginia Tech, Blacksburg, VA 24061, USA.
Corresponding Author: Carly Winton, Email: carlyw02@vt.edu

INTRODUCTION

Germ-line mutations in the *BRCA1* gene, a known tumor suppressor, are linked to an aggressive form of hereditary breast and ovarian cancer known to result in poor clinical outcomes [1, 2]. BRCA1 acts as a global genomic surveyor, playing an important role in both transcription-coupled and DNA damage repair pathways. It associates with its binding partner BARD1 (BRCA1 Associated RING domain protein) and RNA polymerase II (RNAPII) in the nucleus[3]. Since these interactions have yet to be elucidated, we have developed tunable microchips that enable us to isolate BRCA1-associated complexes in patient-derived breast cancer cells for use in both biochemical and cryo-EM imagining.

METHODOLOGY

We extracted the nuclear contents of hereditary breast cancer cell lines expressing wild type and mutant BRCA1 and utilized our antibody-decorated SiN microchips to enrich for BRCA1-associated complexes. We collected images of our complexes using cryo-EM. We processed the images using the PARTICLE software package and the 3D density map of the complexes was calculated using the RELION software package. We utilized antibody labeling and molecular modeling techniques to determine the positions of BRCT and RING domains with respect to the RNAP II core structure within our map.

RESULTS

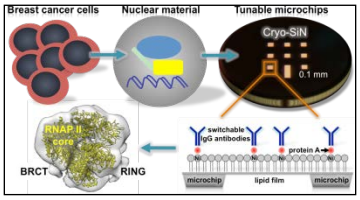

Figure 1: Tunable microchip approach.

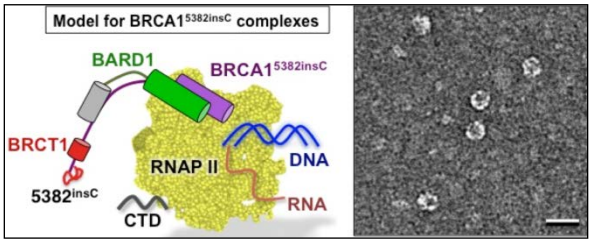

Figure 2: Prediction for the structure a prevalent clinical mutation in the C-terminus of BRCA1 (BRCA1^{5382insC}).

CONCLUSIONS

Our experimental findings allowed us to place the BRCA1-BARD1 heterodimer near the known DNA binding cleft of RNAPII and the hydrophobic cleft of the BRCT proximal to the C-terminal domain (CTD) of RNAPII. Also we found that BRCA1's interaction with BARD1 was decreased in the mutant, which enlightened us to make a prediction about the mutant structure. As the mutation is highly correlated with aggressive forms of breast cancer, understanding subtle differences between the wild type and mutant structure is instrumental towards improving the current poor clinical results.

ACKNOWLEDGMENTS

This work was sponsored by the development funds to D.F.K. from Virginia Tech and was supported by the Institute for Critical and Applied Science (ICTAS) Doctoral Scholars Program.

REFERENCES

1. Miki, Y., et al., Science, 1994. **266**(5182): p. 66-71.
2. Charafe-Jauffret, E., et al., Cancer Res, 2009. **69**(4): p. 1302-13.
3. Friedman, L.S., et al., Cancer Res, 1994. **54**(24): p. 6374-82.

Virginia Tech
Wake Forest University
School of Biomedical Engineering and Sciences
14th Annual Graduate Student Research Symposium, May 13, 2015

LABORATORY EVALUATION OF HEAD IMPACT SENSORS

Abigail M. Zadnik[1], Bryan R. Cobb[1], Steven Rowson[1], and Stefan M. Duma[1]
1. Virginia Tech, Biomedical Engineering and Mechanics
Corresponding Author: Abigail Zadnik, Email: azadnik@vt.edu

INTRODUCTION

As many as 3.8 million sports-related concussions are estimated to occur each year in the United States.[1] Recently, objective ways to assist in concussion diagnoses have come in the form of head impact sensors. These provide a potentially useful tool to parents and coaches in recognizing when a child should be removed from play to avoid a repeated head injury. Unfortunately, the accuracy and reliability of these sensors are not regulated. As sensors become part of the concussion diagnostic process, there is a need for regulation to ensure data is truly representative of what is happening on the field. The objective of this study was to investigate the current ability of commercially-available head impact sensors to accurately measure head impact dynamics.

METHODOLOGY

Five commercially available head impact sensors were evaluated. Sensors were applied to a NOCSAE headform or football helmet according to sensor instructions. The helmeted headform was mounted on a biofidelic neck. Impact tests were conducted using a pendulum impactor with a flat, nylon face. Impacts were performed at four locations and four impact velocities, chosen to be representative of on-field head impacts in sports.[2,3] A reference sensor was used in the headform, and average and standard deviations for percent error were quantified for each test to evaluate sensor performance.

RESULTS

On average, Sensor 1 had the lowest error at 2.2 ±15.5%. Sensor 2 had error of 21.7 ± 77.7%, while all others had errors over 90 ± 100%. Sensor 5 had error as high as 199.0 ± 280.0% (Figure 1). Each sensor also exhibited distinct location dependence. For example, Sensor 3 had 1.4 ± 11.3% error in the front and 140.9 ± 125.4% error in the back. It is evident that the accuracy and reliability differ substantially from sensor to sensor.

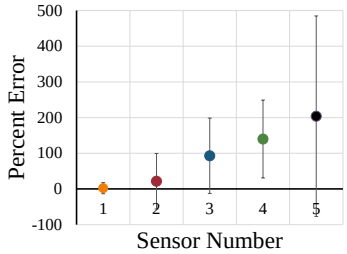

Figure 1: Total percent error for each sensor (with SD).

CONCLUSIONS

The results from comparing these five sensors indicate that not all commercially-available impact sensors are equal, although they are all being sold as such. Sensor 1 performed the best under ideal laboratory conditions, but requires additional on-field tests for a more complete assessment. Sensors 2-5 still require much improvement before they can be possibly deemed reliable for on-field measurements. Seeing as all five of these sensors are currently used in sports, it is imperative that consumers be informed of their reliability. Consistent evaluation of current head impact sensors will also encourage sensor manufacturers to create a more accurate product that can become a tool to aid in diagnosis of sports concussions.

ACKNOWLEDGMENTS

The authors gratefully acknowledge the Lewis Family Foundation for supporting this work.

REFERENCES

1. Langlois JA, et al. *JHTR.* 2006;21(5):375-378.
2. Daniel RW, et al.*Ann Biomed Eng.*2012;40(4):976-981.
3. Pellman EJ, et al. *Neurosurgery.* 2003;53(4):799-814.

PHENOMENOLOGICAL MODEL FOR UNSTEADY AERODYNAMICS OF PLUNGING AIRFOILS AT HIGH FREQUENCIES AND ANGLES OF ATTACK

Mohamed Y. Zakaria[1], Muhammad R. Jahh[1]
1. Department of Biomedical Engineering and Mechanics, Virginia Tech
Corresponding Author: Mohamed Y. Zakaria, Email: zakaria@vt.edu

INTRODUCTION

Flapping flight of insects and birds, which has inspired the concept of flapping micro air vehicles, is characterized by high frequency and angles of attack. Theodorsen's theory for modeling the unsteady lifting force, which assumes flat wake and small angles of attack, is not readily applicable for such flights. This raises the need to develop a model that can be used in the design, performance optimization and control of such vehicles.

METHODOLOGY

We develop a phenomenological model for the unsteady lift on an airfoil undergoing plunging oscillations over a broad range of reduced frequencies ($0.1 < k < 0.9$) and mean angles of attack ($0^\circ < \alpha < 65^\circ$). Experiments were performed in an open jet wind tunnel facility. For each value of the mean angle of attack, the plunging motion is performed at different frequencies to construct the frequency response of the dynamics about this value of the mean angle of attack. A second-order dynamical system is used as the phenomenological model. The model is divided to cover the linear, stall and post-stall flight regimes. In the linear regime, the results show an agreement with Theodorsen's analytical model.

RESULTS AND CONCLUSIONS

The results in the stall regime show lift enhancement over a specific range of operational reduced frequencies. This range can be effectively used as an optimal range in the design of flapping micro air vehicles. In the post stall regime, the behavior is similar to that of the linear regime with the lift significantly attenuated.

Virginia Tech
Wake Forest University
School of Biomedical Engineering and Sciences
14th Annual Graduate Student Research Symposium, May 13, 2015

FOAM STIFFNESS CHARACTERIZATION FOR USE AS A SURROGATE KNEE BOLSTER IN FULL SCALE FRONTAL SLED TESTS

Devon Albert[1], Stephanie M. Beeman[1], and Andrew R. Kemper[1]
1. Virginia Tech—Wake Forest University, Center for Injury Biomechanics, BEAM
Corresponding Author: Devon Albert, Email: dla16@vt.edu

INTRODUCTION

Contact between the knee and knee bolster is a major loading path during frontal motor vehicle collisions (MVCs). In order to simulate frontal MVC lower extremity loading in the laboratory, it is necessary to use surrogate materials for knee bolsters when the use of production bolsters is not possible or feasible. However, the stiffness of the surrogate material must be characterized and compared to production knee bolsters using similar loading conditions. Rupp et al. (2007) and Mahadevan et al. (1994) measured the stiffness of select production bolsters and collectively found that bolster stiffness ranged from 30 to 183 N/mm with an average value of 101 N/mm. The purpose of this research was to find a rigid polyurethane foam that can be used to simulate the stiffness of a sedan knee bolster during frontal sled tests by measuring the foam stiffness.

METHODOLOGY

Indentation tests were performed on three rigid polyurethane foams (65, 90, and 142 psi) using a material testing system (MTS) and a custom indenter. The diameter of the custom indenter (Dia.= 2.25in) was selected based on the average maximum knee-to-bolster contact area reported by Rupp et al. (2007). The impacting face of the indenter had a 1.5 in. radius to simulate the curvature of the knee. Each foam was tested at three loading rates: 1, 100, and 1000 mm/s. The stiffness of each foam was calculated at each loading rate and compared to the knee bolster literature.

RESULTS

The force versus deflection response for each foam during the 1000 mm/s tests are shown in Figure 1. All foams exhibited a two-phase response, where the first phase corresponded to the stiffness before the yield point and the second phase occurred after yielding. Foam stiffness and yield force generally increased with increasing loading rate and compressive strength rating. Figure 1 also shows the average, minimum, and maximum bolster stiffnesses from Rupp et al. (2007) and Mahadevan et al. (1994) along with the Ford Taurus bolster stiffness from a finite element model (FEM) developed by FHWA/NHTSA. While all of the foam stiffnesses reasonably matched literature values, the 65 psi foam was closest to the average literature value and most closely matched the results of the Ford Taurus FEM simulations.

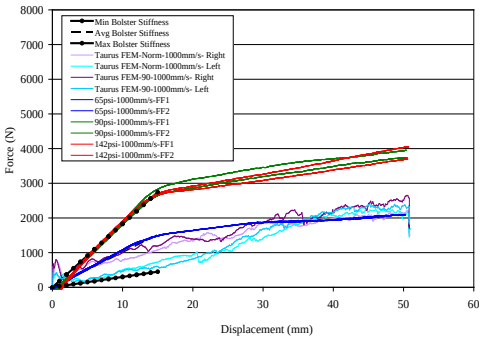

Figure 1: The stiffness of the tested foams, bolster stiffness corridor from the literature, and bolster stiffness from a Ford Taurus FEM model.

CONCLUSIONS

The 65 psi rigid polyurethane foam was found to most closely match the average knee bolster stiffness literature values and the Ford Taurus FEM bolster stiffness.

ACKNOWLEDGMENTS

The authors would like to thank the Toyota Motor Company for sponsoring this research.

REFERENCES

Mahadevan, K. et al. SAE Paper No. 940883, 1994.

Rupp, J.D. et al. Proceedings of the 22nd ESV Conf., Lyon, France; Paper No. 07-0345, 2007.

BRAIN STRUCTURAL NETWORK CHANGES RELATED TO HEAD IMPACT IN YOUTH FOOTBALL

Naeim Bahrami[1], MS; Harish Sharma[1], PhD; Christopher T. Whitlow[1], MD PhD; Jillian E. Urban[1], MS; Mark A Espeland[1], PhD; Youngkyoo Jung[1], PhD; Daryl A. Rosenbaum[1], MD; Gerard A. Gioia[2], PhD; Alexander K. Powers[1], MD; Joel D. Stitzel[1], PhD; Joseph A. Maldjian[1], MD
1. Wake Forest University School of Medicine, 2. Children's National Medical Center
Corresponding Author: Naeim Bahrami, Email: nbahrami@wakehealth.edu

INTRODUCTION

The purpose of this study was to determine if cumulative head impacts over a season of youth football affects brain structural network properties.

METHODOLOGY

Twenty male football players (age: 8-12) without history of prior concussion or neurologic disease from local elementary school teams participated in the study. The Head impact telemetry (HIT) system was used during practices and games for each individual. The HIT system uses sensors embedded in the helmet for kinematic data recording from head impacts. The biomechanical metric used was the risk weighted cumulative exposure (RWE_{CP})[1]. All subjects received pre and post-season MRI, including structural and diffusion tensor imaging (DTI). The scans were acquired on a 3 Tesla Siemens Skyra MRI scanner using a high resolution 20 channel head/neck coil. DTI data were obtained using a 2D single-shot EPI sequence (2.2 x 2.2 x3 mm; 15 diffusion directions with b=1000/2000 each).
DTI probabilistic network processing was performed using FDT-FMRIB diffusion toolbox in FSL[2]. For each subject, 116 nodes were determined based on 116 regions of interest (ROI) from the AAL atlas. For each seed region, 5000×n (n = number of voxels within the region) fibers were measured. The connectivity probability from the seed region to each target region was defined as the number of fibers passing through the target region divided by 5000×n. We created a 116×116 matrix representing the connectivity probability of all ROIs for each subject. Network properties including local and global efficiency, small worldness, node degree, transitivity, betweenness centrality, assortatitivity, triangles, and modularity were computed from this matrix. Linear regression analysis was conducted to determine the association between RWE_{CP} and network properties.

RESULTS

Table 1 reports the regression analysis results demonstrating the association between structural network metrics with respect to total RWE_{CP}. There was a statistically significant linear relationship between the total RWE_{CP} and global efficiency, transitivity, and node degree ($p < 0.05$).

Table 1: Associations between total RWECP and changes in structural network properties

	P-value	R^2
Global Efficiency vs RWE_{CP}	**0.0211***	-0.2751
Local Efficiency vs RWE_{CP}	0.0776	-0.1719
Modularity vs RWE_{CP}	0.1092	0.1439
Node Degree vs RWE_{CP}	**0.0092***	0.3364
Smallworldness vs RWE_{CP}	0.0890	0.1606
Betweenness Centrality vs RWE_{CP}	0.1806	0.1028
Triangles vs RWE_{CP}	0.0631	0.1864
Transitivity vs RWE_{CP}	**0.0164***	0.2944
Assortativity vs RWE_{CP}	0.5267	-0.0239

*$p < 0.05$.
RWE_{CP}, Risk Weighted Cumulative Exposure;
R^2 values with the negative sign illustrate the negative correlation between two designated variables

CONCLUSIONS

These results indicate changes in structural network properties in non-concussed subjects during a single season of football. These findings demonstrate that cumulative subconcussive sports-related impacts may have an effect on the brain.

REFERENCES

1. Urban JE, Davenport EM, Golman AJ, Maldjian JA, Whitlow CT, Powers AK, Stitzel JD, et al. Ann Biomed Eng. 2013; 41 (12): 2474–2487.
2. T.E.J. Behrens, M.W. Woolrich, M. Jenkinson, H. Johansen-Berg, R.G. Nunes, S. Clare, P.M. Matthews, J.M. Brady, and S.M. Smith. Magn Reson Med, 50(5):1077-1088, 2003.

Virginia Tech
Wake Forest University
School of Biomedical Engineering and Sciences
14th Annual Graduate Student Research Symposium, May 13, 2015

CERIUM OXIDE NANOPARTICLES REDUCE THE PRO-OXIDATIVE ENVIRONMENT FOLLOWING TRAUMATIC BRAIN INJURY

Zachary Bailey[1], Adewole Oyalowo[1], Kevin Hockey[2], Beverly Rzigalinski[2], Pamela VandeVord[1]
1. Virginia Tech, Biomedical Engineering and Mechanics
2. Virginia College of Osteopathic Medicine
Corresponding Author: Zachary Bailey, Email: zbailey2@vt.edu

INTRODUCTION

Traumatic brain injury (TBI) affects over two million people each year in the United States, and absorbs a substantial volume of annual healthcare costs. The injury often leads to a decreased quality of life including instances of morbidity and mortality. Further, TBI, including mild TBI (mTBI), is associated with many late-onset neurological disorders which develop years to decades after the initial insult. Despite considerable research efforts in this area, treatment options remain limited.

Free radicals are thought to play a key role in the pathophysiology of TBI and secondary brain injury in particular. The accumulation of free radical damage contributes to poor functional outcomes. Previous work has demonstrated the beneficial effect that cerium oxide nanoparticle (CeONP) administration has following neuronal injury and neurodegeneration [1]. This study was conducted to test the hypothesis that in vivo administration of CEONP will reduce the oxidative stress associated with mTBI which will improve functional outcomes.

METHODOLOGY

A lateral fluid percussion injury (1.5 atm) was administered to Sprague Dawley rats as a model of mTBI. Sham animals underwent surgery procedure without receiving the injury. CeONPs were administered in either 3 doses (1, 3, and 15 min following injury) or 5 doses (additional doses at 24 and 48 hrs following injury). Two concentrations were tested (0.05 and 0.5 mg/kg). Enzyme assays were conducted to assess reactive oxygen species (ROS) metabolism following the final injection. Additional animals were used for behavioral assessments (novel object recognition (NOR), open field task (OF)) up to two weeks post injury.

RESULTS

The mTBI produced acute changes in the activity levels of the enzymes responsible for proper metabolism of ROS. These enzymes include glutathione (oxidized and reduced), superoxide dismutase, and catalase. These changes were ameliorated by CeONP injections. Levels of 4-Hydroxynonenal, a marker for lipid peroxidation, were also returned to sham levels following treatment. While both drug concentrations and both injection schemes showed improvements, five injections of the 0.5 mg/kg was the most effective treatment in returning the enzymes activity to basal levels.

No significant changes were observed between treatment groups during the OF test. Each group showed similar anxiety and activity levels. However, short term memory deficits were restored to sham levels or above during the NOR test after administration of CeONP. The improvement was observed for both concentrations of the 5 injection scheme.

CONCLUSIONS

Oxidative stress is a characteristic outcome following TBI. Our results demonstrated that CeONP treatment following mTBI was effective in improving the pro-oxidative environment. CeONPs were able to return the activity level of several enzymes important to ROS metabolism back to basal levels. The improvements to oxidative stress showed no effect on anxiety or activity levels but correlated with improved memory.

REFERENCES

[1] N. Singh, C. A. Cohen, and B. A. Rzigalinski, "Treatment of neurodegenerative disorders with radical nanomedicine," *Ann N Y Acad Sci*, vol. 1122, pp. 219-30, Dec 2007.

THE EFFECT OF *N*-3-OXODODECANOYL-L-HOMOSERINE LACTONE (ODDHL) ON HYPOXIA-INDUCED PACLITAXEL RESISTANCE IN HUMAN BREAST CANCER CELLS

Brittany N. Balhouse[1], Scott S. Verbridge[1]
1. Virginia Tech, School of Biomedical Engineering and Science
Corresponding Author: Brittany Balhouse, Email: bnbalhou@vt.edu

INTRODUCTION

Hypoxia in the tumor microenvironment is known to induce resistance to chemotherapy drugs, like paclitaxel [1]. OdDHL has been shown to selectively affect breast cancer cell lines by modulating *STAT3* activity [2], which is linked to chemoresistance of breast cancer cells [3]. We hypothesize that OdDHL added to paclitaxel therapy will modulate hypoxia-induced chemoresistance.

METHODOLOGY

The day after seeding, MDA-MB-231 (metastatic breast cancer) cells were subjected to either hypoxia (1% O_2) or normoxia (20% O_2). The cells were then treated with either solely paclitaxel (concentrations of 10, 20, 40, 80 or 160 μM) or paclitaxel and OdDHL (200 μM). After two days of incubation, an alamarBlue® assay was completed to quantify differences in viability. Significance was determined by ANOVA and post-hoc Tukey's tests.

RESULTS

Hypoxia significantly increased the average viability of paclitaxel-treated wells (not shown). There is a trend of decreased viability with the addition of 200μM OdDHL over the range of paclitaxel concentrations (Fig. 1).

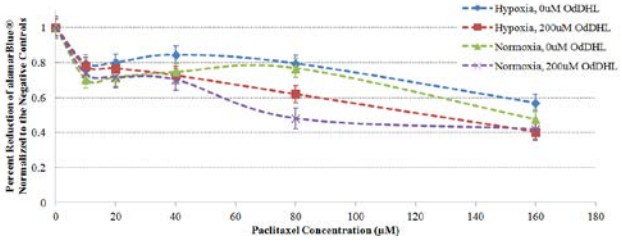

Figure 1: Viability with increasing paclitaxel concentration, quantified as percent reduction of alamarBlue®; decreased percent reduction denotes decreased viability.

There is a significant decrease in average viability with 200μM OdDHL present in both normoxic and hypoxic conditions; 200μM OdDHL has a larger effect in normoxia than in hypoxia (Fig. 2).

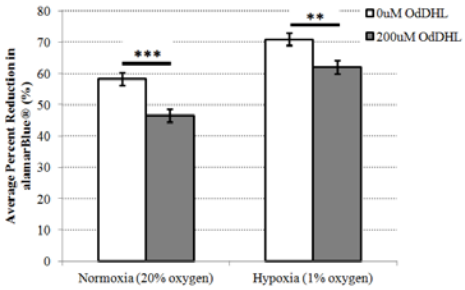

Figure 2: OdDHL effect on viability, averaged over all concentrations of paclitaxel. Decreased reduction of alamarBlue® corresponds to decreased viability. Mean ± standard error; **p<0.01, ***p<0.001.

CONCLUSIONS

OdDHL changed the way in which MDA-MB-231 cells responded to paclitaxel treatment under both normoxic and hypoxic conditions. There was a significant decrease in viability with the addition of 200μM of OdDHL in both normoxia and hypoxia, with a greater effect observed in normoxia. OdDHL could lower the resistance of breast cancer to paclitaxel.

ACKNOWLEDGMENTS

This work was supported primarily by the Institute for Critical Technology and Applied Science (ICTAS).

REFERENCES

[1]. Sullivan, R., et al. Mol Can Ther 2008; **7**(7): 1961-73.
[2]. Li, L., et al. Oncogene 2004; **23**(28): 4894-902.
[3]. Zhou, J., et al. Biochem Pharmacol; 2010. **79**(9): 1242-50.

CONTROLLED RELEASE BIOMATERIALS FOR IL-35 SECRETING MESECHYMAL STROMAL CELLS FOR THE TREATMENT OF TYPE I DIABETES

Jazmine C. Brown[1,2], Chris Rodman[2] , Christopher Porada[1,2] Graca Almeida-Porada[1,2], , Aaron Mohs[1,], Emmanuel C Opara[1,2]
1. SBES (Wake Forest University, Campus)
2. Wake Forest Institute for Regenerative Medicine (WFIRM)
Corresponding Author: Jazmine C. Brown, Email: jazbrown@wakehealth.edu

INTRODUCTION

Type 1 diabetes (T1D) affects approximately three million people in the United States. T1D is usually diagnosed in children/young adults, and results from the damage of insulin-secreting β-cells within the pancreas by deregulated immune cells. There is no cure for T1D; current treatment consists of daily injections of insulin to control blood sugar. While this treatment maintains normal sugar levels in the blood, it does not prevent the severe complications of the disease that can lead to blindness, kidney failure, and an increased risk of heart attack and stroke. This goal of this study was to genetically engineer mesenchymal stromal cells (MSCs) to produce the cytokine, IL-35 for immune therapy in T1D.

METHODOLOGY

Rat MSCs were engineered to secrete IL-25, and this was achieved through transfection using a lentiviral vector encoding a “single-chain” IL-35 cassette and an mCherry fluorescent tag. Successful transfection was verified through fluorescent microscopy as can be seen in Figure 1. With this successful transfection, the immunomodulatory properties of the engineered MSCs will be determined using a T cell suppression assay. This assay will be followed by studies of the MSCs for immune-tolerance in a rat model of autoimmune T1D.

RESULTS

Successful transfection of the rat MSCs as verified using flourescence microscopy are shown in Figure 1. The red coloring is indicative of successful uptake of the IL-35 cassette tagged with mCherry.

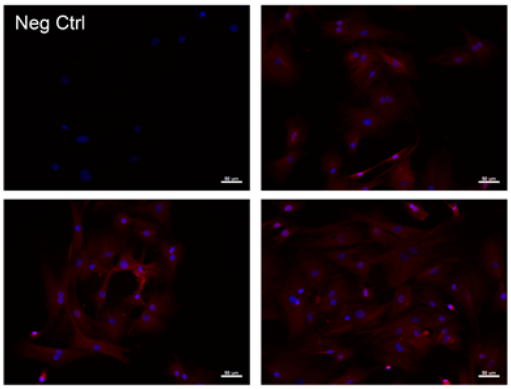

Figure 1: Transduction of rat MSCs verified using flourescence microscopy. Dapi staining was used to label the nuclei to better see individual cells.

CONCLUSIONS

The next steps include verifying the immunomodulatory properties of these engineered MSCs using a T cell suppression assay. Engineered rat MSCs will be co-cultured with splenocytes that are stimulated using concanavalin A. Once the immunomodulatory properties are verified, an in *vivo* study can be done in a rat model.

ACKNOWLEDGMENTS

WFIRM financial support

Virginia Tech
Wake Forest University
School of Biomedical Engineering and Sciences
14th Annual Graduate Student Research Symposium, May 13, 2015

ASYMMETRICAL INJURY RISK IN FRONTAL OBLIQUE IMPACT

Rong Chen[1], Hampton C. Gabler[1]
1. Virginia Tech (School of Biomedical Engineering and Science, Center for Injury Biomechanics)
Corresponding Author: Rong Chen, Email: rjchen@vt.edu

INTRODUCTION

Current vehicles contain several asymmetrical design elements. The steering wheel and various instrument panels are offset to one side, and most engine and transmission arrangements results in an asymmetrical engine compartment. These features of the vehicle raises the questions of whether or not crashworthiness also differs between the left and right side of the vehicle. The research objective of this study was to determine the factors and injury risk of drivers and front passengers in near-side frontal oblique impact.

METHODOLOGY

The analysis is based upon 5,982 cases extracted from the National Automotive Sampling System Crashworthiness Data System (NASS/CDS) database for case years 1997-2012. NASS/CDS is a unique database of in-depth crash investigations. The approach was to compare and contrast injury outcomes for drivers involved in left side oblique frontal impacts against front passengers involved in right side oblique frontal impacts. The distributions of injuries for all drivers were determined by body region and injury severity. In order to be classified as oblique impacts, the vehicle must be involved in frontal crashes with PDOF between 330° to 30°. Furthermore, the most harmful deformation must occur to the front-left or front-right quadrant of the vehicle.

RESULTS

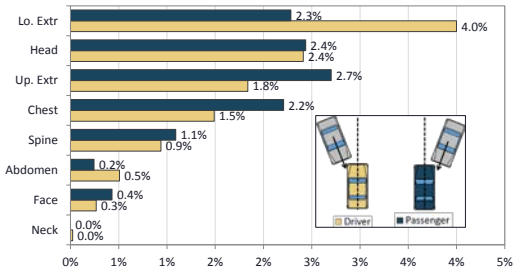

Figure 1: Risk of Moderate (AIS2+) Injury.

Figure 1 shows the distribution of injury risk for the driver and front passenger in oblique frontal crashes. As shown in the figure, the body region with the largest difference in injury risk is the lower extremity. The risk of lower extremity injury for drivers is almost double that of passengers.

One factor which can contribute to the difference in injury risk is the object which the vehicle struck. In U.S. roadways, poles, trees, and other narrow objects are often placed on the right side of the road. Impacts against these narrow objects may not fully engage the vehicle frame rail and can potentially direct the occupant away from the airbag. Our results of the sample of oblique frontal impact shows that approximately 24% of right side oblique frontal impact and 14% of the left side oblique impact involved narrow objects.

Another factor which may contribute to the difference in injury risk is airbag deployment. However, no statistically significant difference were found in the odds of frontal airbag deployment, between left and right side oblique impact of similar crash severity.

Lastly, we examine any potential difference in intrusion between the two sides. Our hypothesis was that the asymmetrical engine and transmission layout may provide protection against intrusion for one side versus the other. Our results showed that the intrusion magnitude was very similar between the two sides, and the distribution of intrusion component was also very similar.

CONCLUSIONS

This study analyzed the factors and injury risk of driver and front passenger in near-side frontal oblique impacts. The results shows that, although the risk of lower extremity injury is greater for drivers, the crash characteristics of the two impact sides are very similar. We found that right side frontal oblique impacts are more against narrow objects, and the result show no difference in the odds of airbag deployment or vehicle intrusion.

Virginia Tech
Wake Forest University
School of Biomedical Engineering and Sciences
14th Annual Graduate Student Research Symposium, May 13, 2015

AN IN VITRO 3D BRAIN INFLAMMATION MODEL

Hyung Joon Cho[1] and Yong Woo Lee[1,2]
1. Virginia Tech-Wake Forest University, School of Biomedical Engineering and Sciences,
2. Virginia Tech, Department of Biomedical Sciences and Pathobiology
Corresponding Author: Hyung Joon Cho, Email: hjcho79@vt.edu

INTRODUCTION

Hydrogels are widely employed as potential biomimetic scaffolds because of their 3D properties mimicking the hydrated microenvironment of native extracellular matrix. In the proposed studies, we designed and constructed *in vitro* 3D hydrogel systems to mimic physiologically relevant environments to investigate specific cellular responses and molecular interactions of microglia.

METHODOLOGY

Type I collagen containing the murine microglial cell line, BV-2 cells, was used to construct an *in vitro* 3D brain inflammation model. Traditional 2D cell culture and *in vivo* studies were used for comparison. To generate brain inflammation in 2D/3D model systems and *in vivo*, BV-2 cells and C57BL/6J mice were exposed to lipopolysaccharide (LPS or endotoxin). Computer simulations of oxygen concentration within the 3D construct and LIVE/DEAD assay were performed to optimize the best cell seeding concentration and culture time. The mRNA and protein expression levels of pro-inflammatory mediators, including TNF-α, MCP-1, IL-6, and IL-1β, were determined by quantitative real-time RT-PCR and ELISA, respectively. The levels of reactive oxygen species (ROS) were visualized by *in situ* dihydroethidium (DHE) assay. The immunoreactivity of activated microglia was observed by immunofluorescence staining. Student's t-test compared mean responses among the respective comparison groups using Sigmaplot 11, and $p<0.05$ was considered significant.

RESULTS

The finite element modeling of oxygen diffusion and cellular oxygen consumption within the 3D structure predicted the optimal cell density of 1×10^6 cells/ml after 72 h growth. In addition, LIVE/DEAD assay showed the highest cell viability and lowest cell cytotoxicity with the predicted cell density after 72 h growth. RT-PCR analyses and ELISA demonstrated a significant up-regulation of TNF-α (Fig. 1) as well as other pro-inflammatory mediators such as MCP-1, IL-6, and IL-1β (data not shown), in LPS-stimulated *in vitro* 2D/3D model systems and *in vivo*. Moreover, the inflammatory responses from 3D cell culture were similar to *in vivo*. Furthermore, *in situ* DHE assays and immuno-fluorescence staining revealed that the LPS-stimulated ROS generation and microglial activation from 3D cell culture was significantly lower and close to *in vivo* compared with 2D cell culture, respectively (Fig. 2).

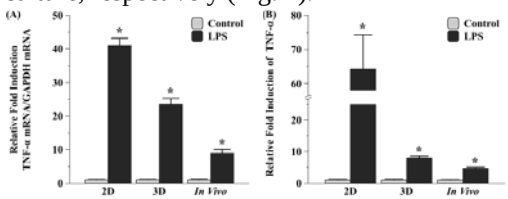

Figure 1: Comparison of TNF-α up-regulation after LPS stimulation. (A) mRNA and (B) Protein expression of TNF-α. *p<0.05 vs. Control.

Figure 2: Comparison of ROS generation and microglial activation after LPS stimulation. (A) *In situ* ROS detection and (B) Immunoreactivity of microglial activation marker. *p<0.05 vs. Control.

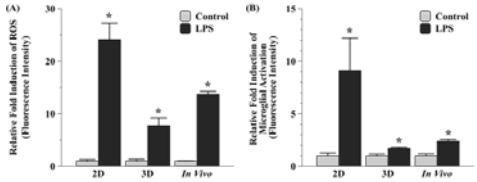

CONCLUSIONS

These results demonstrated that an *in vitro* 3D brain inflammation model system in the present study provides a more physiologically relevant environment than traditional *in vitro* 2D models.

A MICROFLUIDIC PLATFORM TO MODEL THE HETEROGENEOUS EXTRACELLULAR MATRIX OF THE BRAIN TUMOR MICROENVIRONMENT

Megan C. Cox,[1] Asem I. Abdulahad,[2] Timothy E. Long,[2] and Scott S. Verbridge[1]
1. Virginia Tech-Wake Forest University, School of Biomedical Engineering and Sciences
2. Virginia Tech, Macromolecules and Interfaces Institute, Department of Chemistry
Corresponding Author: Megan Cox, Email: meganc4@vt.edu

INTRODUCTION

Cancer is highly heterogeneous, not only among, but also within individual tumors. This is often evident in variations in the extracellular matrix (ECM); however it is not entirely known the mechanisms by which these heterogeneities may be impacting tumor progression. ECM heterogeneity is commonly seen in the most aggressive primary brain cancer, glioblastoma multiforme (GBM), where the average prognosis of a patient is only 12 to 15 months.[1] In GBM, invading tumor cells break down the surrounding ECM proteins, composed mainly of hyaluronic acid (HA), resulting in variations in ECM composition and stiffness, affecting processes, like angiogenesis and metastasis, which play a crucial role in tumor progression and therapeutic resistance.[2] We hypothesize that a microfluidic device capable of generating hydrogel gradients that mimic the heterogeneous ECM of the brain tumor microenvironment will provide insight into the mechanisms by which tumor progression is regulated by the ECM.

METHODOLOGY

Standard photolithography was utilized to pattern channels into PDMS to create an HA molecular weight (MW) gradient, Fig. 1. The dynamics of cellular interactions with soluble low MW HA were analyzed using migration and proliferation studies. A Transwell® assay was used to determine the effect of the HA on U87 cell migration, a human GBM cell line, over 24 hours. Proliferation studies will be presented at a later time.

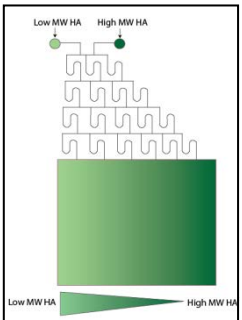

Figure 1: Schematic of HA gradient scaffold

RESULTS

Gradient channels were patterned into PDMS, Fig. 2a. The Transwell® assay illustrated that a low MW HA gradient doesn't induce GBM migration, Fig. 2b.

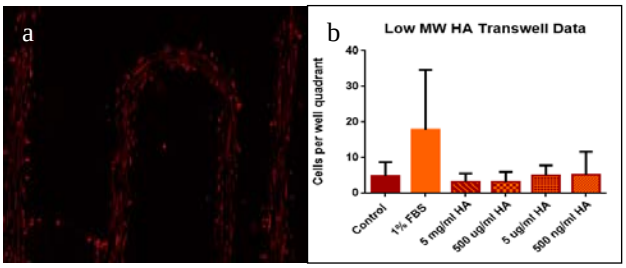

Figure 2: (a) Fluorescent beads in channel, (b) U87 Transwell® migration assay

CONCLUSIONS

The lack of response of the tumor cells to soluble low MW HA could indicate that direct cell-ECM contact is needed for the HA to affect cellular behavior in the tumor. The development of our *in vitro* ECM gradient platform will enable us to analyze direct cell-ECM interactions as well as the impact of ECM heterogeneity on vascular invasion and network formation, potentially uncovering effective new treatment targets.

ACKNOWLEDGMENTS

Funding provided by the NIH under Award Number R21EB019123 and the College of Engineering and ICTAS at Virginia Tech.

REFERENCES

1. Siegel, R et. al, CA:A Cancer Journal for Clinicians
2. Ananthanarayanan et al., Biomaterials, 2011

Virginia Tech
Wake Forest University
School of Biomedical Engineering and Sciences
14th Annual Graduate Student Research Symposium, May 13, 2015

RELATING KINEMATICS TO INJURY RESPONSE OF LOWER EXTREMITY DURING BLAST-INDUCED ACCELERATIVE LOADING

Danielle M. Cristino[1], Warren N. Hardy[1]
1. Virginia Polytechnic Institute and State University, School of Biomedical Engineering and Sciences
Corresponding Author: Danielle Cristino, Email: cristi07@vt.edu

INTRODUCTION

The use of improvised explosive devices has exposed military vehicles to a threat environment characterized by blast-rate accelerative loading in a primarily vertical direction. In this test series, response and tolerance information was obtained from post-mortem human surrogates (PMHS) exposed to underbody blast events in a laboratory setting. Injuries and death due to underbody blast events are significant societal costs and there is a need to understand, predict, and mitigate these effects. In particular, injuries to the lower extremity are frequent and can be debilitating. This effort relates kinematic data to injuries of the lower extremity during testing.

METHODOLOGY

Eight trials with a total of fourteen PMHS were completed. The PMHS were instrumented and placed in a seated position with the inside angle of the knee adjusted to 90 degrees (nominal) or 120 degrees (obtuse). The test apparatus underwent vertical acceleration generated using explosives as the energy source. Two levels of explosives were used: mild and enhanced. The test apparatus had two floor types designated as stiff or soft material.

RESULTS

Foot injuries included damage to the calcaneus, talus, navicular, cuneiform, cuboid, and metatarsals. There was a single pilon fracture of the distal tibia associated with a soft floor and an obtuse knee angle. All injured PMHS (8/14) had calcaneus damage; this damage was independent of floor material and knee angle. The talus generally received minor fracture, except for a single PMHS in the nominal position with soft floor that had complete fracture of the talus. Injuries to the midfoot and forefoot were introduced with reduced floor stiffness. The softer floor material resulted in greater floor deformation, greater rate of floor deformation, and longer contact duration between the floor and foot.

CONCLUSIONS

The tarsal fractures appeared to be the result of a compressive load applied vertically. The more severe case of complete talus fracture occurred in the absence of damage to the tibia. It is suggested that the calcaneus and distal tibia are likely to fail before the talus; however, sustained loading of the talus may have been achieved with the softer floor. Additionally, the softer floor may have influenced the occurrence of midfoot, forefoot, and pilon fractures. The pilon fracture, which is known to typically result from high energy axial loading of the tibial plafond, was not expected to occur in the obtuse condition. This suggests an influence of contact duration, obtuse posture, and foot rotation on this injury. Metatarsal damage may be attributed to a combination of vertical compressive load and the resulting bending moment on the foot and was independent of knee angle.

Lower extremity injury is most likely related to higher acceleration of the floor, which would be associated with larger resultant relative tibia Z-direction and femur X-direction velocity or higher acceleration rate, for a given posture. Femur X-direction speeds are lower for the obtuse condition than the nominal condition. The femur Z-direction speeds were minimal for the obtuse condition.

ACKNOWLEDGMENTS

I would like to thank Andrew R. Kemper, John H. Bolte IV, Kerry A. Danelson, the Army Research Laboratory, and the Aberdeen Test Center.

REFERENCES

W. N. Hardy, J. H. I. Bolte and K. A. Danelson, "Whole-Body Blast-Induced Accelerative Loading, Structure Interaction, and Mechanical Response of PMHS and the Hybrid III ATD," VT/WFU-2013-009, Aberdeen, 2013.

DEVELOPMENT OF THE GHBMC 5TH PERCENTILE FEMALE FINITE ELEMENT MODEL

Matthew L. Davis[1,2], Bharath Koya[1], Jeremy Schap[1], and F. Scott Gayzikl[1,2]
1. Wake Forest School of Medicine
2. Virginia Tech- Wake Forest Center for Injury Biomechanics
Corresponding Author: Matthew L. Davis, Email: mattdavi@wakehealth.edu

INTRODUCTION

To mitigate the societal impact of vehicle crash, researchers are using a variety of tools, including finite element models. Such models are often developed to represent a 50th percentile male occupant (M50) [1]. However, in order to address the effects of size and sex-related geometrical changes, there is interest in developing models of other driving cohorts. This study focuses on the female driver in the 5th percentile of height and weight. As part of the Global Human Body Models Consortium (GHBMC) project, comprehensive image and anthropometrical data of the 5th percentile female (F05) were acquired for the specific purpose of finite element model development. The objective of this study is to review the data collected for this effort, including medical imaging, CAD construction, and meshing techniques employed for model development.

METHODOLOGY

An individual representing the F05 in terms of height (149.9cm) and weight (48.0±0.63kg) was selected. Fifteen external anthropomorphic measurements were acquired to determine eligibility. Surface topography and 52 external bony landmarks were also acquired via a 3D digitizer. Computed tomography (CT), Magnetic Resonance Imaging (MRI), Upright MRI, and external anthropometry were obtained in supine, seated, and standing positions. Soft tissue and bony anatomy that are represented in the F05 finite element model were segmented using supine MRI and CT respectively. NURBS surfaces with tangential continuity were constructed over all segmented data. The CAD dataset was then utilized for mesh development of the GHBMC F05 occupant model [2].

RESULTS

The selected subject closely represented the F05 in terms of height and weight, deviating less than 2% in those measures. For all 15 anthropomorphic measurements, the average subject deviation across all measures was 4.1%. A total of 66 scan series were collected across all modalities for a total of 14,170 images. Abdominal organ volumes and cortical bone thickness were compared to literature sources for verification. The alpha version of the model consists of 850 parts, 2.3 million elements, and 1.3 million nodes. In terms of element quality, stringent thresholds were placed on several criteria: jacobian (>0.3 for all solid elements and >0.4 for all shells), tet-collapse (>0.2 for all elements), and a minimum time step value of 0.01 μs. Figure 1 below shows both the CAD data and the alpha version of the F05 finite element model.

A. B.

Figure 1: A) F05 CAD data. B) F05 Full Body Model

CONCLUSIONS

The methods presented in this study describe the application of a multi-modality image dataset to the ground-up development of an anatomically representative small female finite element model in a driving posture. The small female occupant is the third in the GHBMC family of detailed occupant models (M50, M95). Furthermore, quantitative comparison between various approaches of model output scaling will provide needed insight, particularly as human body modeling is extended to body sizes beyond the average male.

REFERENCES

[1] Gayzik F.S., ABME, 2012
[2] Davis M., et al. IRCOBI, Sept. 2014

Virginia Tech
Wake Forest University
School of Biomedical Engineering and Sciences
14th Annual Graduate Student Research Symposium, May 13, 2015

BREAST RECONSTRUCTION: EVALUATION OF PATIENT SPECIFIC IMPLANT RESPONSES

Katherine E. Degen[1,2], Kurtis Moyer,MD[1,2,3], Robert G. Gourdie, PhD[1,2]
1. Virginia Tech, School of Biomedical Engineering
2. Virginia Tech Carilion Research Institute
3. Plastic Surgery, Carilion Clinic
Corresponding Author: Katherine Degen, Email: ked4p@vt.edu

INTRODUCTION

The single most common complication of breast reconstructive surgery is the formation of a dense scar capsule around the silicone implant called capsular contracture. Nearly all patients will experience this complication, though with different degrees of response, ranging from moderate scarring to major disfigurement and pain at the implant site. Presently, there is no way to predict the degree of contraction capsule formation that individual patients will suffer prospectively, nor is there clinical approach to preventing this complication.

Cx43 has key assignments in wound healing and studies by various groups have demonstrated that targeting Cx43 can lead to improvements in wound closure, and reductions in the inflammatory response reducing scarring following injury [1]. The Gourdie lab has identified a novel peptide (αCT-1) mimicking the carboxyl-terminus of connexin 43 [2] that decreases scarring in skin wounds [3]. Moreover, it was shown that the peptide had efficacy in modulating the response to implanted devices [4]. αCT1 has successfully completed phase II clinical trials in humans for indications in wound healing [5].

METHODOLOGY

Dr. Kurtis Moyer MD, Chief of Plastic Surgery at Carilion, is providing patient samples of scar capsule and de-identified medical information under an active IRB. The standardization of collection is achieved by sampling scar capsule tissue, from around an implanted breast expander device placed by Dr. Moyer, at a precisely defined anatomical location and at a standardized time interval following implantation of the device. Tissue samples are prepared for histology, RNAseq, and patient fibroblast explants.

RESULTS

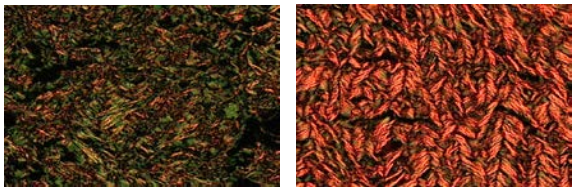

Figure 1: Picrosirius Red Stained Capsules, A) low grade capsules exhibit less mature and less organized collagen than higher capsule grades (B).

Histological analysis has demonstrated that the qualitative clinical scale can be correlated to more quantitative metrics. Initial results suggest that vessel diameter increases while vessel density decreases in higher capsule grades. Capsule thickness does not seem to correlate to capsule severity. Preliminary RNAseq results have identified 5 mRNA species which vary significantly between paired low and high grade capsules.

Peptide treatment of fibroblasts has been found to alter both collagen processing and cell migration patterns in a dose dependent fashion. Future work will investigate mechanism but these results suggest CX43 mimetic peptides could be a promising treatment for capsular contracture.

ACKNOWLEDGMENTS

Carilion Rap9 Grant 2013, 2014
VTCRI Medical Scholars Fellowship

REFERENCES

[1]Degen KE, Gourdie RG. (2012). *Birth Defects Res C Embryo Today*. 96(3):258-70.
[2]Hunter et al. (2005) *Mol Biol Cell.* 16(12):5686-98
[3]Ghatnekar et al (2009) *Regen Med.* 4(2): 205–223.
[4]Soder, et al. (2009) *Plast Reconstr Surg.* 123(5):1440-51.
[5] Ghatnekar et al. (2015) *J. Inv. Derm.(Nature),* 135(1):289-98.

A LONGITUDINAL fMRI STUDY OF WORKING MEMORY IN ALCOHOL USERS

Harshawardhan Deshpande[1, 2], Jonathan M. Lisinski[2], Charles Mueller[2], Warren K. Bickel[2] and Stephen M. LaConte[1, 2]
1. Virginia Tech – Wake Forest School of Biomedical Engineering & Sciences
2. Virginia Tech Carilion Research Institute
Corresponding Author: Harshawardhan Deshpande, Email: harsh87@vt.edu

INTRODUCTION

Chronic dependence on alcohol can impair cognitive control and decision-making [1,2]. In an ongoing longitudinal study, alcohol users are randomly assigned to receive either working memory (WM) training or control training over a period of 6-9 weeks. fMRI data are collected at four assessment sessions (Weeks 1, 14, 20, 26), where subjects perform a series of tasks, including a letter n-back task. The goal of this study is to analyze the effects of the training on the subjects' WM capacity and their ability to control craving for alcohol.

METHODOLOGY

Data collection: fMRI data are collected on a Siemens Trio 3T scanner using an echo planar imaging (EPI) fMRI sequence with imaging parameters: TR/TE = 2000/30 ms, 64×64 acquisition matrix, 4-mm slice thickness, 33 slices, 220-mm field of view. Subjects perform an n-back task, where uppercase letter sequences are displayed with a stimulus duration of 500 ms and an interstimulus interval of 2500 ms (1/3 trials are targets). In the 0-back, subjects respond to a single target, i.e. the letter 'X' by pressing a button. In the 2-back, subjects respond if the letter on screen was identical to one presented two trials back.
Data analysis: Data preprocessing is performed using AFNI [3] and includes slice time correction, motion correction, spatial smoothing and transformation to standard space. For every subject, 2-back – 0-back contrast maps are generated for each time point using general linear model analysis.

RESULTS

Table 1: Current number of completers at each assessment session in the longitudinal study.

Assessment Session	T1	T2	T3	T4
No. of subjects	24	20	19	18

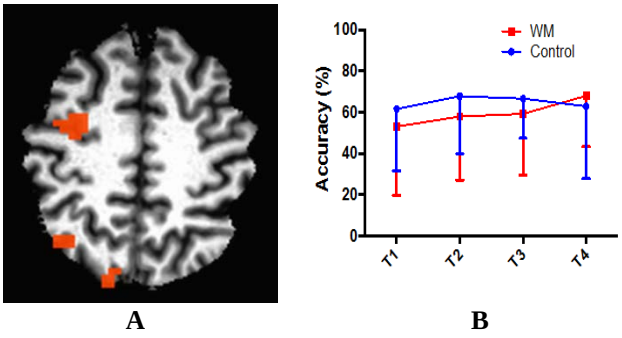

A B

Figure 1: (A) An example 2-back – 0-back map from a single time point for a subject. Increased activity can be seen for 2-back in the left middle frontal gyrus, the left superior parietal lobule and the left precuneus. These regions have been correlated with WM manipulation and visuospatial information processing [4]. **(B)** Subject accuracies for the 2-back task for the WM and control training groups.

CONCLUSIONS

Our preliminary results currently do not show any significant differences in the n-back performance for the two training groups. We are currently analyzing the fMRI data to generate group maps based on the training groups. As this is an ongoing study, we are in the process of collecting more time points as well as adding more subjects.

REFERENCES

[1] Jansen et al. (2011), *Psychological Science*
[2] Bechara et al. (2004), *Neuropsychology*
[3] Cox, R. W. (1996), *Computers & Biomedical research*
[4] Sala-Llonch et al. (2011), *Cortex*

Virginia Tech
Wake Forest University
School of Biomedical Engineering and Sciences
14th Annual Graduate Student Research Symposium, May 13, 2015

A 3D Stratified Colon Model for Colorectal Cancer Progression

Mahesh Devarasetty[1,], Aleksander Skardal[1,], and Shay Soker[1,]
1. Virginia Tech Wake Forest School of Biomedical Engineering and Sciences
Corresponding Author: Mahesh Devarasetty, Email: mdevaras@wakehealth.edu

INTRODUCTION

Colorectal cancer is the second overall leading cause of cancer-related death in the United States. It is the cause of over 50,000 deaths in the United States every year. One reason for the high incidence rate is rapid progression of colorectal cancer cells. Once mutated, these cancers can metastasize and become difficult to treat. Recent investigation of metastasis has identified the queues and factors of the tumor microenvironment to be influential in metastatic progression. This study aims to develop an organized micro-facsimile of colonic microstructure using cellularized hydrogel strata that mimic tissue layers of the intestine. This system can be used to explore the effects of the microenvironment on tumor phenotype in a highly relevant model, with intentions of revealing mechanisms of metastasis and providing a platform for diagnostics.

METHODOLOGY

Each stratum represents a different cell type of native colon anatomy. CACO-2 cells are used for the epithelium, HUVECs are used for the endothelium, and primary rat colon smooth muscle cells (RCSMC) are used for the submucosa. The submucosa is generated using either collagen I or hyaluronic acid (HA) hydrogel mixed with RCSMC at a density of 5 million cells/mL. Endothelial layers and epithelial layers are simple monolayers on either side of the submucosa construct. Constructs are cultured in DMEM (10% FBS) and imaged using a Leica LCS TSI macroconfocal microscope.

RESULTS

Figure 1 shows our cellularized submucosal construct. Constructs at lower collagen concentration demonstrated high propensity for contraction however there was more cytoskeletal disorganization indicated by phalloidin staining. Figure 2 shows our epithelial stratum's response to varying stiffness. There is more columnar shape and cuboidal clustering in the higher stiffness condition; this suggests that stiffer substrates induce a more epithelial phenotype.

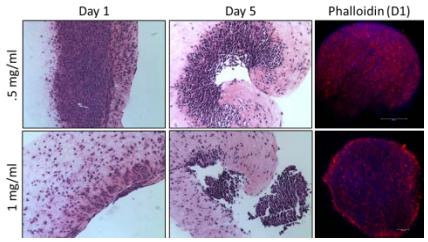

Figure 1: RCSMCs embedded in ColI gel. The first two columns show H&E staining after days 1 and 5, respectively. The third row shows phalloidin staining of the whole construct. Two ColI formulations are show, denoted by each row.

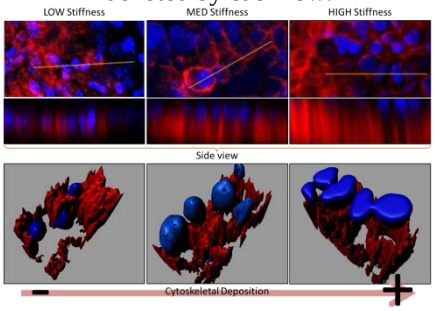

Figure 2: CACO-2 cells grown on varying stiffness HA gels then stained with phalloidin. Top and side views are show in the top two rows, and the third row shows reconstructions of select areas.

CONCLUSIONS

We have demonstrated the techniques to fabricate individual layers of the proposed colon model.

ACKNOWLEDGEMENTS

WFIRM, DoD XCEL, Golfers Against Cancer

EFFECTS OF X-RAY EXCITATION SPECTRUM ON X-RAY FLUORESCENCE COMPUTED TOMOGRAPHY (XFCT)

Xu Dong[1], Guohua Cao[1]
1. School of Biomedical Engineering and Sciences, Virginia Tech
Corresponding Author: Xu Dong, Email: xu14@vt.edu

INTRODUCTION

XFCT has been proposed as a modality for element-specific 3-D imaging of a subject. In this method, X-ray are used to produce characteristic X-rays through interaction with the high atomic number elements in the imaged object. XFCT promises a noninvasive molecular imaging modality of high-Z molecular probes such as gold nanoparticles (AuNPs). However, the insufficient sensitivity still limits the application of XFCT in vivo molecular imaging studies. The imaging sensitivity can be improved by increasing the ratio of x-ray fluorescence photons to background Compton scattered photons. Here we performed simulations to find the optimal spectrum for exciting x-ray fluorescence from gold at lowest radiation dose.

METHODOLOGY

The software *spekcalc*[1] was used to generate the spectrum for simulation. And the system geometry is shown in Figure 1. After the AuNPs voxel is excited by the excitation spectrum, the x-ray fluorescence will be generated isotropically. The detector was put on at the 90°, and it will detect both the fluorescence signal (the wanted signal) and the Compton scattering signal (noise). The dose level, AuNPs concentration, exposure time and all other parameters are fixed, and different excitation spectra are simulated under this system geometry. Finally, the Signal to Noise Ratio (SNR) was obtained through the simulation.

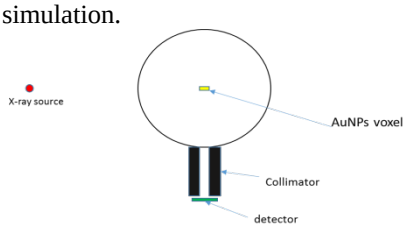

Figure 1: The system geometry used in the simulation.

RESULTS

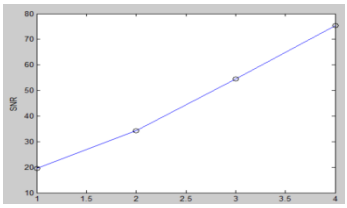

Figure 2: The SNR varies with different Copper thickness as a filter.

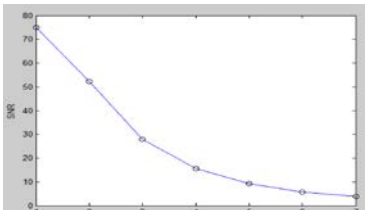

Figure 3: The SNR varies with different spectrum peak energy.

Figure 2 shows how the SNR changes, when the thickness of Copper filter was set as 8mm, 16mm, 24mm and 32mm, which is 1,2,3,4 at the x- coordinate correspondingly. Figure 3 shows how the SNR changes, when the peak energy of spectrum was set as 90KeV, 95KeV, 100KeV, 105KeV, 110KeV, 115KeV, and 120KeV, which is 1,2,3,4,5,6,7 at the x- coordinate correspondingly.

CONCLUSIONS

As the k-edge of Gold is 80.725KeV, when the peak energy is above the Gold k-edge energy, the SNR will become higher with the Copper being thicker and the peak energy being lower.

REFERENCES

[1] Poludniowski, G.G., and Evans P.M. Medical physics 34.6 (2007): 2164-2174.

CONTACTLESS DIELECTROPHORESIS FOR SEPARATION OF CELLS BY MALIGNANCY

Temple A. Douglas[1], Jaka Čemažar[1], Eva M. Schmelz[2], and Rafael V. Davalos[1]
1. Virginia Tech, School of Biomedical Engineering and Sciences
2. Virginia Tech, Department of Human Nutrition, Foods, and Exercise
Corresponding Author: Temple A. Douglas, Email: tadougla@vt.edu

INTRODUCTION

Tumor Initiating Cells (TICs) or cancer stem cells are a small sub-population of cancer cells that can phenotypically self-renew and recapitulate the original tumor [1]. These cells are known to have a unique phenotype from other cancer cells and their normal surrounding tissue. TICs are important indicators of the evolutionary or metastatic population in a tumor, and they contribute to a poor outcome.

Their potential as a diagnostic measure and as a way to understand the development and evolution of tumors makes them an appropriate target for prevention and treatment efforts. Therefore, it is important to develop methods to detect these cells and isolate them for further analysis. Previous work on contactless dielectrophoresis (cDEP) has shown to have potential as a method of separating TICs from other cancer cells with different phenotypes [2]. This poster presents a method of differentiating mouse ovarian surface epithelial (MOSE) cells of different malignancies from each other.

METHODOLOGY

Mouse ovarian surface epithelial (MOSE) cells of increasing malignancy and enriched in TICs (MOSE-L_{FFLv}) were captured using cDEP. These cells were pumped through a microfluidic device containing an array of posts. An electric field was applied across the channel, causing cells to trap on the posts in the chip if the forces balanced [2]. This electric field was applied across the chip, and different voltages were tested for their ability to trap cells based on their phenotype. Cells were sequentially trapped and released by turning on and off the voltage. This trapping was recorded on video.
A computer program was developed to discriminate moving cells from stationary cells in the chip using median filter processing.

RESULTS

Both the MOSE-preIV (malignant cancer cells) and MOSE-L_{FFLv} (very malignant, enriched in TIC-like cells) were run through the chip. The trapping voltage for each cell type was determined.

Table 2: Trapping range of MOSE cells.

	MOSE-preIV (malign ant)	**MOSE-L_{FFLv} (highly malignant)**
5 µl/min	~200V – 270 Vrms	~150V – 200 Vrms
10 µl/min	>300 Vrms	~200V - 270 Vrms

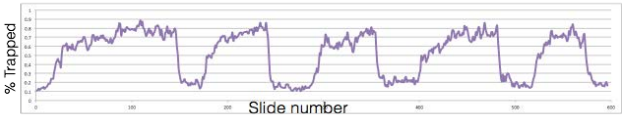

Figure 1: Percent MOSE-FFL cells trapped at 10 µl/min, 268 Vrms and 200 kHz while turning the voltage on/off.

CONCLUSIONS

Through the use of cDEP, it was possible to determine a trapping range for cancer cells of different malignancies. A voltage range (between 270 and 300 Vrms) was found to trap one malignancy level of the MOSE cells while not trapping the other cell type, indicating the possibility for high throughput sorting of different stages of cancer cells.

ACKNOWLEDGMENTS

I would like to thank the MultiSTEPS IGERT.

REFERENCES

1. Zhou, B.S. et al., *NatureReviews Drug Discovery*, 2009
2. Salmanzadeh, A. et al. *Lab on a Chip*, 2013.

Virginia Tech
Wake Forest University
School of Biomedical Engineering and Sciences
14th Annual Graduate Student Research Symposium, May 13, 2015

SUPPORT VECTOR MACHINE CLASSIFICATION OF COMPLEX VALUED FMRI DATA

Amnah M. Eltahir[1], Jonathan M. Lisinski[1], Scott J. Peltier[3], and Stephen M. LaConte[1,2]
1. Virginia Polytechnic Institute and State University
2. Virginia Tech Carilion Research Institute
3. University of Michigan
Corresponding Author: Amnah Eltahir, Email: amnah@vtc.vt.edu

INTRODUCTION

3dsvm is a tool used in support vector machine (SVM) classification of functional magnetic resonance imaging (fMRI) data. This software creates a classifier based on training data that can classify independent test data [1].

When fMRI data are collected, they are encoded as complex valued frequency and phase in what is referred to as "k-space." These data are then converted to an image using a Fourier transform in what is referred to as "image-space."

Typical fMRI studies only use the magnitude of data in the image space. We tested the accuracy of the classifier for fMRI data in both image space and k-space using magnitude, phase and complex data.

METHODOLOGY

Six subjects were scanned. Each subject performed alternating 20 second blocks of left and right finger tapping, using their index fingers to rapidly press the buttons of a fiber-optic button box.

Both magnitude and phase, as well as real, imaginary and complex fMRI data were compared. Two sets of data were collected. One data set was used for training with 3dsvm, while the other was tested. The classifier determined from the brain state which finger was tapping. The data were switched and reclassified. The average accuracies of the classifiers were compared to the findings of the Peltier et al. paper [1].

RESULTS

Accuracies in image and k-space were compared using magnitude, phase and complex data.

Table 1: Summary of 3dsvm results using image space and k-space data.

Trained/Tested	Data 1→2	Data 2→1	Reported
Image Magnitude	99.7±0.3	98.7±0.6	95.5±1.8
Image phase	53.2±9.5	52.6±5.7	58.5±3.6
Image Complex	90.4±7.3	89.2±5.0	93.3±2.3
K-space Magnitude	92.8±2.9	92.8±2.6	94.5±3.0
K-space Phase	63.4±8.4	64.2±1.1	69.0±2.1
K-space Complex	92.3±0.6	88.2±1.6	88.0±4.1

Magnitude data in the image space provided the greatest accuracy. This is what is typically used in MRI studies. The k-space data was comparable with the image space data overall.

CONCLUSIONS

Our results corroborate the findings of the Peltier et al. paper [1]. Accuracy in k-space may improve in future work by developing a standardized k-space similar to the Talairach coordinates, which is the standardized coordinate system used in fMRI studies.

ACKNOWLEDGMENTS
Thank you to the LaConte lab and Dr. Scott Peltier for providing the data and tools to do this work. Thank you to the New Horizons Scholars program for sponsoring me.

REFERENCES

[1] S. J. Peltier, J. M. Lisinski, D. C. Noll, S. M. LaConte. Support vector machineclassification of complex fMRI data. Conf Proc IEEE Eng Med Biol Soc, 1:5381-5384, 2009.

Virginia Tech
Wake Forest University
School of Biomedical Engineering and Sciences
14th Annual Graduate Student Research Symposium, May 13, 2015

GAP JUNCTIONAL COUPLING MODULATES THE CONDUCTION VELOCITY-EPHAPTIC COUPLING RELATIONSHIP

Michael W. Entz II[1], Sharon A. Geoge[1], Michael Zeitz[2], James W. Smyth[2], and Steven Poelzing[1]
1. Virginia Polytechnic Institute and State University, School of Biomedical Engineering and Sciences
2. Virginia Tech Carillion Research Institute
Corresponding Author: Michael W. Entz II, Email: mentz2@vt.edu

INTRODUCTION

Recent studies suggest that ephaptic coupling (EpC) modulates cardiac conduction velocity dependence on gap junctions (CV-GJ relationship)[1,2]. However, it remains unknown whether GJ can modulate the CV-EpC relationship. EpC is modulated by extracellular sodium and potassium, sodium channel availability, and perinxal width as shown in experimental work as well as mathematical models[3].

HYPOTHESIS:

Normal GJ coupling masks the CV-Ep relationship.

METHODOLOGY

Guinea pig ventricles were Langendorff perfused with two solutions with varying Na+ and K+ (solution A – High Ep: $[Na^+]o$=153 and $[K^+]o$=4.6mM, solution B – Low Ep: $[Na^+]o$=145 and $[K^+]o$=7mM). Gap junctions were inhibited with carbenoxolone (CBX) (0, 15, and 30 μM). Sodium channel availability, and thereby Ep coupling, was reduced by increasing pacing rate (200 and 375 beats per minute). Epicardial conduction was quantified by optical mapping. Perinexal width was measured with transmission electron microscopy. Cx43 gap junction expression and phosphorylation levels were evaluated by western blotting.

RESULTS

At modest to no GJ uncoupling (CBX: 0 and 15μM), there were no CV differences between solution A or B, independent of pacing rate. At 30 μM CBX, there were no CV differences between solution A and B at 200 bpm. However, increasing pacing rate to 375bpm only decreased longitudinal and transverse CV in preparations perfused with solution B, suggesting that nominal GJ coupling may mask the CV-Ep relationship. Solution composition did not alter perinexal width, nor did it change total and p368 Cx43 expression. These data suggest that CV changes due to solution composition were not a result of altered perinexal width or GJ coupling.

CONCLUSIONS

We provide evidence that the CV-Ep relationship depends on GJ coupling. These data suggest that Ep coupling may be a novel therapeutic target particularly during loss of gap junctions.

ACKNOWLEDGMENTS

This work was supported in part by grants from the National Institutes of Health (R01 HL102298-01A1 to SP) and Virginia Tech Carilion Research Institute Medical Research Scholars Award to ME.

REFERENCES

1. Veeraraghavan et al. Sodium channels in the Cx43 gap junction perinexus may constitute a cardiac ephapse: an experimental and modeling study. Pflugers Arch, 2015
2. George et al. Extracellular sodium and potassium levels modulate cardiac conduction in mice heterozygous null for connexin43 gene. Pflugers Arch, 2015.
3. Lin et al. Ephaptic coupling in cardiac myocytes. IEEE Trans Biomed Eng, 2013.

RELATING TRAUMATIC BRAIN INJURY IMPACT KINEMATICS TO NEUROCHEMICAL CHANGES AND PHYSICAL DAMAGE IN THE GÖTTINGEN MINIPIG

Elizabeth M. Fievisohn[1], Sujith V. Sajja[1], Pamela J. VandeVord[1,2], and Warren N. Hardy[1]
1. Center for Injury Biomechanics (Virginia Polytechnic Institute and State University, Virginia Tech-Wake Forest School of Biomedical Engineering and Sciences)
2. Salem VA Medical Center, Research & Development Service
Corresponding Author: Elizabeth Fievisohn, Email: lizf87@vt.edu

INTRODUCTION

Current automotive crash test standards use the Head Injury Criterion (HIC) to assess head injury, but this metric does not relate an impact to underlying damage[1]. The overarching goal of this study was to develop an improved injury metric that relates impact parameters to the resulting neurochemical changes and physical damage. The injury caused by the two devices over the course of 24 hours in the Göttingen minipig is described here.

METHODOLOGY

Acute TBI, generated using the translation-input (28-70G) or combined-input injury device (1000-4500 rad/s^2; 7-11 rad/s) (n=13/group and n=3 shams), was characterized using proton magnetic resonance spectroscopy (MRS) to determine neurochemical changes in the brain, and immunohistochemistry (IHC) to define underlying damage in the genu of the corpus callosum. Baseline MRS scans were collected before injury, one hour, 24 hours, and up to 72 hours after injury. IHC staining was used to identify axon cytoskeletal damage with light and heavy neurofilament (NF), astrocyte activation by highlighting glial fibrillary acid protein, microglial activation with iba-1, complete axonal disruption with β-amyloid precursor protein (β-APP), and programmed cell death with cleaved caspase-3.

RESULTS

Two-tailed Student's t-tests showed significant increases in the amount of light and heavy NF present in the experimental animals compared to sham controls for each device ($p<0.05$). No other significant differences were found in the other IHC analyses.

Repeated measures ANOVA with LSD post hoc tests found numerous significant neurochemical changes between the time points within each device experimental group ($p<0.05$). Notably, there were relationships common between the experimental groups that suggest myelin damage[2]. The observed neurochemical changes also indicated important dissimilarities. The translation-input group displayed a neurochemical response suggesting energy crisis with an increase in glutamine[3]. The combined-input group revealed excess glutamate, which is indicative of excitotoxicity[4].

CONCLUSIONS

Importantly, MRS and IHC results will be related to the impact kinematics so that neurochemical changes and underlying damage can be predicted based on the kinematics input. Due to the high incidence of traumatic brain injury, developing a new injury metric will help improve prevention strategies, especially in the automotive industry.

ACKNOWLEDGMENTS

This work was funded in part by the National Highway Traffic Safety Administration.

REFERENCES

1. Versace J. A Review of the Severity Index. *Proc.of the 15th Stapp Car Crash Conf.* 1971; 771-796.
2. Ross B, Bluml S. Magnetic Resonance Spectroscopy of the Human Brain. *The Anatomical Record (New Anat.).* 2001; 265:54-84.
3. Harris JL, et al. Altered Neurochemical Profile After Traumatic Brain Injury: ^{1}H-MRS Biomarkers of Pathological Mechanisms. *Journal of Cerebral Blood Flow & Metabolism*. 2012; 32:2122-2134.
4. Ramonet D, et al. In Vivo Neuroprotective Adaptation of the Glutamate/Glutamine Cycle to Neuronal Death. *Hippocampus*. 2004; 14:586-594.

SINGLE AND DUAL-TASK TURNING IN RECENTLY CONCUSSED ATHLETES AND MATCHED CONTROLS: PRELIMINARY RESULTS

Peter C. Fino[1], P. Gunnar Brolinson[2], and Maury A. Nussbaum[3]
1. Department of Mechanical Engineering, Virginia Tech
2. Edward Via College of Osteopathic Medicine
3. Department of Industrial and Systems Engineering, Virginia Tech
Corresponding Author: Peter Fino, Email: fino@vt.edu

INTRODUCTION

Typical sports-related concussion symptoms resolve within 7-10 days post-concussion [1]. However, use of challenging motor control tasks indicate that deficits can persist beyond this typical timeframe [2]. Changes to turning mechanics due to concussions and their potential impact on performance and / or injury remain unknown. This study examined turning in recently concussed collegiate athletes and matched controls after the athletes were cleared to return to play to examine differences in path curvature and mediolateral (ML) inclinations.

METHODOLOGY

Four recently concussed athletes (C) and four healthy matched controls (H) were tested a mean (SD) of 23 (2) days after each concussion. The C athletes were cleared 12 (3) days post-concussion. Participants walked around a course marked with 1.5 m tall pylons as shown in Figure 1. Participants walked at their normal pace (single task = ST) around the course 14 times, seven laps in each direction. Participants then repeated the procedure while serially subtracting by sevens (dual task = DT).

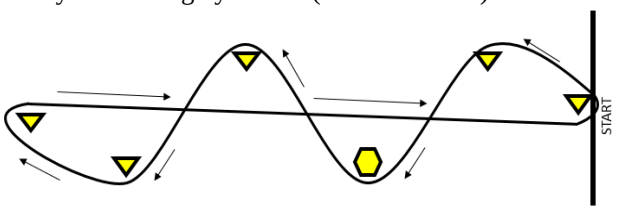

Figure 1: Depiction of the 18 m long course. Triangles indicate pylons, and the hexagon indicates the pylon location where motions were tracked.

Kinematic data were collected at 120 Hz using four ProReflex cameras located around the middle pylon. The upper body center-of-mass (COM_{UB}) location was estimated as the mean of the xiphoid process and T9 vertebral markers. The mean horizontal curvature of each turn and the ML inclination angle (θ) at three heel contacts (Pre-Apex, θ_{Pre}, Apex, θ_{Apex}, Post-Apex, θ_{Post}) were compared using GEE models with compound symmetric covariance structures.

RESULTS

Significant group differences were found for mean curvature ($p = 0.012$) and θ_{Pre} ($p = 0.002$).

CONCLUSIONS

The group differences in curvature and θ_{Pre} support other studies that suggested concussions may affect dynamic tasks, even after athletes return to play [2]. The lower curvatures found here suggest a potential effect on performance as recently concussed athletes take wider, less abrupt turns that may inhibit their ability to respond to competitive demands. Furthermore, the decreased θ_{Pre} suggests delayed anticipation of the turn and may manifest in declined performance and / or increased injury risk. It is unclear whether these differences are caused by the neurophysiology of the concussion or due to potential detraining during recovery. Overall, these results encourage further research examining the effects of concussions on turning behaviors and on the competitive readiness of athletes returning from concussions.

ACKNOWLEDGMENTS

The first author (PCF) was supported by an NSF Graduate Research Fellowship (Grant No. DGE 0822220).

REFERENCES

1. McCrory P, et al. *Br J Sports Med* 45.5, 250-258, 2013.
2. Powers KC, et al. *Gait Posture* 39, 728-732, 2014.

Virginia Tech
Wake Forest University
School of Biomedical Engineering and Sciences
14th Annual Graduate Student Research Symposium, May 13, 2015

THE HISSING COCKROACH AS A MODEL FOR ADAPTABLE MICROFLUIDIC SYSTEMS

Joel Garrett[1], Rafael Davalos[1], Jake Socha[1]
1. Virginia Tech, Department of Biomedical Engineering and Mechanics
Corresponding Author: Joel Garrett, Email: jfg@vt.edu

INTRODUCTION

All insects use pressure gradients produced by metabolism to move gas diffusively through an internal tracheal system. Some species augment this gas exchange using tracheal compression, a volume displacement of the tracheal tubes that generates bulk flow of air. At least three distinct behaviors are thought to affect such flow: abdominal pumping, collapse of internal tracheal tubes, and active opening and closing of spiracles. The specific coordination of these events should influence internal and external airflow patterns, and therefore may vary with changing environmental conditions and metabolic demands.

Understanding the mechanisms by which insects manipulate airflow within their bodies is a promising avenue of research for developing novel biologically-inspired technologies. Particularly within the realm of microfluidics, the internal physiology of insects could result in devices that are able to produce efficient flow at small size and with low energy requirements, mix fluids at very low Reynolds numbers, or provide effective 3D geometries for perfusion schema within engineered tissues.

METHODOLOGY

Due to its relatively large size and conveniently visible spiracle anatomy, the Madagascar hissing cockroach *Gromphadorhina portentosa* is a useful model for studying the coordination of respiratory behaviors. We used these roaches to study how the animal modifies its respiratory behavior to compensate for a reduced and excess availability of oxygen. The Advanced Photon Source at Argonne National Laboratory was used to capture X-ray video of internal abdominal structures, while the abdomen and abdominal spiracles were recorded using separate visible-light video cameras. Micro computed tomography (µCT) was carried out on sacrificed specimens to construct detailed 3D renderings of the internal structures.

RESULTS

Quantitative assessment of abdominal pumping reveals a significant increase in abdominal pump frequency correlating with reduced oxygen concentrations. We also observed a significant increase in spiracle conductance below a critical hypoxia threshold (3% O_2). This increased average conductance seems to be a result of increased "flutter" time of the spiracles between abdominal pump events.

CONCLUSIONS

We have observed that the hissing cockroach is able to modulate its respiratory functions in response to hypoxic and hyperoxic environments. Understanding how the hissing cockroach modulates its respiratory behavior in response to changing atmospheres contributes to our growing understanding of ventilation by tracheal compression in insects. Additionally, by drawing on the dynamics of this system as inspiration for microfluidic pumps, we have gained new insight into potential areas of development for flow systems that adapt to changing conditions and seamlessly integrate advective and diffusive flow.

ACKNOWLEDGEMENTS

Supported by NSF 0938047 and DE-AC02-06CH11357. Thanks to the Socha lab, the Davalos lab, and Dr. Jason Davis.

Virginia Tech
Wake Forest University
School of Biomedical Engineering and Sciences
14th Annual Graduate Student Research Symposium, May 13, 2015

A REVIEW OF RAPID PROTOTYPING APPLICATIONS FOR SURGICAL IMPLANTS

Gregory J. Gillispie[1], Philip J. Brown[1], and Joel D. Stitzel[1]
1. Center for Injury Biomechanics (Wake Forest, BME)
Corresponding Author: Gregory Gillispie, Email: ggillisp@wakehealth.edu

INTRODUCTION

Additive manufacturing (AM), commonly known as 3D printing, is a process in which material is laid down layer by layer according to a computer model. This method is beneficial for complex parts and for manufacturing small quantities because more common processes have geometric limitations and the high initial costs for tooling. AM is a rapidly expanding field, especially for medical applications where each patient is unique and complex geometries are the norm. Anyone with access to a 3D printer can develop a novel idea for its use. Applications have been growing so quickly and are published so rarely that communication has become a rate limiting factor for the implementation of these beneficial technologies[1].
According to the classification system proposed by Tuomi et. al[1], the medical uses for AM can be placed into five areas, one of which is inert implants. These are implanted in the body long-term, but do not contain live cells. Most reviews of AM technology have been broad in scope and do not touch the category of implants in depth, which is what this review will attempt to do.

METHODOLOGY

Journal publications and news articles have been used to gather information. Additionally, physician interviews will be conducted for supplemental information on unpublished works.

RESULTS

Dental implants are the most well-established 3D printed implants and occupy the largest share of the market at $175 million in 2014[2]. Similarly, 99% of hearing aids made are 3D printed[3]. Another major success has been prosthetics. Hands for children can be made cheaply to combat the fast rate they outgrow them and better fitting limb sockets decrease irritation in adults. These are all class 1 medical devices with minimal regulations, which has greatly facilitated their success[3].
Inside the body, porous titanium can be printed to facilitate boney ingrowth[4]. Cranial and maxillofacial surgeries frequently employ 3D printed implants. Patient anatomy is very individualized and perfectly matching implants are important from a visual standpoint. Each skull fracture location and pattern is unique, making a universal cranial plate nearly impossible[3]. The first whole bone printed and implanted was a mandible in the U.K. The company ConforMIS has been printing both components of total knee replacements since 2011 with excellent results. Chinese doctors have successfully printed and implanted a full clavicle, scapula, spinal axis, and pelvic ileum after removing cancerous tumors.

CONCLUSIONS

As additive manufacturing continues to grow, so will its applications for implants. Future work is needed to provide more clinical trials because many uses to date have been case studies. Additionally, an organized platform for sharing techniques would be very beneficial. This review has also highlighted that nearly all developments in this field come from outside the U.S. The major advantage of printed implants is their uniqueness which becomes a disadvantage when going through the strong regulation such as the FDA.

REFERENCES

1) A novel classification and online platform for planning and documentation of medical applications of AM, Tuomi 2014. **2)** Tissue engineering and dental implants set to boost 3D printing in healthcare to a $1.2 billion market by 2020, Matthews 2015. **3)** Adding value in additive manufacturing: researchers in the UK and Europe look to 3D printing for customization, Banks 2013. **4)** Additive manufacturing technology as a novel approach to fabricate functionally graded titanium implants, Lin 2013.

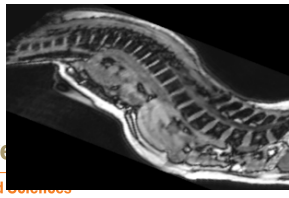

14th Annual Graduate Student Research Symposium, May 13, 2015

A METHOD TO QUANTIFY SUPINE TO PRONE THORACOABDOMINAL DEFORMATION AND ORGAN MIGRATION IN A SET OF HEALTHY YOUNG ADULTS

Berkan Guleyupoglu[1, 2], Josh C. Tan[1, 2], Craig A. Hamilton[1, 2], and F. Scott Gayzik[1, 2]
1. Wake Forest University School of Medicine
2. Virginia Tech – Wake Forest University School of Biomedical Engineering and Sciences
Corresponding Author: F. Scott Gayzik, Email: sgayzik@wakehealth.edu

INTRODUCTION

Medical imaging is a valuable tool in the study of biomechanics. Imaging in different postures (i.e. prone vs. supine) furthers understanding of how the body adapts and morphs internally to postural changes. Such data can inform computational modeling and medical device design optimization and in particular allows for the development of computational human body models which can be used as a platform to virtually evaluate design concepts. However, medical image data used in biomechanics studies are often retrospectively acquired, and researchers are unlikely to encounter scans of healthy individuals with the pulse sequences, resolution, and anatomy desired in the data set. The purpose of this study was to obtain a dataset and evaluate the effects of prone to supine postural adjustment in a set of healthy young adults, specifically analyzing thoracoabdominal compression and organ migration. [1]

METHODOLOGY

We prospectively acquired scans in both prone and supine postures from 22 healthy young adults; M:F 1:1, with age, height, and weight of 28.8±7.0 years, 173.0±7.8 cm and 70.6±10.9 kg. While prone, subjects' arms were superior to the head and supported by a foam insert at the axilla. Breath held, T1-weighted MRI scans were acquired using a Siemen's Skyra 3T with an in-plane resolution of 1.56 mm (TR: 4.10 ms, TE: 1.23 ms, thickness: 2 mm, matrix: 256x256, FOV: 400 mm).

RESULTS

Gross compression was found to be 9.0% (71.6±12.9 mm prone vs. 78.7±12.4 mm supine; p=0.0013). Gender differences were not noted. Liver and spleen compression were found to be 17.7% (110.4±4.1 mm prone vs. 134.8±2.6 mm supine; p<0.0001) and 3.5% (53.8±1.9 mm prone vs. 57.3±2.9 mm supine) respectively. Liver migration occurred with an average of 8.3 mm posterior movement, 11.4 mm rightward movement and 15.1 mm superior movement. The spleen migrated on average 4.1 mm anteriorly, 6.1 mm towards to right side of the body and 1.7 mm superiorly.

Figure 1: Subject in supine (B) and prone (T) postures, sagittal view.

CONCLUSIONS

Posture has a significant effect on gross thoraco-abdominal and liver compression as well as liver migration. No significant effects were found for the spleen. This dataset can be used to further understand how supine to prone positioning can affect morphology and migration of thoraco-abdominal contents in healthy young adults. Gender differences were not noted in the initial study of gross compression. The data obtained from this set may be of use in computational biomechanics studies, surgical simulation, and medical device design.

ACKNOWLEDGMENTS

This work was sponsored by the U.S. Army Research Lab through cooperative agreement W911NF-13-2-0039

REFERENCES

[1] Gayzik FS, et al., Annals of BME, 2011, Vol 39, pp. 2568-2583.

Virginia Tech
Wake Forest University
School of Biomedical Engineering and Sciences
14th Annual Graduate Student Research Symposium, May 13, 2015

HUVEC AND MPC GROWTH AND MATURATION IN VITRO

Laura Hernandez-Cruz[1,2], Zhan Wang [2], and Shay Soker[1,2]
1. Virginia Tech – Wake Forest School of Biomedical Engineering and Sciences
2. Wake Forest Insitute of Regenerative Medicine
Corresponding Author: Laura Hernandez-Cruz, Email: lahernan@wakehealth.edu

INTRODUCTION

Healthy function of skeletal muscle involves the cooperation of several cell types. This work explores the behavior of two types of cells involved in skeletal muscle development: fluorescently labeled myogenic progenitor cells (MPC) and human umbilical vein endothelial cells (HUVEC) both individually and in co-culture.

METHODOLOGY

Primary MPC were derived from transgenic GFP mice. The cells were seeded on a tissue culture plate coated with a Matrigel solution. Fluorescent images were taken every two days using an inverted microscope. The images were analyzed for an understanding of MPC differentiation in vitro.

In order to observe the formation of capillary like structures, a capillary formation assay was conducted with mKate labeled HUVEC. A Matrigel coated 96 well plate was seeded with HUVEC. Images were taken at selected intervals over 24 hours. These images were studied for the formation and dissociation of capillary-like structures.

For the co-culture of HUVEC and MPC, the cells were seeded on a Matrigel coated tissue culture plate in a 1:1 ratio. A mixed media of equal parts myogenic and endothelial cell media was used. As before, images were taken every other day to observe the behavior of both types of cells.

RESULTS

Individual myogenic progenitor cells are initially visible as single cells. Over time, these cells elongate and fuse with adjacent cells to form myotubes. These myotubes continue to grow longer and reach their peak around 11 days after seeding.

The fluorescent images of the HUVEC assay showed the formation of capillary-like structures from the individual HUVEC and the beginning of their dissociation. The most highly developed capillary-like structures were observed at 12 hours. At 24 hours, significant dissociation of the structures had occurred.

In co-culture, MPC continued to fuse together and form myotubes as in solitary culture. HUVEC did not form capillary-like structures but remained as single cells.

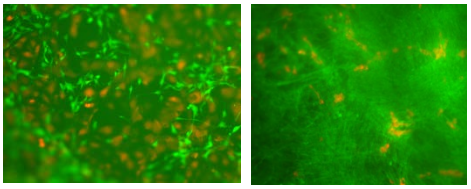

Figure 1: The co-culture of mKate labled HUVEC and GFP MPC at day 1 (left), and day 4 (right)

CONCLUSIONS

Using fluorescence microscopy, it is possible to see the MPC fiber formation and HUVEC formation of capillary-like structures. In co-culture, MPC are able to continue forming fibers, while HUVEC are unable to form capillary like structures.

Future studies will focus on methods to modulate the growth and development of MPC and improve HUVEC development in co-culture.

ACKNOWLEDGMENTS

Thanks to Etai Sapoznik for helping with the labeling of the HUVEC

TWO- AND THREE-DIMENSIONAL *IN VITRO* MODELS OF BLAST-INDUCED NEUROTRAUMA

Nora Hlavac[1], Samuel Miller[1], Pamela VandeVord[1,2]
1. Virginia Tech, Biomedical Engineering and Mechanics
2. Veteran Affairs Medical Center, Salem, VA
Corresponding Author: Nora Hlavac, Email: nhlavac@vt.edu

INTRODUCTION

Blast-induced neurotrauma is a growing concern in military personnel, with about 75% of casualties in recent military endeavors involving explosives [1]. Astrocytes play a critical role in the central nervous system's response to injury [2]. Astrocyte reactivity to injury is characterized by increased proliferation as well as up-regulation of particular activation markers [2-3]. The role of astrocyte activation in both neuroprotection and degeneration has been explored [2, 4], however, the response is still not completely understood. This study aimed to compare two- and three-dimensional *in vitro* models in which cells were exposed to overpressure profiles characteristic of blast. The effects of both exposure and environment were assessed by measuring cell viability and gene expression changes of potential reactivity biomarkers.

METHODOLOGY

C6 astroglioma cells (ATCC, CCL-107) were used in two- and three-dimensional *in vitro* models to characterize acute astrocyte response and reactivity to a peak overpressure of 18-20 psi (124-138 kPa). A custom shock wave generator was used to expose the cells to overpressure. Cell viability was measured at 24 and 48 hours post-exposure using an MTT assay. Changes in gene expression were also evaluated using real-time, reverse transcription polymerase chain reaction (RT-PCR) at 48 and 72 hours post-exposure. Fold changes for each target (Table 1) were calculated relative to a sham group (similar testing methods with the exception of exposure to overpressure).

Table 1: Gene targets of interest for astrocyte reactivity.

Target	Classification/Function
Glial fibrillary acidic protein	intermediate filament, mechanical strength
β-actin	cytoskeletal protein, shape, integrity
Vinculin	cytoskeletal protein, anchors actin
Piezo2	transmembrane protein, cation channel, mechanosensor
Ezrin	peripheral membrane protein, adhesion, communication
Mitogen-activated protein kinase kinase 1	enzyme, stimulates MAP kinases pathways (proliferation)

RESULTS

Minimal cell death occurred in either model as a result of overpressure exposure (Figure 1). Changes in gene expression of GFAP were significant in both models ($p<0.05$), with up-regulation occurring at different time points. This suggests different time periods of activation relative to environment. Piezo2 was up-regulated in the three-dimensional model at 72 hours, but not in the two-dimensional model. Actin expression was not significantly different for either model, suggesting that the integrity of the actin cytoskeleton was not compromised as a result of overpressure exposure.

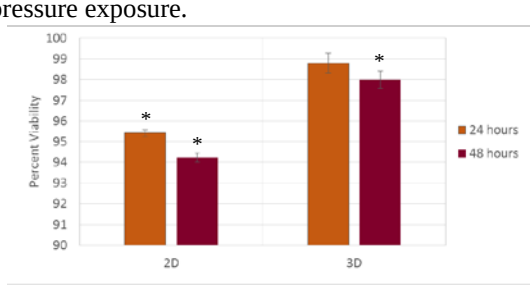

Figure 1: Cell viability at 24 and 48 hours post-exposure. *$p<0.05$ compared to sham at 100%

CONCLUSIONS

Overall, the peak overpressure used in this study did not cause significant loss of cells. However, results suggest that astrocytes have differential periods of activation in response to shock wave exposure depending on their surrounding environment.

REFERENCES

[1] Cernak I, Noble-Haeusslein LJ (2010) J Cereb Blood Flow Metab 30, 255-66.
[2] Buffo A, et al. (2010) Biochem Pharmacol 79 (2), 77-89.
[3] Sofroniew MV (2009) Trends Neurosci 32(12), 638-47.
[4] Pekny M, et al. (2014) Neurosci Lett 565, 30-8.

Virginia Tech
Wake Forest University
School of Biomedical Engineering and Sciences
14th Annual Graduate Student Research Symposium, May 13, 2015

GEOMETRICAL CUES MEDIATE THE INVASION OF ENDOTHELIAL CELLS IN COLLAGEN I HYDROGEL

Yahya Hosseini[1], Masoud Agah[1,2], and Scott S. Verbridge[2]
1. Virginia Tech, The Bradley Department of Electrical and Computer Engineering
2. Virginia Tech, Department of Biomedical Engineering and Mechanics
Corresponding Author: Yahya Hosseini, Email: hosseini@vt.edu

INTRODUCTION

Endothelial cells sprout and form neovessels from sharp corners of microchannels but it is unknown how cells respond to the curvature index, which represents the topography of basement membrane structures of blood vessels, or to more complex geometries such as bifurcations. To understand these effects, we have fabricated collagen hydrogel devices with different degrees of sharpness and curvature controlled by microfabrication strategies. The effects of geometrical cues and matrix microstructure were analyzed by measuring the invasion frequency and distance of endothelial cells from sites of interest.

METHODOLOGY

Collagen hydrogel with the final concentration of 7.5–10mg/ml was pipetted onto a coverslip with supports on both sides, then, a PDMS stamp is cast against the neutralized solution and polymerized at 37°C for 30 minutes. Figure 1.a shows the confocal image of one of the fabricated sharp structures in collagen hydrogel.

RESULTS

Human umbilical vein endothelial cells were seeded on top of the devices uniformly to fill the channel with structures. Growth factors (VEGF:33ng/ml and TPA:33ng/ml) were added on days 1 and 3, along with fresh media, and on day 5 cells were fixed. Figure 1.b shows the confocal image of cell invasion from one of the sharp sites. Table 1 shows the dimension of the curved and sharp structures, invasion frequency per structure, and average invasion distance per structure (n=15). As it can be noted, the invasion frequency is higher from sharper and curved structures compared with less sharp and curved structures. Furthermore, sharp corners are deformed to rounded structures and cell invasion is slightly higher from curved structures for geometries b and c.

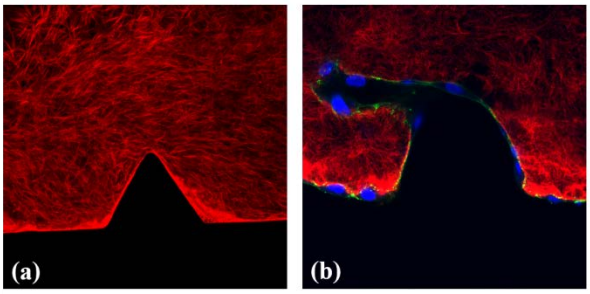

Figure 1: Confocal image of fabricated sharp structure in collagen hydrogel (a) before cell culturing, and (b) 5 days after cell culturing

	depth (μm)	*width (μm)*	*Invasion Frequency*	*Invasion Distance (μm)*
Sharp *a*	100	50	1.4	81.7
Curved *a*			1.33	88.4
Sharp *b*		125	0.6	93.5
Curved *b*			1	86.0
Sharp *c*		250	0.46	77.3
Curved *c*			0.53	112.3

Table 1: Dimension of different structures along with cell invasion distance and frequency.

CONCLUSIONS

The results obtained from this study can give us new insights on the effect of biologically-inspired geometries on the growth of tumor by cell sprouting from specific sites, and to further investigate the effect of anti-angiogenic factors to reduce tumor growth.

ACKNOWLEDGMENTS

We would like to thank the *Institute for Critical Technology and Applied Science* (ICTAS), the National Science Foundation (CBET-1403304), and the National Institutes of Health (NIBIB-R21EB019123) for financially supporting this project.

HEMOSTATIC NANOPARTICLES MITIGATE INTERNAL BLEEDING AND LUNG PATHOLOGY AFTER BLAST POLYTRAUMA

W. Brad Hubbard[1], Margaret Lashof-Sullivan[2], C. Shaylen Hall[1], Carly Norris[1], Erin Lavik[2] and Pamela VandeVord[1,3]
1. Virginia Tech, School of Biomedical Engineering and Sciences
2. Case Western Reserve University, Department of Biomedical Engineering
3. Research Services, Veterans Affairs Salem, VA
Corresponding Author: Dr. Pamela VandeVord, Email: pvord@vt.edu

INTRODUCTION

In response to the lack of therapeutics for internal bleeding following a traumatic event, we synthesized hemostatic dexamethasone nanoparticles (hDNP) to help alleviate internal hemorrhaging. Blood loss is the primary cause of death at acute time points post injury in both civilian and battlefield traumas and there is a lack of internal bleeding therapeutics available for in theatre usage. This study examines potential therapeutic effects of hDNP on acute physiology and subacute recovery in lung pathology after blast polytrauma.

METHODOLOGY

hDNP consist of a block copolymer, poly (lactic-co-glycolic acid) – poly (l-lysine) – poly (ethylene glycol) conjugated to a peptide, glycine-arginine-glycine-aspartic acid-serine (GRGDS). These particles were evaluated as treatment in a rodent polytrauma model. Rats placed into hDNP and control groups (control DNP and Lactated Ringer's) were exposed to blast and given injection. Physiology recordings were collected one hour after injury. Seven days post-blast, lung tissue was extracted and stained with H&E. Fluorescent protocols for TNF-alpha, caspase-3, and TUNEL were performed and quantified.

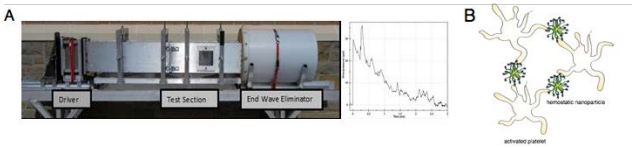

Figure 1: (A) Advanced Blast Simulator at VT and representative blast wave. (B) Schematic of the role of hDNP binding with activated platelets.

RESULTS

Oxygen saturation and heart rate were increased in the hDNP and control groups compared to other blast controls. Amount of hemorrhaging in the lung was decreased in hDNP and control groups compared to blast controls. Markers of cellular death and inflammation were decreased in hDNP compared to blast controls at 7 days.

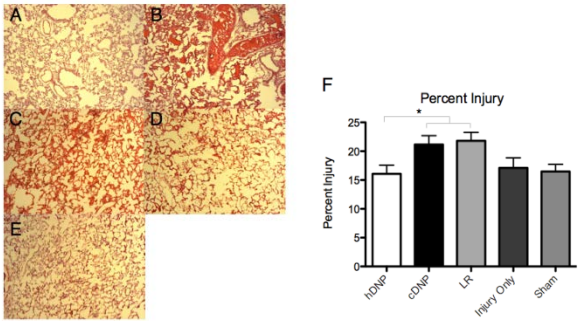

Figure 2: Representative H&E staining for (A) hDNP (B) cDNP (C) LR (D) IO and (E) Sham. (F) The hDNP and sham demonstrated a decreased lung injury level compared to the cDNP and LR groups (* $p < 0.05$).

CONCLUSIONS

Targeting activated platelets creates efficiency of dexamethasone's therapeutic effect (Lashof-Sullivan, 2014). Administration of hDNP has the potential to be a viable option for open field trauma care because of its effectiveness in reducing lung damage and improving oxygen exchange as well as ease of delivery. Treatment with hDNP significantly increased acute oxygen saturation, decreased acute hemorrhaging and alleviated cellular damage of lungs at a subactute stage.

ACKNOWLEDGMENTS

The authors would like to recognize the funding sources: DOD CDMRP Program W81XWH-11-1-0014 and NIH Director's New Innovator Award number DP20D007338.

REFERENCES

Lashof-Sullivan, M. M., et al. *PNAS* **2014,** *111* (28), 10293-8.

ENHANCED ENDOTHELIAL CELL ATTACHMENT VIA ANTIBODY CONJUGATION: TOWARD KIDNEY IMPLANTATION USING AUTOLOGOUS CELL SOURCES

Jennifer Huling[1], Ethan Bassin[1], In Kap Ko[1], Anthony Atala[1] and James Yoo[1]
1. Wake Forest Institute for Regenerative Medicine, Wake Forest School of Medicine
Corresponding Author: Jennifer Huling, Email: jhuling@wakehealth.edu

INTRODUCTION

The only definitive treatment for end stage renal disease is renal transplantation, however a shortage of kidney donors has created a long waiting lists for patients. Recent progress in whole organ decellularization techniques suggests that this method could eventually be used in transplantation. One major challenge for long-term in vivo success of bioengineered kidneys is vascular patency, which requires complete endothelial reseeding of the decellularized organ matrices. Preliminary efforts to re-endothelialized decellularized kidneys saw detachment of the endothelial cells after implantation. To address this issue, we developed an endothelial cell seeding method, in combination with antibody conjugation technique that enhances endothelial cells attachment.

METHODOLOGY

Primary endothelial cells (pEC) were collected from adult pigs. Appropriate phenotype was confirmed with CD31 staining. To prepare the flow chamber, glass slides were coated with collagen to mimic the ECM environment in a decellularized kidney. CD31 antibody was attached to the collagen surface with an EDC/NHS crosslinking reaction. Antibody-coated slides were placed in the flow chamber and protein blocked before introducing the pECs. After the cells settled onto the bottom of the flow chamber, increasing flow through the chamber induced cell detachment. Cell numbers were counted with ImageJ. Two control groups were tested: collagen-only slides and antibody coated slides seeded with CD31 pretreated cells.

RESULTS

Cell detachment was significantly reduced with the addition of CD31 antibody. At the highest flow rate only 14% or the original seeded cells remained on the collagen only surface. In contrast, 73% of the cells remained on the antibody-coated surface. Pre-treating the cells with the CD31 antibody interfered with the cell's ability to bind with the surface-bound CD31, resulting in higher detachment rates. These results support the idea that antibody coating the vessels in a decellularized kidney would prevent cell detachment after implantation and help prevent clotting.

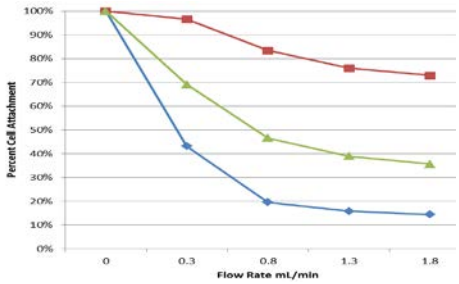

Figure 1: Cell detachment data. Red: Antibody, Green: Pre-treatment, Blue: collagen only.

CONCLUSIONS

Conjugation of CD31 antibody to collagen surfaces reduces detachment of primary procine endothelial cells.

ACKNOWLEDGMENTS

This study was supported, in part, by the SENS Research Foundation.

REFERENCES

Arenas-Herrera JE, Ko IK, Atala A, Yoo JJ. Decellularization for whole organ bioengineering. Biomed Mater. 2013 Feb;8(1).

Badylak SF, Taylor D, Uygun K. Whole-Organ Tissue Engineering: Decellularization and Recellularization of Three-Dimensional Matrix Scaffolds. Annu Rev Biomed Eng. 2011;13(1):27–53.

FLUID SHEAR STRESS IMPACTS OVARIAN CANCER VIABILITY AND ORGANIZATION

Alexandra R. Hyler[1], Rafael V. Davalos[1], Paul C. Roberts[2], Mark A. Stremler[1], and Eva M. Schmelz[1]
1. School of Biomedical Engineering and Sciences, Virginia Tech, Blacksburg, VA
2. National Institutes of Health, Bethesda, MD
Corresponding Author: Alexandra Hyler, Email: ahyler@vt.edu

INTRODUCTION

All cells exist in a physiological environment that is impacted by chemical and physical factors. These stimuli affect tissue growth, organization and function but also contribute to diseases such as cancer. Epithelial ovarian cancer (EOC) has a 5-year survival rate below 30% since the majority of cases are diagnosed after the cancer has metastasized where cells disseminate throughout the peritoneal cavity and are exposed to physical stresses.[1]
While neoplastic progression is a topic of much interest, there are few investigations *in vitro* into the effects of fluid flow induced shear stress on EOC. We utilized our MOSE model for this investigation since it uniquely transforms and progresses *in vitro* from a premalignant, non-tumorigenic (MOSE-E) to a transitional, malignant (MOSE-L) and finally, to a highly aggressive, malignant phenotype (MOSE-L_{FFLV}).[2]
We hypothesize that even at relatively small, physiological values of shear stress, long-term exposure to this mechanical force will significantly and differently impact the various stages of EOC cell survival, spheroid formation and cell cytoskeleton structure.

METHODOLOGY

We first estimated the shear stress for our system to be ~1.37-1.99 dyne/cm^2 which is physiologically relevant.[3] Cells were seeded and placed immediately (-imm-) onto or allowed to adhere (-adh-) before placement onto a Lab Rotator. Cell viability (hemocytometer count), spheroid formation (imaging) and cytoskeleton structure (indirect immunofluorescence) were assessed at each, successive 96h time period (3 total). ANOVAs were used to determine significance ($p < 0.05$ considered significant).

RESULTS

Figure 1 presents the spheroid formation results.

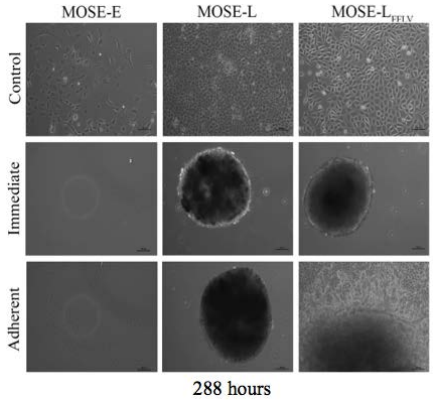

Figure 1: Spheroid formation of MOSE cells subjected to continual shear stress force of < 2 dyne/cm^2.

Additionally, cell viability and cytoskeleton structure results already completed will be presented.

CONCLUSIONS

Physiological magnitudes of shear stress significantly impact MOSE cell viability at all stages of disease. Additionally, the continual fluid shear stress induces cell death in benign cells. Shear stress induces spheroid formation in the slow-developing and fast-developing stages of ovarian cancer. Lastly, cytoskeleton structure is heavily impacted by continual fluid shear stress.

ACKNOWLEDGMENTS

This work was supported by NSF IGERT Grant 0966125.

REFERENCES

1. Avraham-Chakim, L. et al. *PLoS One*. Apr 2013;8(4).
2. Roberts PC, et al. *Neoplasia*. Oct 2005;7(10) 944-956.
3. Even-Tzur, N., et al. *Biophysical J*. Sept 2008;95(6) 2998-3008.

Virginia Tech
Wake Forest University
School of Biomedical Engineering and Sciences
14th Annual Graduate Student Research Symposium, May 13, 2015

TARGETED CELLULAR ABLATION BASED ON MORPHOLOGY OF MALIGNANT CELLS

Jill W. Ivey[1], Eduardo L. Latouche[1], Michael B. Sano[1,2], Rafael V. Davalos[1], Scott S. Verbridge[1]
1. Virginia Tech-Wake Forest University, Department of Biomedical Engineering and Mechanics
2. Stanford University School of Medicine, Department of Radiation Oncology
Corresponding Author: Jill Ivey, Email: jivey@vt.edu

INTRODUCTION

Glioblastoma multiforme (GBM) is an extremely lethal brain cancer, with an average survival time of less than 1 year. The nearly universal recurrence of GBM tumors is attributable to the failure of current therapies to selectively target malignant cells without destroying healthy brain tissue or leaving behind cells that will repopulate a tumor We hypothesize that malignant GBM cells exhibit distinct physical characteristics that can provide targets for selective killing using physical techniques. We have developed 3D tissue models, with tunable tissue microenvironment, to study cell responses to irreversible electroporation therapy (IRE) and how these responses correlate to physical properties of cells.

METHODOLOGY

3D tissue mimics of type 1 collagen were created. Scaffolds were seeded with human glioblastoma cells (U87), normal human astrocytes (NHA), rat glioblastoma cells (C6), or rat astrocytes (D1TNC1). Cell morphology was controlled by varying collagen concentration (0.2% w/w or 2.0% w/w). Cells were exposed to different electroporation regimes, 1µs pulse high-frequency irreversible electroporation (HFIRE) or 100µs IRE pulses. Live/dead staining and finite element modeling was used to determine lethal thresholds. The morphology of the cells are analyzed by confocal microscopy.

RESULTS

We created tissue mimics in which U87 cells exhibited a significantly smaller area in the higher density collagen as compared with lower density collagen. Using this *in vitro* model we determined that these cell sizes determined lethal thresholds for IRE but not for HFIRE pulses with IRE lesions being larger for larger cells. HFIRE was shown to exhibit intracellular effects, as nuclear size becomes an important variable in HFIRE lethal thresholds but not IRE thresholds. The glioma cell lines exhibited increased nuclear area compared to astrocytes. HFIRE lethal thresholds are lower for malignant cells while IRE thresholds are similar across cell types.

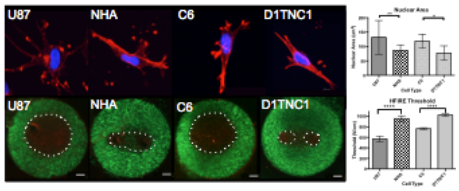

Figure 1: HFIRE threshold correlation with nuclear area

CONCLUSIONS

Though the exact mechanism of cell killing with HFIRE is not yet known, our results suggest a mechanism that is different than that of long IRE pulses which target the plasma membrane, and that, unlike for IRE, is cell type dependent among cells of similar size. The HFIRE killing mechanism is such that the biophysical structure of malignant cells allows for the selective targeting of these cells using a range of electric field distributions that induce no damage to the healthy cells studied but elicit a death response in malignant cells. A threshold in such a range at the edge of the tumor may be effective at killing the invasive glioblastoma cells that render surgery to be an ineffective treatment for GBM, and infiltrative tumors more broadly.

ACKNOWLEDGEMENTS

This work was supported by the R21 Award from the NCI and funding from ICTAS at Virginia Tech.

REFERENCES

Davalos RV, Mir LM, Rubinsky B. Tissue ablation with irreversible electroporation. Ann Biomed Eng. 2005; 33(2):223-31.

APPLICATION OF FEEDBACK THROUGH ELECTROMAGNETIC STIMULATION OF SHAPE MEMORY ALLOYS

Paola Jaramillo[1], Alexander Leonessa[1,i] , and Nicole Abaid[2]
1. Virginia Tech, Department of Mechanical Engineering
2. Department of Biomedical Engineering and Mechanics
Corresponding Author: Paola Jaramillo, Email: paolajc@vt.edu

INTRODUCTION

We have developed a setup capable of generating suitable stimulation currents through linear and nonlinear closed loop controllers driven by contraction measurements. Preliminary tests were carried out using shape memory alloys (SMAs), which are structures that behave as thermo-mechanical actuators [1].

In particular, we used Biometal, a Ni-Ti SMA, which contracts and expands, similar to muscles, when heated and cooled, respectively. For the development of the system, a primary coil connected to a current amplifier driven by a data acquisition system, and a secondary coil connected to the Biometal, are selected. Current from the control input is forced through the primary coil generating a magnetic field. By magnetic induction, voltage is then produced in the secondary coil, generating a current that causes the Biometal to contract in a preassigned fashion.

METHODOLOGY

The Biometal is mounted on the setup to evaluate the electromagnetic system. Three different types of controllers: a linear Proportional-Integral (PI) control, and two nonlinear controllers: a Model Reference Adaptive controller (MRAC) and an Adaptive Augmented PI controller (ADP-PI) are tested.

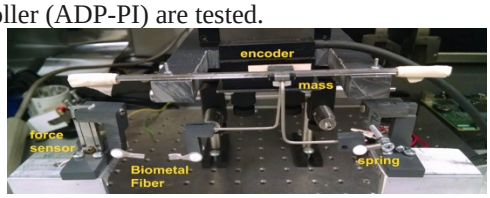

Figure 1: Experimental setup for Biometal contractions.

The experimental setup is illustrated in Fig. 1. A Biometal is fixed at one end and connected to the mass-spring system. The trajectory of the mass is measured using an optical encoder. The instantaneous position of the mass is used as feedback to control the desired stimulation and the corresponding Biometal response.

A digital signal output is generated as the product of a Pulse Width Modulation (PWM) signal with low frequency of 100Hz and high frequency sine function of 10,000Hz. The control algorithm modulated between 0μs to 2000μs generates the duty cycle of the PWM signal.

RESULTS

The results presented are the trajectory responses due to the Biometal contraction for the 3 controllers on Fig. 2.

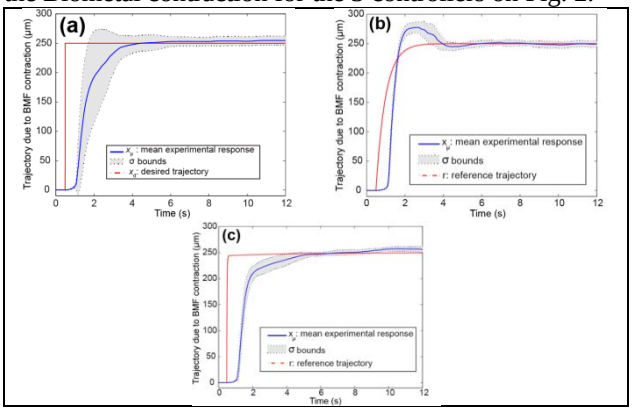

Figure 2: Mean step trajectories due to Biometal contraction using (a) PI, (b) MRAC, and (c) ADP-PI.

CONCLUSIONS

This study emphasizes the advantage of model-free closed-loop systems applied for stimulation able to handle the nonlinearities inherent in the Biometal.

REFERENCES

[1] Leo, Donald J. *Engineering analysis of smart material systems*. John Wiley & Sons, 2007.

[i] This material is based upon work supported by (while serving at) the National Science Foundation

Virginia Tech
Wake Forest University
School of Biomedical Engineering and Sciences
14th Annual Graduate Student Research Symposium, May 13, 2015

COMPARISON OF CEREBRAL BLOOD FLOW AND ARTERIAL TRANSIT TIME MAPPING METHODS: LOOK-LOCKER ASL, HADAMARD ENCODED ASL, AND MULTI-TI ASL WITH VARIABLE BOLUS AND TR

Megan E. Johnston[1] and Youngkyoo Jung[1,2]
1. Wake Forest School of Medicine, Biomedical Engineering
2. Wake Forest School of Medicine, Radiology
Corresponding Author: Megan E. Johnston, Email: megjohns@wakehealth.edu

INTRODUCTION

A new PCASL acquisition scheme is proposed involving varying the bolus duration, TI, and TR titled multi-TI Arterial Spin Labeling (ASL) with variable bolus and TR, referred to as "Multi-TI Integrated ASL." This method is implemented and compared with other existing CBF and ATT estimation methods: ASL with Look-Locker acquisition[2] and Hadamard Encoded ASL[3].

METHODOLOGY

Five healthy subjects were imaged (2 M/3 F, 28.6 +/- 3.2 years old). All ASL images used pseudo-continuous labeling and a 2D EPI acquisition 24 slices, in-plane resolution 3.4x3.4 mm, and matrix size of 64x64x24. All other ASL parameters are listed in Table 1. All images were registered to the first volume, smoothed using a 5 mm Gaussian kernel. CBF and ATT were estimated using an unconstrained nonlinear optimization function in Matlab (fminsearch) to find a solution minimizing the difference between the data and the ASL kinetic model. A correlation between the data and the model fit was calculated on a voxel basis and the correlation coefficient (rho) and the p-value were found. Voxels with a p-value of greater than 0.05 were rejected.

Table 1: Summary of ASL parameters

	Look Locker	Hadamard Encoding	Multi-TI Integrated ASL
TR (ms)	5700	5100	3000 (avg)
Bolus Duration (ms)	1600	600	0/700/1400/1600
Flip Angle (deg)	45	90	90
TI increment (ms)	800	600	700
Number of TIs (time points)	5	8	7 for T_1 mapping 6 for Perfusion
Scan Time (min)	5:53	5:31	5:39
Avgs in 6 min	31	8	8

RESULTS

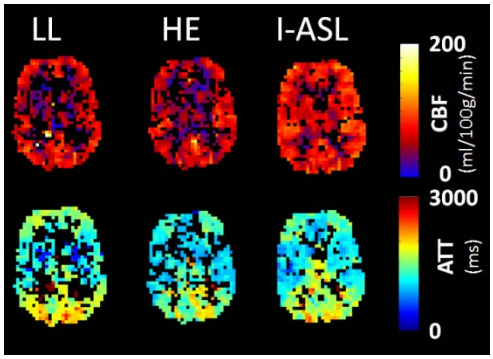

Figure 1: Slices from CBF and ATT maps after p-value masking (p <0.05) from one subject.

Table 2: Summary of ASL method comparisons

	Look-Locker	Hadamard Encoded	Multi-TI Integrated ASL
Mean GM CBF (ml/100g/min) (mean±std)	58.77±31.4	53.24±20.8	66.94±20.4
Mean GM ATT (ms) (mean±std)	1651.5±631	1461.4±554	1477.2±495
MeanGM Rho (mean ± std)	0.843±0.173	0.795±0.184	0.851±0.149
GM % survival p-value mask (mean±std)	50.7±10.4 %	59.3±13.9%	67.3±7.5%

CONCLUSIONS

The study shows that Multi-TI Integrated ASL can be a time efficient method for simultaneous CBF and ATT estimation which fits the perfusion model well.

REFERENCES

1. Gonzalez-At et al. MRM, 2000 **2.** Gunther, et al., MRM, 2001. **3.** Dai, et al., MRM, 2013. **4.** Dai, et. al., MRM, 2012.

SKULL THICKNESS MORPHING FOR AN AGE AND SEX SPECIFIC FE MODEL OF THE SKULL

Derek A. Jones[1, 2], Jillian E. Urban[1, 2], Elizabeth M. Lillie[1, 2], and Joel D. Stitzel[1, 2]
1. Virginia Tech-Wake Forest University Center for Injury Biomechanics
2. Wake Forest University School of Medicine
Corresponding Author: Derek A. Jones, Email: derjones@wakehealth.edu

INTRODUCTION

Over 1.7 million people in the United States sustain a traumatic brain injury (TBI) each year, 52,000 of whom die [1]. It has been shown that skull thickness affects the propensity for TBI and skull fracture [2, 3]. Therefore, it is very important to consider accurate measurements of full and cortical thickness of the skull when studying head impact. Though there have been various finite element (FE) models used in this field of research, many of the most frequently used FE models of the head and skull are constructed based on 50th percentile male geometry. The objective of this study was to develop a methodology to morph existing FE head models to specific ages and sexes using skull thickness regression data in order to better predict injury.

METHODOLOGY

Paired homologous landmark and cortical thickness measurement data were used from 123 clinical head computed tomography (CT) scans [4]. The homologous landmark full thickness data points were used in conjunction with a FE model morphing method, specifically the Thin Plate Spline (TPS) method [5]. In order to create an age and sex specific skull model, the Global Human Body Models Consortium (GHBMC) 50th percentile male (M50) head was used as a starting model [6]. A case study of relaxation parameter, λ, was conducted for a 65 year old male.

RESULTS

The GHBMC M50 skull was morphed to a full thickness representative of a 65 year old male (Figure 1). The frontal bone was subject to the most dramatic change. The best relaxation parameter was determined to be 0.5 based on visual inspection and quantitative analysis (Table 1). The average error for this chosen morph was 0.231 mm and 95 percent of the error was below 0.942 mm.

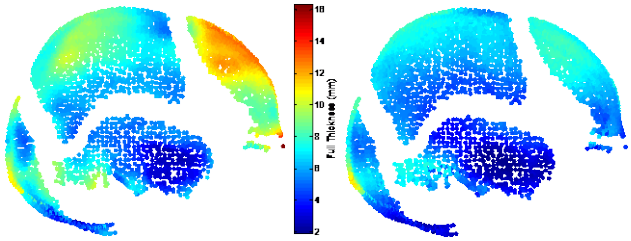

Figure 1: Comparison of GHBMC M50 skull thickness (left) with that of representative 65 year old male (right). Landmarks on suture lines were removed.

Table 1: Summary of Absolute Value of Morphing Error.

Relaxation (λ)	Mean error (mm)	S.D. error (mm)	95th percentile error (mm)
0.5	0.231	0.334	0.942
1	0.294	0.379	1.116
3	0.441	0.445	1.383
5	0.535	0.478	1.538
10	0.673	0.542	1.735
50	1.002	0.835	2.722

CONCLUSIONS

This methodology including TPS and thickness regression data is a valid method to generate age and sex specific FE models of the human skull for the adult population (ages 20-100). Further work is needed to morph the cortical thicknesses within the corresponding full thickness morphs to provided improved anatomic accuracy.

REFERENCES

[1] Coronado et al. *MMWR Surveill Summ*, 2011. [2] McElhaney et al. *J Biomech*, 1970. [3] Hubbard *J Biomech*, 1971 [4] Lillie et al. *J Bone Miner Res*, In Review. [5] Stayton *Evolution*, 2009. [6] Mao et al. *J Biomech Eng*, 2013.

Virginia Tech
Wake Forest University
School of Biomedical Engineering and Sciences
14th Annual Graduate Student Research Symposium, May 13, 2015

IMPROVING BRAIN-SKULL INTERFACE THROUGH APPLICATION OF MESH SMOOTHING ALGORITHM

Mireille E. Kelley[1, 2], Logan E. Miller[1, 2], Jillian E. Urban[1, 2], and Joel D. Stitzel[1, 2]
1. Wake Forest University School of Medicine, Biomedical Engineering
2. Virginia Tech – Wake Forest Center for Injury Biomechanics
Corresponding Author: Mireille E. Kelley, Email: mekelley@wakehealth.edu

INTRODUCTION

With an average of 53,000 traumatic brain injury (TBI)-related deaths per year in the US, TBI is a leading cause of disability and injury-related death [1]. The mechanisms of TBI are not fully understood, so developing an anatomically accurate, high resolution finite element (FE) model of the head is important for studying these injuries. The objective of this study is to adapt the Taubin smoothing algorithm for application to an FE model of the human head to improve the brain-skull interface and provide a more powerful tool for predicting brain injury.

METHODOLOGY

For this study, the FE model of the brain developed by Miller et al. known as the atlas-based brain model (ABM) will be used [3]. A custom MATLAB program was developed for the mesh smoothing algorithm [4], [5]. First, each node is classified into categories and assigned a number to signify its order as surface (4), interface (3), interior (2), or fixed (1). Then, neighbors for each node are found based on the distance from the central node and are subject to constraints. Lastly, smoothing is applied to every node in the FE mesh using the smoothing parameters λ and μ, where $\lambda < 0$ and $\mu < -\lambda$ [6]. Warpage, aspect ratio, skew, and jacobian, were measured to optimize the smoothing parameters and maintain good element quality [7], [8].

RESULTS

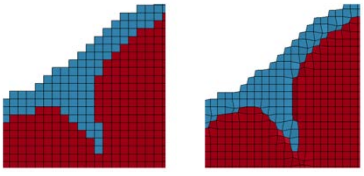

Figure 1: Brain model before smoothing (left) and after smoothing (right).

Table 1: Percent of elements failing element quality tests.

	Accepted Range	Measured (#, %)
Number of elements	--	1993972
Jacobian (% fail)	>0.30	3991 (0.20%)
Warpage (% fail)	<50.00	44 (0.00%)
Aspect Ratio (% fail)	<8.00	0 (0.00%)
Skew (% fail)	<60.00	0 (0.00%)

CONCLUSIONS

A smoothing algorithm was developed to smooth the interfaces between parts of the ABM. The results demonstrate that the algorithm successfully smoothed the stair-stepped interfaces between the brain, CSF, and skull while maintaining element quality. The smooth interfaces may improve the accuracy of the stress and strain measurements in FE simulations by creating a more realistic interface. The smoothing algorithm presented here will ultimately lead to an improved FE model of the brain and allow for more accurate brain injury prediction.

ACKNOWLEDGMENTS

The authors acknowledge Elizabeth Lillie for help with development of the ABM and the Wake Forest University Graduate School for funding this research.

REFERENCES

[1] V. G. Coronado, *et al.*, *MMWR Surveill Summ*, May 6 2011.
[2] R. J. Cloots, *et al.*, *Ann Biomed Eng*, Jul 2008.
[3] L. Miller, et al., ed: BMES, 2014.
[4] Y. Chen and M. Ostoja-Starzewski, *Acta Mechanica*, 2010.
[5] G. Taubin, *IEEE Comput Graph Appl*, 2012.
[7] C. Untaroiu, *et al.*, *Ann Biomed Eng*, 2013.
[8] H. Mao, *et al.*, *J Biomech Eng*, 2013.

3D BIOPRINTING OF BONE CONSTRUCTS FOR CRANIOMAXILLOFACIAL RECONSTRUCTION

Carlos V. Kengla[1,2], Young-Joon Seol[1], James J. Yoo[1,2], Anthony Atala[1,2], and Sang Jin Lee[1,2]
1. Wake Forest School of Medicine, Wake Forest Institute for Regenerative Medicine
2. Wake Forest University, School of Biomedical Engineering and Sciences
Corresponding Author: Carlos Kengla, Email: ckengla@wakehealth.edu

INTRODUCTION

For three decades, tissue engineering efforts have sought to remedy insufficient and misshaped bone healing with Bone Tissue Engineering (BTE); however, the clinical impact is largely unfelt for CFM reconstructive surgery. The advent of 3D fabrication methods now known as 3D printing has helped the BTE field through realization of scaffolds with complex shapes and incorporated inner architecture producing favorable environments for bone tissue formation. Our research seeks to improve CFM bone regeneration by integrating complex anatomical shapes, enhanced architecture, and stem cell population.

METHODOLOGY

Polycaprolactone (PCL) is mixed with tricalcium phosphate nano-powder (TCP) in chloroform to form homogenous 1:1 mixture by weight. The solvent is evaporated with vacuum pressure and heat after which the material is ground by cryomilling. For cell printing, cells are released from culture dishes with trypsin, followed by washes in PBS, and then mixing with bio-ink hydrogel. The bio-ink hydrogel is a thermosensitive gel composed of gelatin, fibrin, glycerol, and hyaluronic acid. The materials are then printed using the custom built Integrated Organ Printing system. Structures for printing are designed with Mimics/3-Matic software developed by Materialise and custom software. Structure designs are converted to tool paths and machine code by custom software. Rat calvaria defects (8mm diameter) were treated with 8mmx1mm disks with or without hAFS cells. Patient specific implants are being designed for rabbit mandibular defects.

RESULTS

By 5 months, calvaria defects treated with PCL/TCP scaffolds demonstrated evidence of bone ingrowth largely restricted to the defect margin. Defects treated with hAFS cells printed within the scaffolds showed bone ingrowth with accompanying vasculature, seen via CD31+ staining. See Figure 1. Further studies in rabbits will incorporate patient specific implant design based on medical imaging. Our workflow is capable of producing implants with multiple architectures integrated into a single implantable construct. See Figure 2.

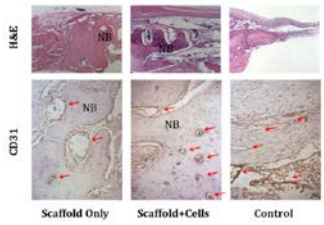

Figure 1: 5 Month histology of rat calvaria defect.

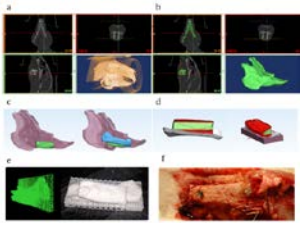

Figure 2: Implant design workflow starting from CT for mandibular bony defect construct.

CONCLUSIONS

We demonstrate that bioprinting can simultaneously deliver a supporting polymeric template and 3-D patterned deposition of cell-laden hydrogels in a precise manner to promote bone regeneration. Furthermore, this can mimic patient specific anatomical bone structures.

ACKNOWLEDGMENTS

This work was supported by the Armed Forces Institute of Regenerative Medicine (W81XWH-08-2-0032).

Virginia Tech
Wake Forest University
School of Biomedical Engineering and Sciences
14th Annual Graduate Student Research Symposium, May 13, 2015

DOES MURRAY'S LAW APPLY TO THE TRACHEAL SYSTEM IN INSECTS? A 3D STUDY OF THE BEETLE *PLATYNUS DECENTIS*.

Melissa Kenny[1] and Jake Socha[1]
1. Virginia Tech, Department of Biomedical Engineering and Mechanics
Corresponding Author: Melissa Kenny, Email: mck66@vt.edu

INTRODUCTION

The architecture of fluid transport systems has been well studied in diverse taxa, some of which have evolved network geometries that tend toward minimizing energy loss. Three basic principles apply to these networks; (1) transfer processes must occur over short spatial distances, (2) large and small vessels must be used for bulk flow and exchange sites respectively, and (3) flow velocities must be limited across transfer sites. A fourth principle is also utilized for optimal design, termed (4) Murray's law, stating that at any branch point: $\Sigma r^3_{parent} = \Sigma r^3_{daughters}$. This relationship balances the costs of forcing flow against the fluid's viscosity with maintaining the system. Evidence of Murray's law has been found in many eukaryotic taxa spanning from mammals to sponges and plants, but it has not yet been studied in the tracheal network of insects.

METHODOLOGY

To test Murray's law in an insect, we utilized synchrotron microtomography of the beetle, *Platynus decentis*, which uses convective airflow to aid in respiration. Data were collected at beamline 2-BM at the Advanced Photon Source at Argonne National Laboratory. 3D segmentation and measurement of tracheal tubes was performed using Avizo software. An orthogonal cross-section of each tube was selected, approximately 1-2 diameter lengths away from the junction. MATLAB was used to create a binary image, fit an ellipse to the tube's cross section, and measure the effective radii of each tube (Figure 1).

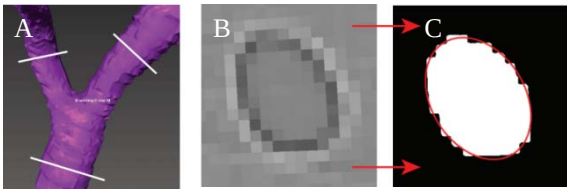

Figure 1: (A) Resonstructed branching group with indicated cross section. (B) Tracheal tube cross-section. (C) Binary image of cross section with best fit ellipse.

RESULTS

The ratio of ellipse major and minor axis length for each cross section was calculated. Parent tubes had a ratio of 1.24 ± 0.27 (n=131) and daughter tubes had a ratio of 1.18 ± 0.17 (n=269). The ratio of the parent radius cubed to the sum of the daughter radii cubed (=1 for Murray's law) was found to be 1.134 ± 1.048 (Figure 2). The best-fit exponent (x=3 for Murray's law) was found for each branching group with an average of 1.99 ± 0.75 (n=104).

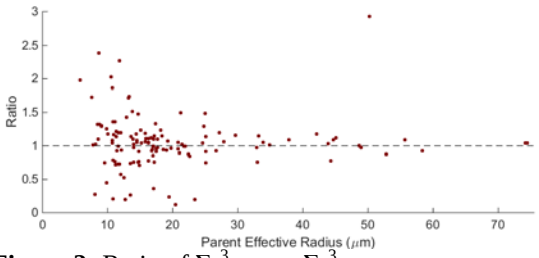

Figure 2: Ratio of Σr^3_{parent} to $\Sigma r^3_{daughters}$ versus parent effective radius for branching groups.

CONCLUSIONS

Our data suggest that Murray's law does not apply to the tracheal system of this beetle. Further analysis indicates that a diffusion-based design, in which the squares of the radii were used, provided a better a fit, with an average exponent of approximately 1.99. Future work should focus on looking at other insect species and correlating specific geometries with local patterns of collapse. This collapsing behavior, which is not often seen in biological transport networks, could provide an explanation for why Murray's Law does not seem to apply.

ACKNOWLEDGMENTS

We thank Talia Weiss, Joel Garrett, Britt Horton, and the Socha Lab. Supported by NSF 0938047.

NOVEL INTEGRATED *IN VITRO* GASTROINTESTINAL AND HEPATIC MODEL FOR INVESTIGATING DRUG TOXICITY

Rebekah Less[1] and Padma Rajagopalan[1,2,3]
1. Virginia Tech – Wake Forest School of Biomedical Engineering and Sciences, Biomedical Engineering
2. Virginia Tech, Department of Chemical Engineering
3. ICTAS Center for Systems Biology of Engineered Tissues
Corresponding Author: Rebekah Less, Email: lessx002@vt.edu

INTRODUCTION

The interactions between the liver and gastrointestinal (GI) tract, result in metabolism of nutrients, the biotransformation of chemical compounds, and in drug disposition. Single-organ systems lack the complex inter-cellular and inter-organ communication that occurs *in vivo* and therefore are unable to properly model first-pass metabolism that has been shown to be critical for assessing drug metabolism. To date, there have been very few reports of an integrated liver and GI model for the assessment of pharmaceutical absorption and metabolism. Drug delivery and efficacy are rarely studied on more than one organ or tissue at the same time. Because of these gaps in *in vitro* modeling, there is a critical need to design and assemble integrated engineered tissues that can provide a holistic and representative understanding of drug absorption and metabolism *in vivo*. The present study focuses on integrating an *in vitro* GI model with an organotypic multi-cellular 3D liver model for toxicity evaluations.

METHODOLOGY

Caco-2 (human colon adenocarcinoma) cells were purchased from ATCC (Manassas, VA). Hepatocytes were obtained through the surgical excision of rat livers. Acetaminophen (APAP) was used as model toxins to study absorption, metabolism, and toxicity in this integrated organ system. Transepithelial electrical resistance (TEER) measurements were conducted to measure tight junction integrity of intestinal monolayers. Hepatic urea production was quantified using a colorimetric reaction assay with diacetyl monoxime.

RESULTS

A significant decrease in TEER resistance was observed in Caco-2 monolayers after a 24 hour treatment with 10 mM APAP (77.8 ± 7.6% of control) ($p<0.01$). These results indicate a disruption in the tight junction integrity in Caco-2 monolayers after treatment with toxins. In order to mimic the GI-liver interaction observed *in vivo*, we cultured hepatocytes in APAP treated and Caco-2 conditioned hepatocyte medium (CM Model) or Caco-2 cells were cultured on Transwell® inserts and placed above CS hepatocyte cultures (Transwell® Model). Results showed a significant decrease in hepatic function (as determined by urea secretion) in models containing Caco-2 cells or Caco-2 soluble factors after 2.5 mM APAP ($p<0.01$), however a significant decrease in urea secretion is not observed at any APAP treatment (up to 10 mM) in the collagen sandwich model (Figure 1).

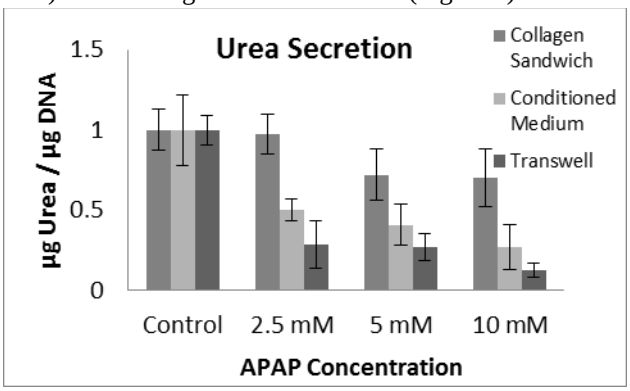

Figure 1: Urea secretion by hepatocyte models after treatment with Acetaminophen (APAP)

CONCLUSIONS

Results suggest the integration of GI tract and liver models can increase sensitivity of drug toxicity models *in vitro*, creating a need for more complete drug absorption, metabolism, and toxicity assessment system. By integrating both organ models (GI tract and liver) in toxicity testing, a more complete evaluation of drug absorption and metabolism can be generated.

NON-ITERATIVE INTERIOR TOMOGRAPHY WITH 2D SVD

Rui Liu[1,2], Hengyong Yu[2]
1. Wake Forest University, School of Biomedical Engineering and Sciences
2. University of Massachusetts Lowell, Department of electronic and engineering
Corresponding Author: Hengyong Yu, Email: hengyong-yu@ieee.org

INTRODUCTION

A 2D singular value decomposition (SVD) based method is reported for ultra-fast interior tomography. When the system matrix is overdetermined, the SVD based reconstruction method guarantees accurate reconstruction from noise-free projections.

METHODOLOGY

One way to find the solution is to solve the pseudo inverse. We employ the SVD method to get the inverse. When a subregion inside the ROI is known for our knowledge based interior tomography, the columns of the system matrix corresponding to those known pixels can be eliminated. We only need to do the SVD for corresponding to the unknown part of the pixels.

RESULTS

In our simulations, we assume that the phantom is in a rectangular region. The system matrix should be overdetermined. A modified Shepp-Logan phantom and self-designed image resolution phantom are reconstructed. The number of detector cell is 261 and 121 views are uniformly sampled using an interior scan configuration with scanning range of 360 degrees. The results are shown in Fig. 1. The whole image can be exactly reconstructed when assuming the overdetermined matrix. The reconstructions outside the FOV are unstable. Neither singular values of full nor interior projection matrices decreases to zero rapidly. When a subregion is known inside the FOV, the interior problem can be stably and uniquely solved. The total known pixel number is 24086 and the unknown pixel number is 22139. The difference between the reconstructed image and the ground truth is shown in Fig. 2. Without considering noise, the 2D SVD-based method can exactly reconstruct all the unknown pixels. After adding the noise, we use Truncated SVD method and Tikhonov regularization to depress noise.

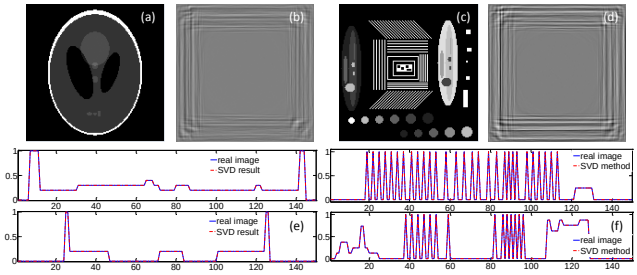

Figure 1: (a) and (c): reconstructed results. (b) and (d): differences with truth. (e) and (f): vertical and horizontal profiles of the ground truth and reconstructed results.

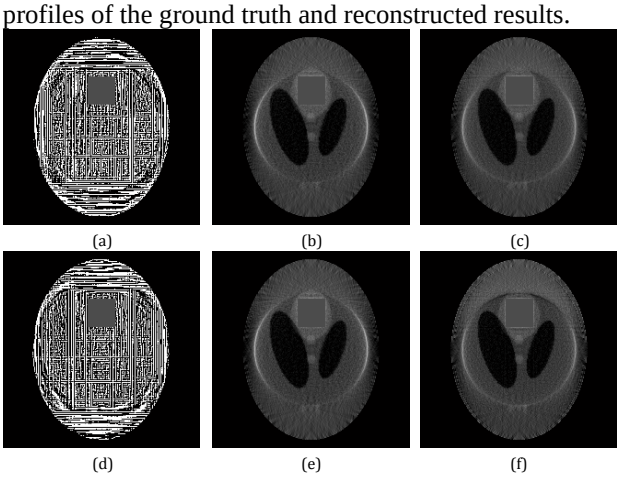

Figure 2: Given a subregion inside the FOV and the compact support. With different noise levels. (a), (d): SVD method; (b) and (e): TSVD; (c) and (f): modified Truncated SVD.

CONCLUSIONS

When a subregion is known, it is possible to accurately reconstruct the pixels inside the FOV. In conclusion, we have demonstrated the feasibility to perform interior tomography using the 2D SVD-based reconstruction method. It is possible to accurately reconstruct an interior ROI from local noisy projections. Therefore, the reported method may offer a faster way for accurate CT reconstruction.

DIFFUSION-BASED ULTRASENSITIVE BISULFITE CONVERSION ON CHIP

Sai Ma[1] and Chang Lu [1, 2]
1. School of Biomedical Engineering and Sciences, Virginia Tech
2. Chemical Engineering, Virginia Tech
Corresponding Author: Chang Lu, Email: changlu@vt.edu

INTRODUCTION

Extensive studies have demonstrated that DNA methylation has played a major role in many biological procedures, such as cellular proliferation and differentiation. Bisulfite genomic sequencing is regarded as the gold-standard technology for analyzing DNA methylation. This technology is based on the different consequences after cytosine and 5-methycytosine (5-mC) treated with sodium bisulfate. The cytosine in DNA will be converted to uracil residues and recognized as thymine in subsequent PCR amplification and sequencing. On the other hand, the 5-mC will remain the same so that it can be distinguished from cytosine.

One of the major concerns of bisulfite conversion is the degradation of DNA. Under known conditions, at least 80% (up to 98%) of the DNA is degraded due to the non-specific degradation under acidic conditions. To obtain decent sequencing coverage in the whole genome, hundreds of nanograms (up to 2 μg) input DNA is needed. This results in huge problem when dealing with rare samples, such as blood sample and embyro. In addition, the bisulfite conversion usually takes 4~16 hours in traditional protocols. The long incubation time results in high conversion rate, but also significantly affects the integrity of DNA. To reduce the amount of DNA needed, we developed a diffusion-based microfluidic chip to minimize sample loss by decreasing reaction time without compromising conversion rate. In addition, the diffusion strategy eliminates the need for column based DNA purification which also improves the sensitivity of the assay. This strategy will potentially be used for reduced representative bisulfite sequencing (RRBS) and whole genome bisulfite sequencing (WGBS) with limited DNA samples.

METHODOLOGY

Our microfluidic device has a simple structure that includes a reaction chamber connected with two loading chambers on both sides [1]. The connections between the reaction chamber and the two loading chambers could be cut off by closing two-layer valves. This simple microfluidic platform allows the replacement of small molecules inside the reaction chamber by diffusion from/into the loading chambers under the concentration gradient, while preserve the large DNAs inside throughout such process.

RESULTS

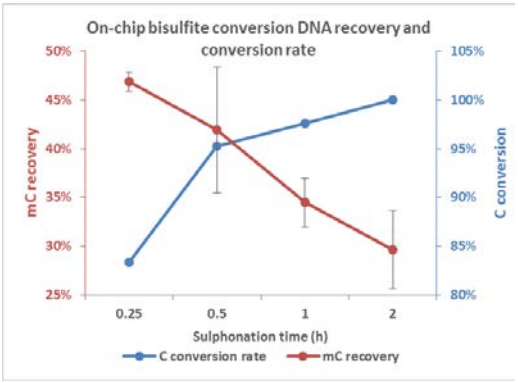

Figure 1: ~300bp fully methylated DNA (mC) is used for analyzing DNA recovery by qPCR. ~300bp unmethylated DNA sequence with methylated adapter (C) is used for evaluating conversion rate by Sanger sequencing.

ACKNOWLEDGMENTS

We acknowledge financial support from Virginia Tech ICTAS NanoBio Trust, NSF CBET grants 1016547 and 0967069, NIH NCI R21CA174577.

REFERENCES

(1) Ma, S.; Loufakis, D. N.; Cao, Z.; Chang, Y.; Achenie, L. E. K.; Lu, C. *Lab on a Chip* **2014**, *14*, 2905.

AN OPTIMIZED THRESHOLDING RECONSTRUCTION APPROACH FOR THE L_p $(0 < p < 1)$ REGULARIZATION PROBLEM

Chuang Miao[1] and Hengyong Yu[2]
1. VT-WFU School of Biomedical Engineering and Sciences, Wake Forest University Health Sciences, Winston-Salem, NC
2. Department of Electrical and Computer Engineering, University of Massachusetts, Lowell, MA, USA
Corresponding Author: Chuang Miao, Email: cmiao@wakehealth.edu

INTRODUCTION

Recently, the analytical solution of the $l_{1/2}$ regularization has been developed in a thresholding form, distinguishing it from other l_p $(p \neq \frac{2}{3},\ 0 < p < 1)$ regularizations [1]. Here, we report the general thresholding algorithm based on the derived analytic thresholding representation for any l_p $(0 < p < 1)$ regularization

METHODOLOGY

We consider the following l_p regularization problem:

$$\min_{x\in\mathbb{R}^N}\{\|y - Ax\|^2 + \lambda\|x\|_p^p\}, \qquad (1)$$

where $\lambda > 0$ is a regularization parameter. Recently, we derived the analytic thresholding formula for any l_p $(0 < p < 1)$ regularization [2],

$$h_{,p}(x) = \begin{cases} x - sgn(x)\cdot\frac{\lambda p}{2}\left(|x| - \frac{p}{2}(1-p)^{\frac{p-1}{2-p}}\lambda^{\frac{1}{2-p}}\right)^{p-1}, & |x| > \frac{2-p}{2}(1-p)^{\frac{p-1}{2-p}}\lambda^{\frac{1}{2-p}} \\ 0, & otherwise \end{cases}. \qquad (2)$$

RESULTS

Figure 1: Reconstructed images from 9 views. From left to right, the images correspond to p=1, p=0.9 and p=0.1 after 5000 iterations, respectively. The initialization are selected as the result of p=1 after 10000 iterations.

The representative CT reconstruction results are shown in Figure 1, and the corresponding root-mean-square-error (RMSE) curves for p=0.1 and p=0.9 are shown in Figure 2. When p=1 (soft thresholding), it cannot reconstruct the phantom image exactly from 9 views. While both p=0.9 and p=0.1 can exactly reconstruct the phantom (i.e. RMSE<10^{-3}), p=0.1 reconstructs a smaller RMSE (see Figure 2).

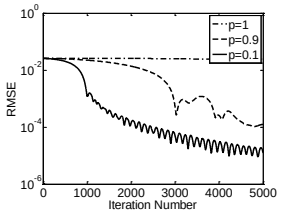

Figure 2: RMSE curves for p=1, 0.9 and 0.1.

CONCLUSIONS

In this work, we reported the analytic thresholding representation for l_p regularization. The phantom experiments in CT applications show the enhanced sparsity with smaller p $(0 < p < 1)$ compare to the soft thresholding algorithm $(p = 1)$. This can help to significantly reduce patient dose in realistic applications, which is a big concern in the CT imaging field.

REFERENCES

[1] Xu, Z.B. et al., *L-1/2 Regularization: A thresholding representation theory and a fast solver.* IEEE Transactions on Neural Networks and Learning Systems, 2012. 23(7): p. 1013-1027.

[2] C. Miao and H. Yu, *A general thresholding solution for lp (0<p<1) regularized CT reconstruction*. IEEE Trans. on Image Process (Submitted).

DESIGN BEHIND IMPROVING EFFICIENCY IN ENDOTRACHEAL TUBE CHANGES

Jared D. Mitchell[1], Philip J. Brown[1], and Michael A. Olympio[2]
1. Virginia Tech – Wake Forest School of Biomedical Engineering
2. Wake Forest University School of Medicine
Corresponding Author: Jared Mitchell, Email: jmitche@wakehealth.edu

INTRODUCTION

Endotracheal tubes, also known as breathing tubes, are catheters inserted into the mouth to provide an airway for gas exchange in the lungs. Endotracheal tubes are commonly used on patients with obstructed airways or lose or deficient function of the diaphragm. An endotracheal tube can also accumulate the buildup of mucus and provide a pathway for pathogens to infiltrate the body. For these reasons, endotracheal tubes are removed and replaced often [1,2].

Our goal was to design a device that would allow for a quick and easy changing of the endotracheal tube. Designing an apparatus to assist the changing of the endotracheal tubes would allow medical practitioners to perform what normally takes roughly 45 seconds [1], in nearly 5.

METHODOLOGY

Using Solidworks, we developed a mouthpiece, blade, and handle that, after assembled, allowed for removal of an endotracheal tube needing replacement.

RESULTS

We have designed an endotracheal tube changer (handle, blade, and mouthpiece) allowing administers of ET changes to work efficiently. To prevent the tube changer from opening, the handle is equipped with a clasp as well as an altered blade (seen in later designs) allowing for increased pliability. The main goal is to allow this to be very practical and simply. In order to do so, we developed a mouthpiece that mates with the handle seamlessly. This helps not only to make sure you are in the right position, but also to lock you into place. The design put forth (Figure 1C) allows for a nearly fool-proof and straight forward system.

Figure 1: Endotracheal tube changer design iterations.

CONCLUSIONS

The final design (Figure 1C) will allow for quicker, easier, and more efficient changing of endotracheal tubes. This will drastically reduce the amount of time that patients are without oxygen.

ACKNOWLEDGMENTS

Dr. Michael Olympio, Wake Forest Innovations

REFERENCES

1) Benumof (2007), Ezri T and Warters RD, Chapter 15: Indications for tracheal intubation, pp. 371–8
2) Olympio, Michael A. Devices with Mouthpieces That Allow for Rapid Change Out of Endotracheal (ET) Tubes and Related Methods. WFU Health Sciences, assignee. Patent WO2014099780 A1. 26 June 2014.

Virginia Tech
Wake Forest University
School of Biomedical Engineering and Sciences
14th Annual Graduate Student Research Symposium, May 13, 2015

EFFECTS OF SUBCONCUSSIVE HEAD IMPACTS IN A SINGLE SEASON OF HIGH SCHOOL FOOTBALL ON RESTING-STATE FMRI CONNECTIVITY NETWORKS

Fatemeh Mokhtari[1], MS, Christopher Lack[2], MD,
Christopher T. Whitlow[2], MD, PHD, Joel D. Stitzel[1], PHD, Joseph A. Maldjian[2], MD
1. Virginia Tech-Wake Forest School of Biomedical Engineering and Sciences
2. ANSIR Laboratory, Department of Radiology-Neuroradiology, Wake Forest School of Medicine
Corresponding Author: Fatemeh Mokhtari, Email: fmokhtar@wakehealth.edu

INTRODUCTION

There are over 5 million athletes playing organized football in the United States, with a vast majority in high school leagues. Football players are subject to more concussion risk compared to other contact sports. Although several studies have been done to explore serious and instant external appearance of concussion, the weaker effects of repeated subconcussive impacts, that cause mild traumatic brain injuries (mTBI), have been mostly remained unknown. The purpose of this study is to determine if resting-state functional magnetic resonance imaging (rsfMRI) networks interconnections change after a single season of high school football.

METHODOLOGY

Thirty high school football players without history of prior concussion participated in this study. Six minutes of rsfMRI was obtained pre- and post-season from each subject. For each subject, fMRI data was band-pass filtered and registered to the same subject structural data. Independent component analysis (ICA) was performed for each scan. For 16 scans, ICs were manually classified to noise and signal. This data was used to train the FMRIB's ICA-based Xnoiseifier (FIX) classifier. FIX attempts to auto-classify ICA components into “signal" vs. ”artifact" components, so that the artifact components can be removed from the 4D FMRI data. Artifact removal and motion correction were performed using the FIX classifier. Group ICA (gICA) on the cleaned data resulted in twenty-nine gICA maps. Dual regression was performed in order to obtain subject versions of the group maps. Removal of noise and artifact components from the gICA maps was performed on the basis either of the components’ frequency spectra or of the gICA spatial maps. For each subject an interconnectivity matrix between the subject version of gICA networks was created by computing pairwise partial temporal correlations. Significant changes between pre- and post-season network interconnectivity were evaluated using paired t-tests corrected for multiple comparisons.

RESULTS

Seventeen networks were identified using gICA after removal of artifact components. Interconnectivity between the frontoparietal network (often associated with attention and memory processing) and a network centered in the extrastriate cortex (involved in processing visual stimuli) showed a significant increase after a season of football using paired t-tests corrected for multiple comparisons (p-value <0.05) (Figure 1).

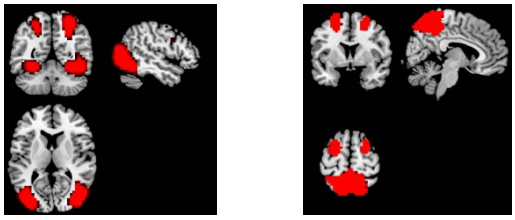

Figure 1: Significantly increased connectivity between frontoparietal network and extrastriate cortex network (post-season connectivity > pre-season connectivity).

CONCLUSIONS

Our findings indicate significant changes in brain connectivity between fronto-parietal and visual networks after a season of football in the absence of clinical concussion. While this suggests changes in brain connectivity networks associated with mild traumatic brain injury (1), possible developmental changes will also need to be considered in future work.

REFERENCES

1. Sharp, D. J et al., Brain 2011, 134: 2233–2247.

COLLAGEN ORIENTATION AND DENSITY ANALYSIS: DEVELOPMENT OF A PROGRAM FOR QUANTIFICATION OF SCAR TISSUE METRICS

Jade Montgomery[1], Robert G. Gourdie[1]
1. Virginia Tech Carilion Research Institute
Corresponding Author: Jade Montgomery, Email: jmont@vt.edu

INTRODUCTION

The orientation and density of collagen fibers within a tissue is often an important metric for studies observing wound healing and scar tissue formation, among others. A primary differentiating factor between scar tissue and uninjured skin is the density and entropy of orientation of the underlying collagen matrix[1]. Scar tissue has a denser and more ordered collagen matrix, giving it a paler appearance and lower tensile strength than uninjured skin.

For our research into wound healing, we wished to quantify the density and entropy of orientation of collagen fibers in a multitude of skin tissue samples. However, given the complexity of analysis and large volume of samples to examine, manual examination was out of the question. A program utilizing features of both MATLAB and Image-J was developed and is outlined in this paper.

METHODOLOGY

First, skin samples obtained from a clinical trial were stained with Picrosirius Red, a stain designed to highlight collagen. The entirety of the stained skin samples was imaged under a birefringence slide scanner at 20x.

The images of the samples were then passed through Image-J's Orientation-J Analysis plugin in a batch process, saving the resulting image maps with hue and saturation respectively corresponding to orientation and coherency. Image masks were manually created for each image file, highlighting the position and rotation of the tissue for analysis by the program as shown in Figure 1. Discrepancies in the images, such as cracks in the slide which showed up as bright lines, were excluded in the mask file in order to prevent them affecting the final analysis.

The MATLAB program then took each subset of images (original, image orientation map, and mask) for analysis. From the mask files the program determined the location, orientation, and any skewing of the tissue, and translated the original and orientation images into a set of rectangles. These rectangles were then split into squares, and each square individually analyzed for entropy of orientation and normalized brightness to approximate density. The program outputs these numbers calculated for all of the images in an excel file formatted to be read directly into the statistics software JMP. From here, p values related to row, column, and other variables to be tested can be determined with relative confidence compared to other less comprehensive methods.

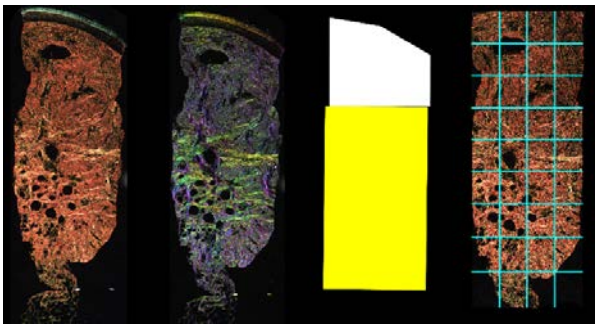

Figure 1: From left to right: original picrosirius image, image orientation map, mask image, and sample data broken up into individual squares for analysis.

CONCLUSIONS

Our program is able to successfully quantify the entropy of orientation and density of large swathes of data with minimal user interaction, outputting data that can be quickly evaluated for significance in statistics software. The program is currently being used in several different ongoing studies with minimal modifications.

REFERENCES

1. McDougall, S., et al. *Philos. Trans. A. Math. Phys. Eng. Sci.* 364, 1385–405 (2006).

Virginia Tech
Wake Forest University
School of Biomedical Engineering and Sciences
14th Annual Graduate Student Research Symposium, May 13, 2015

THORACIC SBRT INDUCES EARLY DETERIORATION OF CORTICAL BONE IN RIBS

Catherine Okoukoni[1,2], Sarah Lynch [2], Ashley Weaver PhD [2], A. William Blackstock MD[1], Brian E. Lally MD[1], Michael T. Munley, PhD[1] and Jeffrey S. Willey, PhD [1]
1. Wake Forest School of Medicine, Departments of Radiation Oncology
2. Wake Forest School of Medicine, Departments of Biomedical Engineering
Corresponding Author: Catherine Okoukoni, Email: cokoukon@wakehealth.edu

INTRODUCTION

Thoracic stereotactic body radiation therapy (SBRT) leads to an increased incidence of spontaneous rib fractures often occurring early after treatment. The etiology of radiation induced rib fracture (RIRF) is unclear, but likely results from bone damage and deterioration. Spontaneous fractures are believed to initiate within cortical bone; cortical thickness is a major determinant of the bone strength. Unfortunately, thin laminar structures comprising the bone cortex of ribs are poorly visualized on clinical CT images due to limited spatial resolution. The objective of this study was to assess early radiation effects on the cortical thickness of ribs after SBRT using a novel cortical thickness mapping technique capable of resolving thickness differences >30μm (1).

METHODOLOGY

Rib cortical thickness maps were constructed from pre-treatment and follow-up CT scans acquired 4 months after SBRT for 40 patients treated for primary and metastatic lung malignancies. Patients were treated with several dose fractionation schedules: 50 Gy × 10 fractions (fr) (n = 5), 50 Gy × 5 fr (n =13), 45 Gy × 3 fr (n =5), and 54 Gy × 3 fr (n =7). Post-treatment scans were registered to corresponding pre-treatment scans using rigid body transformation. Regions of interest (ROI) along the length of each rib were defined in 10 Gy increments (0 - 50 Gy) and clustered into the following groupings for analysis based on absorbed dose: 0-10 Gy; 20-30 Gy; 30-40 Gy; and 40+ Gy. Regions receiving dose on the internal and external surface were analyzed independently, and irradiated regions with volumes <0.5cc were excluded. The mean cortical thickness within each ROI was determined pre-SBRT and post-SBRT and the percent difference was calculated. Data were compared using Kruskal-Wallace ANOVA to identify main effects of dose on cortical thickness with Dunn's post-hoc analysis for between group differences.

RESULTS

Exposure to radiation at doses >20 Gy resulted in significant thinning of cortical bone at the both the internal ($p = 0.029$) and external ($p=0.008$) rib surfaces. While no significant cortical thinning was observed at either the internal (+0.5%) or external (-2.9%) surfaces in ribs absorbing 0-10 Gy; significant thinning occurred at, i] the internal surface at locations absorbing 20-30 Gy (-12.7%; $p=0.013$), 30-40 Gy (-12.3%; $p = 0.017$); and marginally lower at 40+ Gy (-9.5%; $p = 0.08$); and ii] the external surface at ROIs absorbing 20-30 Gy (-12.0%; $p = 0.004$), 30-40 Gy (-15.4%, $p = 0.003$), and 40+ Gy (-9.6%, $p=0.024$). This substantial thinning of cortical bone at both external and internal surfaces could greatly increase the risk of spontaneous fracture.

CONCLUSIONS

SBRT induced rapid thinning of the cortical bone throughout ribs that absorb >20Gy. This thinning of cortical bone in irradiated regions of the rib likely contributes to the occurrence of RIRF in patients treated with SBRT.

REFERENCES

Treece GM, Gee AH, Mayhew PM, Poole KE (2010). High resolution cortical bone thickness measurement from clinical CT data. Med Image Anal 14: 276.290.

TRANSFERRIN-MODIFIED SINGLE WALLED CARBON NANOHORNS FOR SELECTIVE UPTAKE INTO CANCER CELLS

Allison M. Pekkanen[1], Matthew R. DeWitt[1], Timothy E. Long[2], and M. Nichole Rylander[3]
1. Virginia Tech- Wake Forest School of Biomedical Engineering and Sciences, Blacksburg, VA
2. Virginia Tech, Department of Chemistry, Macromolecules and Interfaces Institute
3. University of Texas at Austin, Department of Mechanical Engineering
Corresponding Author: Allison Pekkanen, Email: apekk@vt.edu

INTRODUCTION

Transferrin is an iron carrying protein essential for cellular metabolism and transport of iron. The cellular receptor for transferrin is significantly overexpressed in the highly metabolic cancer cells, especially breast and bladder cancers. Due to this overexpression, the transferrin protein is an attractive targeting moiety for selective uptake into tumor cells.

Single walled carbon nanohorns (SWNHs) are a relatively unexplored nanoparticle with a large surface area for modification, internal volume, and act as a photothermal agent for thermal treatment of tumors. They have previously been modified with quantum dots for real-time imaging and cisplatin for chemotherapeutic treatment of AY-27 rat bladder cancer cells *in vitro*. (1-3)

This investigation examines the conjugation of transferrin protein to the surface of SWNHs for selective uptake into cancer cells.

METHODOLOGY

Transferrin was conjugated to SWNH surfaces through carbodiimide chemistry in water. Along with the transferrin, 5(6)-FAM was simultaneously attached to SWNH surfaces to afford fluorescence tracking (SWNH-Tf). MCF-10A and MCF-7 (transferrin receptor normal expressing and overexpressing cells) as well as AY-27 cells were evaluated for cellular uptake of SWNH-Tf with flow cytometry.

RESULTS

Following synthesis, transferrin conjugation was confirmed through BCA assay, which detects the presence of total protein. As shown in Figure 1, increasing feed concentrations of transferrin protein causes an increase in total protein detected through BCA assay.

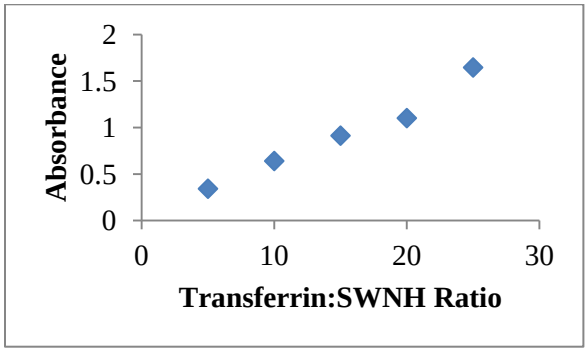

Figure 1: BCA Assay of SWNH-Tf with varying concentration of transferrin.

In addition to protein presence, increasing concentrations of SWNH-Tf induces increased cellular uptake in AY-27 cells, both in the number of cells containing particles as well as the average fluorescence intensity in each cell.

CONCLUSIONS

Transferrin can be successfully conjugated to the surface of SWNHs along with 5(6)-FAM for targeted fluorescence tracking. These particles can be evaluated for cellular uptake via flow cytometry, enabling targeted particles for photothermal therapy.

REFERENCES

1.Zimmermann K, Inglefield D, Jr., Zhang J, Dorn H, Long T, Rylander C, et al. *J Nanopart Res*. 2013;**16**(1):1-18.
2.DeWitt MR, Pekkanen AM, Robertson J, Rylander CG, Nichole Rylander M. *J Biomech Eng*. 2014;**136**(2):021003-.
3.Pekkanen AM, DeWitt MR, Sirrine JM, Geohegan DB, Long TE, Rylander MN. *Nanomedicine : nanotechnol, biol, and med*. 2015;**In review**.

Virginia Tech
Wake Forest University
School of Biomedical Engineering and Sciences
14th Annual Graduate Student Research Symposium, May 13, 2015

INCLUSION OF THE CROSS SCATTERING COMPONENT IN THE SYSTEM MATRIX FORMATION FOR THE ITERATIVE RECONSTRUCTION ALGORITHM IN COMPUTER TOMOGRAPHY

Olga V. Pen[1], Guohua Cao[1]
1. Virginia Polytechnic Institute and State University, School of Biomedical Engineering and Sciences
Corresponding Author: Olga V. Pen, Email: olgapen@vt.edu

INTRODUCTION

Ever since its introduction in 2005, dual-energy computer tomography becomes more and more popular clinical diagnostic tool. However, the 3-D reconstruction based on the projections obtained by the dual-energy double-source, double-detector systems is still riddled with numerous artifacts that eventually degrade the image quality and make diagnostics less reliable.

Compton scattering which naturally occurs as the x-ray passes through the matter is one of the major sources of these artifacts. In case of dual energy CT, the specific problem lies in the fact that not only the detector registers the scatter introduced by its "own" source, but also the scatter introduced by the source aimed at another detector.

However, it can be estimated based on the geometry of the path of the incoming photon, level of its energy and the attenuation coefficient of the material. Several physical laws exist that allow calculating of the predicted scattering.

Modern iterative reconstruction algorithms can calculate the radiological path of the ray and, by utilizing the measurements obtained by the detector, reconstruct the attenuation map of the object. However, the precision of this reconstruction is hindered by the fact that no allowances are made for the fact that the detector measurements contain the additional scattering component. Introduction of this component to the system matrix formation step of the iterative reconstruction could provide us with higher quality images.

METHODOLOGY

1)

Linear integral model based on the Siddon algorithm [1] is planned to be utilized to model the propagation of rays within the matter, thus providing us with the system geometry. With this model, the measured signal can be represented as:

$$Ax = b \quad (1)$$

Where A is a system matrix representing the geometry of the ray passing through the system, x – attenuation that ray experienced while passing, b – signal measured by the end of the path. Introduction of the additional component C that takes into account the geometrical properties of the ray, as well as the attenuation encountered by a scattered photon, would transform this formula into:

$$Ax_1 + Cx_2 = b \quad (2)$$

Calculation of the C matrix is achieved by modeling the scattered ray propagation with the Klein-Nishina Compton scattering probabilistic formula that would take into account the cross scatter angle [2]. Development of the C-matrix calculation algorithm and incorporation of scattering component into existing iterative reconstruction algorithms is the purpose of this work.

PREDICTED RESULTS AND CONCLUSION

The improved forward projection modeling should improve the performance of the whole algorithm, thus providing us with the more precise reconstruction results.

ACKNOWLEDGMENTS

Author is especially grateful to her advisor, Dr. Guohua Cao, and a Ph. D. candidate Hao Gong for support and advices.

REFERENCES

1) Fast calculation of the exact radiological path for a three-dimensional CT array Medical Physics, Vol. 12, No. 2. (1985), pp. 252-255, doi:10.1118/1.595715 by Robert L. Siddon
2) Strategies for scatter correction in dual source CT - Petersilka, M. and Stierstorfer, K. and Bruder, H. and Flohr, T., Medical Physics, 37, 5971-5992(2010), DOI: http://dx.doi.org/ 10.1118/1.3504606

QUANTIFYING HEAD IMPACT EXPOSURE IN COLLEGIATE WOMEN'S SOCCER

Jaclyn N. Press[1] and Steven Rowson[1]
1. Virginia Tech, Department of Biomedical Engineering and Mechanics
Corresponding Author: Jaclyn Press, Email: jaclynp@vt.edu

INTRODUCTION

With a concussion injury rate of 0.41 per 1000 athlete-exposures, women's soccer ranks among the top five sports with the highest rate of concussion when compared to 14 other popular men's and women's collegiate sports including football and ice hockey.[1] In order to better understand concussive injuries in female soccer players, we aim to quantify the head impact exposure in collegiate women's soccer through on-field measurement of head impacts. This study uses both visual analysis and sensor-recorded measurements when quantifying head impact exposure.

METHODOLOGY

A total of 26 players from the Virginia Tech Women's Soccer Team consented to participate in this study and IRB approval was obtained prior to testing. Head impact sensors were placed behind the ear of every participating player before each game and practice to record linear and rotational head accelerations (Fig. 1). Data were downloaded from each sensor following each game and practice. Results collected were then compared to video recordings of each event in order to manually verify each impact sustained as well as categorize the type of impact that occurred.

Figure 1: Head impact sensor behind the ear of a player.

RESULTS

Out of a total 26 practices and 20 games, 1703 real impacts were identified through video analysis. Of these impacts, 89.6% were headers. The remaining impacts were a mixture of head to head, head to body, head to ground, and unintentional ball to head contact. The average number of impacts per player per practice was 1.66 ± 0.91 and the average number of impacts per player per game was 1.63 ± 1.86. Impact totals varied by position.

The sensors reported a total of 17,865 impacts, 8999 of which were classified as real. True/false positive and negative impact classifications were used to construct a positive predictive value (PPV) curve (Fig. 2). This curve suggests that the optimal linear acceleration threshold for the sensors would be 34g, where 65.8% of positive recorded impacts are true positive results.

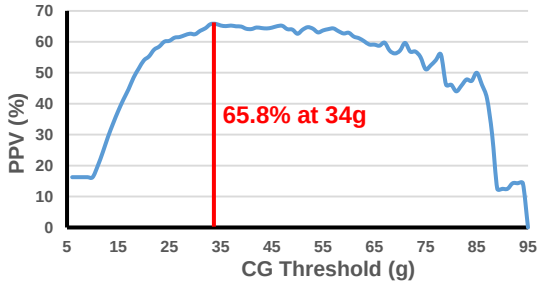

Figure 2: PPV across a span of linear acceleration thresholds.

CONCLUSIONS

Large discrepancies were found between the number of impacts actually sustained by the players and those that were recorded by the sensors. The recorded head accelerations are higher than expected, especially rotational. While this study quantified head impact exposure in collegiate women's soccer, it also identified some of the challenges in using sensors to measure head impacts from athletes on the field. The results of this study should be considered by others when using such sensors.

REFERENCES

[1] Hootman, J et al., *J Athl Train*, 42(2):311-319, 2007.

TREATING OVARIAN CANCER WITH IRREVERSIBLE ELECTROPORATION: IRE THRESHOLD OF SYNGENEIC MURINE OVARIAN CANCER CELLS

Andrea Rolong[1], Eva M. Schmelz[2], and Rafael V. Davalos[1]
1. Virginia Tech – Wake Forest University School of Biomedical Engineering and Sciences
2. Virginia Tech, Department of Human Nutrition, Foods, and Exercise
Corresponding Author: Andrea Rolong, Email: andrear2@vt.edu

INTRODUCTION

Ovarian cancer is the fifth leading cause of cancer-related deaths in women in the United States [1]. An estimated 21,290 women will receive a new diagnosis of ovarian cancer and approximately 14,180 patients will die from the disease in 2015 [1].

Irreversible electroporation (IRE) is a non-thermal ablation technique with the capability to treat otherwise inoperable tumors. One of the main characteristics that sets IRE apart from the more commonly used ablation modalities such as cryoablation, radiofrequency, high intensity focused ultrasound, microwave, and laser, is its non-thermal mechanism for inducing cell death; IRE uses a series of short (≈100μs), high-intensity pulsed electric fields (PEFs) to destabilize the cellular membrane, which in turn disrupts homeostasis and leads to cell death [2].

Even though IRE has been gaining attention due its success in treating tumors with intricate morphologies such as cancers of the pancreas, liver, kidney, and prostate, the potential of this technique to treat ovarian cancer has not yet been investigated. The study presented here used a mouse syngeneic murine ovarian cancer model representative of different stages of the disease [3] and comprises the first step in evaluating the use of IRE to treat ovarian cancer by determining the different thresholds for cell death.

METHODOLOGY

Collagen I 3D tumor models were used to determine cell death threshold from IRE. The death region was imaged by fluorescent microscopy where live cells express enhanced green fluorescent protein (eGFP) and dead cells do not. The lesion size was measured and compared to a numerical model developed in COMSOL Multiphysics 4.3a to correlate the lesion size to the electric field induced in that region as described by Arena et al [4].

RESULTS

Results in collagen hydrogels are consistent with theory; they show that larger cells have lower electric field thresholds than smaller ones for a particular cancer type.

Table 1: Summary of results - IRE of ovarian cancer cells

Cell Type	Ovarian Cancer Stage	Average Diameter in Cell Suspension (μm)	Cell radius (μm)	Electric Field Threshold for Cell Death (V/cm)
MOSE-E	Early Stage	19.61 ± 0.78	9.805	448.47 ± 17.9
MOSE-L	Late Stage	16.05 ± 0.53	8.025	484.84 ± 11.2
MOSE-L_{FFLv}	Highly aggressive, Stem-like properties	16.35 ± 0.61	8.175	504.13 ± 7.83

CONCLUSIONS

IRE is a new treatment modality that may offer great potential to successfully treat ovarian cancer as it uses short, high-intensity electric pulses to kill cells without damaging neighboring vital structures. Future studies will look at targeting the more aggressive malignant cells.

ACKNOWLEDGMENTS

This work was supported by the NSF IGERT DGE-0966125 (MultiSTEPS)

REFERENCES

1. *Cancer Facts & Figures 2015*, cancer.org.
2. Davalos, R.V., et al., Ann Biomed Eng, 2005.
3. Roberts, P.C., et al., Neoplasia, 2005.
4. Arena, C.B., et al., Biophys J, 2012.

IMAGE QUALITY ASSESSMENT IN NOVEL FIBER BASED FLUORESCENT IMAGING

Etai Sapoznik[1,2], Guoguang Niu[2], Peng Lu[3], Yu Zhou[2], Tracy L. Criswell[2], Yong Xu[3], Shay Soker[1,2]
1. VT-WFU School of Biomedical Engineering and Sciences
2. Wake Forest Institute for Regenerative Medicine
3. Department of Electrical and Computer Engineering
Corresponding Author: Etai Sapoznik, Email: esapozni@wakehealth.edu

INTRODUCTION

A critical issue in tissue engineering is the inability to monitor cellular growth and interactions within tissues in real-time. Current imaging tools either require sacrifice of sample for histological analysis, or have limits with penetration and working distance. The fiber-based imaging system developed by our group offers a new approach for localized excitation of fluorescent targets [1] which allows for deeper penetration and larger working distance. Our ultimate goal is to develop a novel imaging tool for non-invasive monitoring of engineered tissues. *Our current objective is to assess the effect that physical parameters have on image quality; specifically, the image quality as a function of fluorescent marker used.*

METHODOLOGY

Mouse endothelial cells (MS1) have been labeled by one of three fluorescent nuclear localized proteins; GFP (green), mCherry (red), or iRFP (far-red). Cells were sorted using FACSAria and seeded on Poly (e-caprolacetone) (PCL) scaffold. The scaffold was electrospun with embedded hollow core fibers (HCF). Samples were put in an imaging chamber containing cell medium which was placed on a motorized stage. Optical fiber with coated polished tip (mirror) was used for laser light delivery and inserted into the HCF. We used three lasers for the fluorescent targets (blue-473 nm; green-532 nm; red-660nm) which excited GFP, mCherry, and iRFP respectively. Fluorescent emission was then collected by Electron Multiplying Charge Coupled Device (EMCCD) detector with matching band-pass filter. An image was then reconstructed based on multiple excitation points and normalized for laser power fluctuations. To assess the quality of the reconstructed image we chose to look at the local mean contrast to noise ratio (CNR) in multiple fluorescent nuclei targets which were segmented from the image based on local maxima points using MATLAB

RESULTS

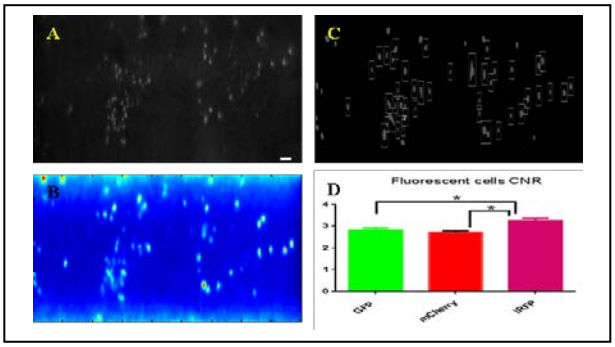

Figure 1: (A) example control image iRFP (scale bar 60μm) (B) Reconstructed image (C) reconstructed image segmented binary mask with analyzed objects (D) mean CNR values for each fluorescent marker

All fluorescent targets were visualized through the opaque scaffold and the segmentation detected most fluorescent targets (Figure 1 A-D). iRFP had the highest CNR while GFP and mCherry had lower and comparable CNR.

CONCLUSIONS

Fluorescent emission wavelength has an effect on the resulting image which is expected to be even more significant with increase in scaffold thickness and collagen content [2]. One aspect of image processing we anticipate to use would involve the registration of control and reconstructed images. This would give another indicator for image quality comparison as well as an estimate for potential deblurring of reconstructed image based on scaffold physical parameters.

REFERENCES

[1] Hofmann, M. C et al. Tissue Engineering Part C: Methods (2012) 18(9): 677-687.
[2] Niu, G., E. Sapoznik, et al. Journal of tissue engineering and regenerative medicine. (2014)

Virginia Tech
Wake Forest University
School of Biomedical Engineering and Sciences
14th Annual Graduate Student Research Symposium, May 13, 2015

DRIVER EVASIVE ACTION PRIOR TO REAL-WORLD INTERSECTION CRASHES

John M. Scanlon[1], Kristofer D. Kusano[1], and Hampton C. Gabler[1]
1. Biomedical Engineering and Mechanics Department, Virginia Tech
Corresponding Author: John Scanlon, Email: john91@vt.edu

INTRODUCTION

There are approximately 4,500 fatal crashes in the U.S. each year [1]. Intersection Advanced Driver Assistance System (I-ADAS) is a developing active safety system that detects oncoming vehicles then alerts the driver of a potential collision. The objective of I-ADAS is to allow the driver additional time to avoid an imminent crash, which makes it highly dependent on avoidance maneuvers followed by drivers during real-world intersection crashes. The objective of this study was to use real-world crashes to determine the frequency, timing, and degree of driver evasive action prior to intersection crashes.

METHODOLOGY

Pre-crash vehicle speed, braking application, and evasive steering were downloaded from 1,735 Event Data Recorders (EDR) of vehicles involved in intersection crashes investigated as part of National Automotive Sampling System / Crashworthiness Data System (NASS/CDS) years 2000 to 2013. Pre-crash movement classifiers were assigned to each vehicle based on their velocity and acceleration profiles prior to the crash. To ensure that any significant steering input observed was an attempted evasive maneuver, the vehicles included in the study were required to have been travelling straight through the intersection, could not have been driving on a curved road prior to the intersection, and could not have been performing a lane change. Braking application at the last EDR-recorded time point was assumed to indicate evasive braking. A steering wheel angular displacement of 16 degrees or greater at any time point prior to impact was assumed to indicate an evasive steering maneuver.

RESULTS

Evasive action was found to occur in 84% of all crashes. Steering was the most frequent evasive maneuver. A more detailed analysis revealed evasive braking to be dependent on the traffic control device (stop sign or signal) and pre-crash movement of the vehicle. Drivers that completely stopped evasively braked 40% of the time, whereas drivers travelling through the intersection evasively braked 72% of the time. Drivers entering the intersection from a stop sign evasively braked 22.5% of the time, whereas drivers entering the intersection at traffic lights or with no traffic control device evasively braked 66% and 82% of the time, respectively.

Drivers were found to evasively steer earlier than brake. Three-quarters (77%) of drivers began braking in the last second prior to impact. In contrast, over two-thirds of drivers (69%) began evasive steering 1-4 seconds before impact. Drivers evasively braked at stop signs or with no traffic control device earlier than drivers with a stop light.

The median average evasive braking deceleration for all cases was found to be 0.56 g. The median evasive steering angular displacement was found to be 32 degrees.

CONCLUSIONS

This paper highlights important characteristics of driver evasive behavior prior to intersection characteristics. The results should be considered by automakers designing I-ADAS, and by government regulatory agencies which may be considering a future I-ADAS vehicle test.

ACKNOWLEDGMENTS

The authors would like to acknowledge the Toyota Collaborative Safety Research Center (CSRC) and Toyota Motor Corporation for funding this study.

REFERENCES

[1] Kusano, K. D. and H. C. Gabler (2013). "Comprehensive target populations for current active safety systems using national crash databases." Traffic injury prevention 15(7): 753-761.

EFFECT OF GEOMETRIC AND MATERIAL PROPERTY CHANGES IN THE THORACIC SKELETON FOR AN OLDER OCCUPANT FINITE ELEMENT MODEL

Samantha L. Schoell[1,2], Ashley A. Weaver[1,2], Nicholas A. Vavalle[1,2], and Joel D. Stitzel[1,2]
1. Wake Forest School of Medicine
2. Virginia Tech- Wake Forest Center for Injury Biomechanics
Corresponding Author: Samantha L. Schoell, Email: sschoell@wakehealth.edu

INTRODUCTION

The shape, size, bone density, and cortical thickness of the thoracic skeleton vary significantly with age, which can affect the injury tolerance especially in at-risk populations such as the elderly. Computational modeling has emerged as a powerful and versatile tool to assess injury risk. However, current computational models only represent certain ages in the population. One current finite element (FE) model is the Global Human Body Models Consortium (GHBMC) v4.2 average male occupant model [1]. The objective of this study is to develop an older occupant GHBMC model representative of a 65 year old (YO) male with a focus on the thoracic skeleton. The biomechanical response of the 65 YO model will be studied through simulations of a frontal hub impact to assess the effects of geometric and material property changes with age.

METHODOLOGY

Development of the 65 YO model involved morphing the baseline GHBMC model using thin-plate spline interpolation to accurately capture the geometric changes in the thoracic skeleton. To evaluate the role of material property changes with age, techniques and data from the literature were implemented. Golman et al. utilized a statistically significant correlation between age and ultimate strain based on two previous studies to adjust the ultimate plastic strain of the ribs [2]. El-Jawahri et al. developed a 75 YO FE model and implemented rib material properties based on aging functions for femur data [3]. Ito et al. also developed a 75 YO FE model based on both aging functions for rib and femur data [4]. Kent et al. developed an elderly FE model based on aging functions for another set of femur data [5]. To evaluate the thoracic response, a frontal hub impact was simulated. A total of 9 simulations were performed to study the influence of geometric and material property changes alone as well as the combination of both changes.

RESULTS

A summary of the predicted rib fractures is provided in Figure 1. Abbreviated Injury Scale (AIS) 98 injury severity for each simulation was determined using the number of predicted rib fractures. In all cases, adding geometric changes in addition to material property changes increased the number of rib fractures predicted on average by 219%.

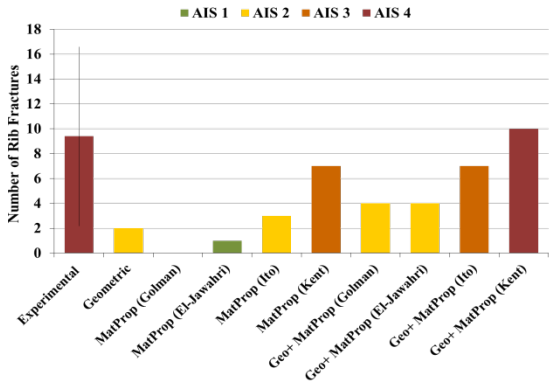

Figure 1: Summary of predicted rib fractures.

CONCLUSIONS

The development of age-specific FE models will lead to an improved understanding of the complex relationship between thoracic geometry, age, and injury risk. The improved understanding will aid in changes in restraint design to not only reduce injuries but also save lives**.**

REFERENCES

[1] Vavalle NA, *Ann Biomed Eng*, 41(3): 497-512, 2013.
[2] Golman AJ, *Acc Anal Prev*, 64:1-8, 2014.
[3] El-Jawahri RE, *Stapp Car Crash*, 54:407-430, 2010.
[4] Ito O, *SAE Technical Paper*, 01-0381, 2009.
[5] Kent R, *Stapp Car Crash*, 49:231-249, 2005.

COMPUTATIONAL MODELING OF DRUG DELIVERY ACROSS THE BLOOD-BRAIN BARRIER (BBB) FOR THE TREATMENT OF AUTISM SPECTRUM DISORDER (ASD)

Jamelle Simmons[1], Luke Achenie[2,3], and Yong W. Lee[1,3]
1. Virginia Tech, School of Biomedical Engineering and Sciences (SBES)
2. Virginia Tech, Department of Chemical Engineering
3. Virginia Tech Center for Autism Research (VTCAR)
Corresponding Author: Jamelle Simmons, Email: jmsimm13@vt.edu

INTRODUCTION

Autism Spectrum Disorder (ASD) is a neurodevelopmental disability defined by deficits in social interaction, communications, and restricted and repetitive interests. With the prevalence rates for ASD rising from 1 in 150 children and 2000 to 1 in 68 children in 2010 accompanied by healthcare costs in the billions the economic burden of the disorder and its prevalence are only expected to rise [1-5].

There is no single cause for ASD and factors such as environment, biology, and genetics can increase the risk for children making this a multifactorial problem [1]. One product of the intersection of these factors are documented increases in oxidative stress levels in brain tissue leading to neuronal loss. Previous work in our lab has documented elevated levels of reactive oxygen species (ROS), microglial activation, and neuronal loss in 3 week old male autism mice. The enzyme Xanthine Oxidase (XO) was found to be elevated in autism mice compared to controls. This compound is capable of increase the amount of oxidative by products in purine catabolism and we hypothesize that the inhibition of this enzyme will reduce neuronal damage caused by oxidative stress.

METHODOLOGY

Transwell® Co-culture blood-brain barrier (BBB) models of rat astrocytes (C6) and rat brain capillary endothelial cells (RBE4) were created where rates of free diffusion across the barrier could be measured over time. Sodium fluorescein salt (NaFl) is used as a fluorescent tracer to measure the permeability of the culture systems. This data is then used to construct Partial Differential Equation (PDE) diffusion models across each culture system. These models can then be used to predict diffusion behavior in future cell culture systems.

RESULTS

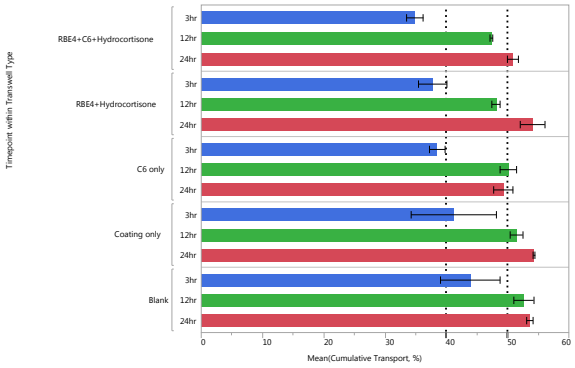

Figure 1: Cell culture cumulative transport (%) of NaFl.

We found slower transport rates for RBE4 monolayers and RBE4+C6 co-cultures compared to C6 alone and Transwell® controls within the first 12 hours of transport.

CONCLUSIONS

With our co-culture systems confirming diffusion trends, we can construct initial PDE models of these systems for later validation studies. Once completed, we will be able to obtain estimate of how XO inhibitors can cross the BBB by means of diffusion.

ACKNOWLEDGMENTS

Virginia Tech Center for Autism Research (VTCAR)

REFERENCES

[1] http://www.cdc.gov/ncbddd/autism/facts.html
[2] Lord, C., et al. *Neuron, 28*, 355-363.
[3] Levy, S., et al. *J. Dev & Behav Ped., 31*(4), 267-275.
[4] http://www.cdc.gov/ncbddd/autism/data.html
[5] Lavelle, T., et al. (2014). *Pediactrics*, E520-9.

POWER SPECTRAL DENSITY ANALYSIS AND FREQUENCY CONSIDERATIONS FOR ELECTROPORATION

Daniel C. Sweeney[1], Suyashree P. Bhonsle[2], Rafael V. Davalos[1]
1. Virginia Tech, School of Biomedical Engineering and Sciences
2. Virginia Tech, Bradley School of Electrical Engineering
Corresponding Author: Daniel C. Sweeney, Email: sweeneyd@vt.edu

INTRODUCTION

Irreversible electroporation (IRE) is a focal ablation technique that utilizes intense pulses of electrical energy to generate a clinically-relevent lesion [1]. Nano-scale defects caused by the intense electric field in the cellular membrane are spontaneously generated to create this lesion ultimately causing cell death [2]. Recent studies have implicated the pulse on-time as the major factor in the determination of the homogenaeity of the ablated tissue region [3]. However, designing the electroporation signal in the time-domain obfuscates the independent frequency content of the input and output signals.

Historically, pulse parameters have been thought of as pulsed DC fields (IRE) [4] or as having the frequencies similar to that of their pulse on-time high-frequence electroporation (H-FIRE) [5]. However, power spectral density analysis (PSD) of the input signal indicates that far more frequency content is applied to the tissue during H-FIRE and conventional IRE. Understanding the frequency response for a given tissue will enable its bulk physical properties to be more accurately assessed and optimized for electroporation. Additionally, an appropriate waveform can be designed to optimize the therapy for a particular tissue in the frequency domain using PSD analysis. By minimizing the apparent tissue impedance for a given frequency band to balance potentially expensive the hardware considerations for the application of higher frequency components, a treatment can be designed to provide the best treatment outcomes and minimize hardware requirements [5].

METHODOLOGY

Liver tissue was chosen for these experiments due to its macroscopic homogenaeity. Prior to and following pulsing, the impedence spectrum was measured using a potentiostat from 1.0 Hz – 1.0 MHz. Pulses were delivered with a custom-built generator and voltages were recorded using probes before and after the tissue sample.

RESULTS

Table 1: Summary of Pulse PSD Simulation Results

Pulse Scheme [μs]	**Dom. Frequency Centers** [Hz]
2-5-2-5	71k, 214k, 357k
2-7.5-2-7.5	56k, 167k, 278k, 389k
2-10-2-10	42k, 125k, 208k, 375k

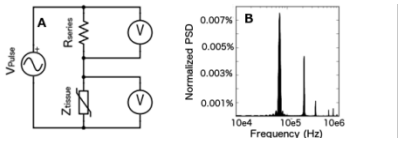

Figure 1: *(A)* Measurement Circuit and *(B)* 2-5-2-5 Pulse PSD between 10 kHz and 1 MHz.

CONCLUSIONS

For square wave pulses with inter-pulse delays, the frequency content is distributed between two decades (10 kHz – 1 MHz) rather than a single representative frequency. The observed tissue response will be dependent on each of the applied frequency components rather than a single frequency.

ACKNOWLEDGMENTS

We thank the MultiSTEPS IGERT and Dr. Ahmed Safaai-Jazi for his invaluable input over the past months.

REFERENCES

[1] Edd et al., *IEEE Trans Biooed Eng*, 2006.
[2] Davalos et al., *Ann Biomed Eng*, 2005
[3] Sano et al., *Bioelectriochemistry*, 2014.
[4] Charpentier et al., *HPB*, 2010.
[5] Arena et al., *IEEE Trans Biomed Eng*, 2012

Virginia Tech
Wake Forest University
School of Biomedical Engineering and Sciences
14th Annual Graduate Student Research Symposium, May 13, 2015

CINNAMON OIL AS A THERAPEUTIC AGENT FOR BREAST CANCER

Marc Thompson[1], Dr. Eva Schmelz[2], Dr. Lissett Bickford[1]
1. Department of Biomedical Engineering and Mechanics, Virginia Tech, Blacksburg, VA, United States
2. Department of Human Nutrition, Foods and Exercise, Virginia Tech, Blacksburg, VA, United States
Corresponding Author: Marc Thompson, Email: Marct@vt.edu

INTRODUCTION

A lack of effective treatment options for metastatic cancer warrants considering alternative approaches that limit systemic toxicities. Studies show that bioactive dietary agents or *neutraceuticals* slow or eliminate cancer progression, with marked immediate cytotoxicity when applied directly to cancer cells as compared to clinically approved chemotherapeutics. In this study, we observe the effects of trans-cinnamaldehyde, the active ingredient in cinnamon oil and a documented anti-inflammatory and anti-cancer agent, on highly invasive triple negative breast cancer cells. By considering bioactive dietary agents, a treatment that selectively kills cancer cells and potentially reverses precancerous conditions may be possible. Here, we examine the influence of trans-cinnamaldehyde on cancer cell viability as well as migration and invasion, which are, hallmarks of cancer progression.

METHODOLOGY

Chemotherapeutic drugs Cisplatin, Carboplatin and Paclitaxel were compared to natural anti-cancer agents frankincense oil, garlic oil and cinnamon oil, to measure potential cytotoxic effects on the MDA-MB-231 triple negative breast cancer cell line. Cells were seeded at 30,000 cells/mL and grown for 3 days. Cells were treated with 10, 25 and 50 µg/mL of each previously stated agent, for 24 hours. Post treatment, an Alamar Blue cell viability assay was performed to determine the cytotoxic effects of agents, results seen in Figure 1.

As the agent conferring the greatest immediate level of cytotoxicity, cinnamon oil was chosen for further studies. The ingredient, trans-cinnamaldehyde, was confirmed as the key active component of cinnamon oil through Gas Chromatography-Mass Spectrometry (GC-MS) and subsequent cytotoxicity analyses.

RESULTS

Initial tests show cinnamon oil displays greater cytotoxicity on the MDA-MB-231 cell line than other botanical agents and current chemotherapeutics. (Figure 1). Isolated trans-cinnamaldehyde was further shown to be the key active ingredient based on subsequent cytotoxicity analysis and GC-MS (data not shown).

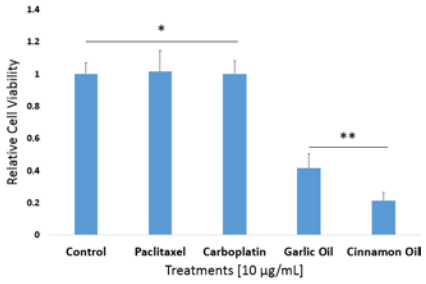

Figure 1: Viability of breast cancer cells after 24-hour agent exposure. *Not significant. **Significant at $p<0.01$. n = 4 per condition.

CONCLUSIONS

Trans-cinnamaldehyde was determined to be the active anticancer component of cinnamon oil, resulting in marked cytotoxic effects in the observed cancer cell line. Further studies must be performed to elucidate further viability, mobility, and evasive effects on progressive forms of breast cancer.

ACKNOWLEDGEMENTS

The authors wish to acknowledge the Cunningham Fellowship for support for M. Thompson.

REFERENCES

Kwon et al. BMC Cancer 2010, 10:392

DETECTION OF SPECIFIC NUCLEIC ACID SEQUENCES IN A MIXED SOLUTION WITH SOLID-STATE NANOPORES

Fanny Wang[1], Osama K. Zahid[1], and Adam R. Hall[1,2]
1. Wake Forest University School of Medicine, Department of Biomedical Engineering
2. Wake Forest University School of Medicine, Comprehensive Cancer Center
Corresponding Author: Adam R. Hall, Email: arhall@wakehealth.edu

INTRODUCTION

Short nucleic acid sequences play an important role in biology. For instance, highly conserved bacterial rRNA sequences (50-150 nt) can be used as indicators of contamination or infection and miRNAs (20-25 nt) can regulate gene expression, which is of even greater importance than the presence or absence of the gene itself.

Here, we describe a novel approach for detecting these sequences with solid-state (SS-) nanopores[1]. Here, two reservoirs of electrolyte solution are connected through a nanopore, and when a voltage is applied, an ionic current is initiated through the pore. The transit of ions produces a baseline current that is altered transiently (known as an "event") when a charged biomolecule in solution threads through the opening. In our technique, events are produced only when a target sequence is present.

METHODOLOGY

SS-nanopores were fabricated using focused helium ion milling[2]. Calibrated exposure times were used to form nanopores of 7.3-8.6 nm diameter. Biomolecules were prepared by mixing a biotinylated 34 bp oligonucleotide ('bait') with an equal amount of a complimentary sequence ('target'), incubating at 95°C, and cooling to synthesize dsDNA. This annealing step was performed in the presence of two additional oligos (maximum 25% homology) to show specificity. 1 μM reactions were incubated with monovalent-streptavidin ('MS', Howarth group, Oxford U.), a high-affinity, highly charged protein tag, to promote translocation. Detection is dependent on reduction of translocation speed by analyte attachment (drag-regulated nanopore detection)[3].

RESULTS

The highly charged MS travels through the pore too quickly to be detected. Binding to ssDNA only does not supply sufficient drag to reduce translocation speed to a resolvable level. However, dsDNA slows the process and enables events to be detected (Fig. 1a). Our assay produces events predominantly if homology with a known biotin oligo (bait) is achieved to form dsDNA (Fig. 1b).

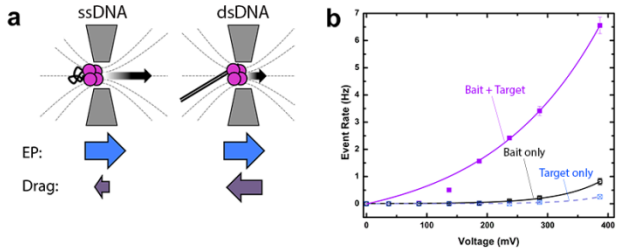

Figure 1: (a) Schematic of mechanism, showing greater drag resistance for dsDNA, making its translocation slower and resolvable. 'EP' is electrophoretic force. (b) Nanopore event rate *vs* voltage for target ssDNA only, biotin bait ssDNA only, and annealed bait+target dsDNA.

CONCLUSIONS

This research demonstrates that target DNA sequences can be detected specifically with a SS-nanopore through formation of dsDNA with a biotinylated (bait) sequence. Future directions include investigating the length limit of the assay and applying it to miRNA and rRNA sequence identification.

ACKNOWLEDGMENTS

We thank J. A. Ruzicka and E. W. Taylor at UNCG for contributions to this project.

REFERENCES

1. Dekker C., doi:10.1038/nnano.2007.27, 2007
2. Yang, J., doi:10.1088/0957-4484/22/28/285310, 2011
3. Carlsen, A., doi: 10.1021/nl501340d, 2014

INTERACTION OF NEGATIVE PRESSURE WOUND THERAPY AND ELASTOMERIC MATERIALS FOR BONE HEALING

Rui Wang[1,2], William D. Wagner[1,2]
1. Virginia Tech – Wake Forest University School of Biomedical Engineering and Sciences
2. Wake Forest University Department of Plastic and Reconstructive Surgery
Corresponding Author: Rui Wang, Email: rwang@wakehealth.edu

INTRODUCTION

Complications associated with spine leads to the most common cause of disability and loss of productivity. It contributes to the No.1 aggregation OR cost (Weiss et al. 2014). Since the start of the 21st century, negative pressure wound therapy (NPWT) has transformed traumatic wound management through improve healing rate. However, few have suggested its applications for bone repair, and little is known about its potential pathways on osteogenesis. The aim of this work is to study the interaction of negative pressure with an elastomeric material during bone formation. The graft material was fabricated by electrospinning a composite of collagen type I (Col I), poly (1, 8-octanediol citrate) (POC) and chondroitin 6-sulfate (CS), named bone repair material (BRM). The central hypothesis of this project was: BRM interacts with negative pressure to regulate osteoblast proliferation and differentiation, and to contribute to spinal fusion.

METHODOLOGY

The proliferation of osteoblast was measured. Molecular pathway of osteoblastic differentiation was studied through temporal gene expressions to shed light on the interactions of BRM and negative pressure.

RESULTS

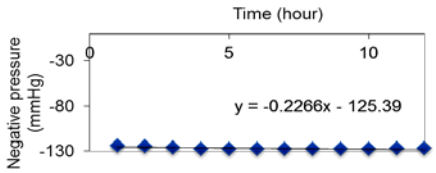

Figure 1: Pressure in the culture chamber was held at a constant -125mmHg continously for 12 hours.

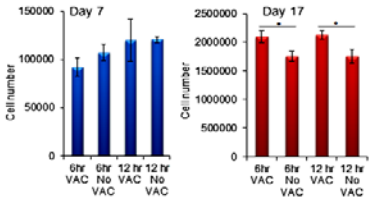

Figure 2: The proliferation at day 7 and day 17 under negative pressure treatment on tissue culture plastic dish.

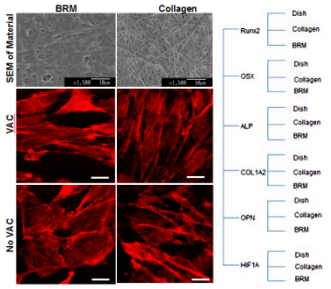

Figure 3: The morphology of hFOB human osteoblast (left) and tested gene expression (right).

CONCLUSIONS

Early time negative pressure was translated into late functional effects as BRM demonstrated a synergistic effect with negative pressure.

ACKNOWLEDGMENTS

Deparment of Plastic and Reconstructive Surgery. Dr. Aaron Goldstein, and Patrick Thayer for the kind gift of the rat MSC and technical assistant in RT-PCR.

REFERENCES

Weiss et al. Agency for Healthcare Research and Quality 2014.

Virginia Tech
Wake Forest University
School of Biomedical Engineering and Sciences
14th Annual Graduate Student Research Symposium, May 13, 2015

DEGRADABLE SCAFFOLDS FOR NEGATIVE PRESSURE WOUND THERAPY APPLICATIONS

Harleigh J. Warner[1,2], William D. Wagner[1,2]
1. Department of Plastic and Reconstructive Surgery, Wake Forest Baptist Medical Center
2. School of Biomedical Engineering and Sciences, Virginia Tech and Wake Forest University
Corresponding Author: Harleigh J. Warner, Email: hwarner@wakehealth.edu

INTRODUCTION

Myocardial ischemia-reperfusion injury and traumatic brain injury are both characterized by edema and inflammation. It has been shown previously that treatment of infarcted myocardial tissue with mechanical resuscitation using negative pressure wound therapy reduces cell death after ischemia-reperfusion.[1]The purpose of this study was to produce an ideal degradable sponge material for use in negative pressure wound therapy thus omitting an additional surgery for removal. An ideal sponge should be biocompatible, able to pull negative pressure for 2-3 days and be fully degradable in 7-10 days. We hypothesized that a material consisting of combinations of poly(lactic co-glycolic acid) (PLGA), poly(lactic co-caprolactone) (PL-CL), and poly-caprolactone (PCL) would provide the necessary properties.

METHODOLOGY

Sponge Fabrication: 11 compositionally distinct sponges were produced using combined salt leaching and solvent displacement protocols.
Accelerated Degradation Testing: Sponges were weighed and placed in a 0.025M NaOH solution. Sponges were lyophilized and weighed at 20, 40, 60, 90, 120, 240, and 480 minutes to determine sponge half-life.
Mechanical Testing: The compressive moduli were measured using an Electroforce Test Instrument. Compressive modulus was calculated as the slope of the linear portion of the stress strain curve in the range between 0.4 and 0.5 strain.
In Vivo Rat Testing: Sponges were implanted subcutaneously into the dorsal scapular region and examined histologically after 21 days.
All data presented in mean ± SD (n=3)

RESULTS

Sponges composed of 70:30 PLGA (50:50):PCL had the fastest degradation of all sponges tested with a degradation half-life of 17.5 days. These sponges had a compressive modulus most similar to the current clinical sponge, PVA. (70:30 PLGA:PCL : 0.051± 0.009 MPa; PVA: 0.024±0.015 MPa).

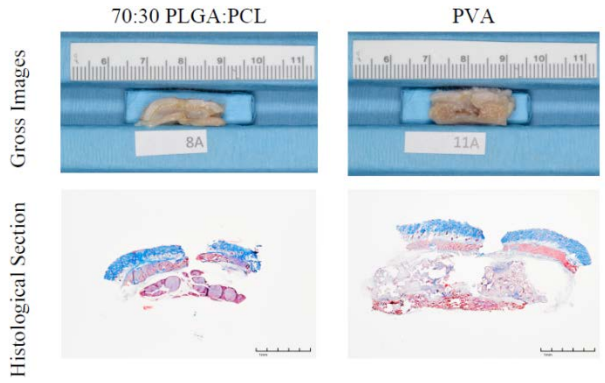

Figure 1: Gross and Masson's trichrome stained histological images of sponges.

Based on histological data, 70:30 PLGA:PCL showed extensive degradation at day 21 with minimal fibrosis (blue) surrounding the sponge. The PVA sponges did not degrade and displayed fibrotic tissue infiltration.

CONCLUSIONS

From the 11 sponges fabricated and evaluated for this study, the degradable sponge composed of 70:30 poly (lactide co glycolide) (50:50) and poly (caprolactone) had properties most similar to the clinically used PVA sponge.

REFERENCES

1. Jordan, J. E., et al. *J Cardiac Surg.* (2014) 29:116-123

Virginia Tech
Wake Forest University
School of Biomedical Engineering and Sciences
14th Annual Graduate Student Research Symposium, May 13, 2015

BLAST INJURY AUGMENTS PRO-INFLAMMATORY MACROPHAGE PHENOTYPE IN RAT HIPPOCAMPUS

Michele Waters[1], Venkata Siva Sai Sujith Sajja[1], Mark Van Dyke[1], Pamela VandeVord[1]
1. Virginia Tech, Biomedical Engineering
Corresponding Author: Michele Waters, Email: mwaters1@vt.edu

INTRODUCTION

Macrophage differentiation and infiltration following traumatic brain injury (TBI) play critical roles in tissue remodeling. However, healing is complicated by the prolonged presence of pro-inflammatory (M1) macrophages (associated with tissue destruction) and the rapid decline of anti-inflammatory (M2) macrophages (linked with tissue remodeling) at the site of injury. In particular, the cellular and molecular mechanisms underlying the cognitive impairment associated with blast-induced neurotrauma (BINT) are poorly understood. Therefore, in the present study, a temporal response of hippocampal M1 and M2 macrophage activation was undertaken following blast-induced TBI in a rat model.

METHODOLOGY

An established rat model of BINT was used to examine M1 and M2 macrophage activation.[1] After experiencing a single peak overpressure (~17 psi), brains were collected at 1, 2, 4, or 12 wks post blast. Sagittal sections were stained for M1 and M2 macrophage markers (CD86 and CD206) and imaged in the hippocampal region. Fluorescence area was quantified, and results were compared to previously published cognitive data.

RESULTS

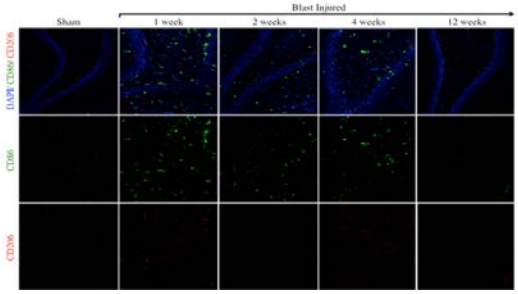

Figure 1: Macrophage staining of rat hippocampus. CD206 (M2; red)/ CD86 (M1 marker; green); sham (far left) and injured animals 1-, 2-, 4-, and 12-weeks (second left to far right) after blast exposure.

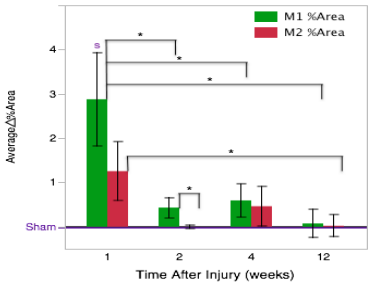

Figure 2: Average Change in %Area of Macrophages

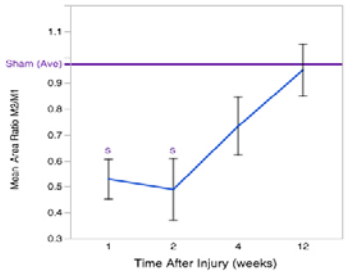

Figure 3: Average Ratio of M2/M1 Marker Area

CONCLUSIONS

Percent total area of M1 immunofluorescence staining was significantly increased 1-week following blast injury compared to the sham group and other time points; the average ratio of M2-to-M1 area was significantly reduced at 1- and 2-weeks following blast injury compared to sham groups. This phenotype imbalance positively correlates with previously reported cognitive deficits in animals following BINT.

ACKNOWLEDGMENTS

We would like to acknowledge the DOD/CDMRP.

REFERENCE

1. Cho, H.J., et al., Neuroscience, 2013. **253**: p. 9-20.

Virginia Tech
Wake Forest University
School of Biomedical Engineering and Sciences
14th Annual Graduate Student Research Symposium, May 13, 2015

PELVIC RESPONSE OF A TOTAL HUMAN BODY FINITE ELEMENT (FE) MODEL DURING SIMULATED UNDER BODY BLAST (UBB) IMPACTS

Caitlin M. Weaver[1] and Joel D. Stitzel[1]
1. Wake Forest University, School of Biomedical Engineering and Sciences
Corresponding Author: Caitlin M. Weaver, Email: cweaver@wakehealth.edu

INTRODUCTION

This study focuses on the pelvic injury response of the Global Human Body Models Consortium (GHBMC) 50th percentile seated FE human body model (v4.3) [1]. The input data used for this study was obtained from testing performed by the Biomechanics Product Team (BIO PT) for the U.S. Army Warrior Injury Assessment Manikin (WIAMan) project. The purpose of the WIAMan effort is to create an enhanced capability to assess risk to Soldiers in the UBB environment for use in live-fire test and evaluation and protection technology development. This includes the creation of a soldier-representative, biomechanically-validated anthropomorphic test device (ATD). Evaluation of GHBMC model fidelity and injury response is based on biofidelity targets (corridors) created using pelvis accelerations obtained from experimental testing of UBB-type loading using post mortem human subjects (PMHS) [2].

METHODOLOGY

Acceleration pulses obtained from accelerometers attached to the floor and seat of experimental test vehicle rigs were used to perform UBB FE simulations. Acceleration data from nodes in the S1 region of the pelvis of the GHBMC were extracted from the simulations. The extracted S1 acceleration data was compared to S1 data recorded from the experimental biofidelity corridors created from preliminary WIAMan experimental test data. Corridors were created using data filtered at 345, 1050, and 1750Hz. The corridors were generated using a standard approach determined by a Biofidelity Response Corridor working group. The approach aligns non-normalized signals using the Nusholtz method, transforms signals to principal component space using eigenvectors and eigenvalues, and generates ±1 and ±2 standard deviation equivalent corridors [3].

RESULTS

The FE S1 acceleration showed good correlation with the biofidelity corridors. An analysis was performed using an objective rating method (CORrelation and Analysis, CORA) using these corridor curves. The ±1 and ±2 SD curves were used for the inner and outer corridor limits, respectively. The average corridor curve was used as the cross-correlation reference. The CORA analysis showed good correlation (70% or higher) with an average of 70.7%, 83.5%, and 82.5% for the data filtered at 345, 1050, and 1750Hz, respectively.

CONCLUSIONS

The initial work for this FE study has shown good correlation for results comparison between PHMS experimental testing and FE human body model acceleration outputs of the S1 region of the pelvis. Further FE UBB impact simulations and additional human body model metrics will be compared to the experimental biofidelity corridors. To date, the comparison of full body UBB experimental testing to drive and compare with full body FE simulation metrics for UBB is unique. This data was acquired with the explicit purpose of enhancing vehicle and soldier survivability.

ACKNOWLEDGMENTS

The authors would like to acknowledge the US Army Research Lab, the John Hopkins Applied Physics Lab, and SMART program for their support and collaboration.

REFERENCES

[1] Vavalle, N. A., et. al. ABME, Mar 2013.
[2] Chancey, C., et. al. USAMRC Ind. Day, Mar 2011.
[3] Nusholtz, G. S., et al. SAE Int. J. Trans. Safety, 2013.

Virginia Tech
Wake Forest University
School of Biomedical Engineering and Sciences
14th Annual Graduate Student Research Symposium, May 13, 2015

A NOVEL SOLID-STATE NANOPORE ASSAY FOR THE DETECTION OF DNA EPIGENETIC MODIFICATIONS

Osama K. Zahid[1], Fanny Wang[1], and Adam R. Hall[1,2]
1. Wake Forest University School of Medicine, Department of Biomedical Engineering
2. Wake Forest University School of Medicine, Comprehensive Cancer Center
Corresponding Author: Adam R. Hall, Email: arhall@wakehealth.edu

INTRODUCTION

Increasing evidence implicates DNA epigenetic modifications and modified DNA as important biomarkers for both development and disease susceptibility. Two such modifications have been widely studied: 5-methylcytosine (5-mC) and 5-hydroxymethylcytosine (5-hmC), both with significant links to cancer. Conventional assays to differentiate and quantify these modifications are laborious, require sophisticated equipment, and demand large amounts of starting material. Therefore a detection technique that is inexpensive, rapid, and sensitive is desirable. Solid-state (SS-) nanopores are an ideal candidate for this purpose. Briefly, two reservoirs of electrolyte solution are attached through a single nanoscale pore drilled in an insulating membrane. An applied voltage facilitates molecular translocation through the pore, which can be detected with resistive pulse sensing.

METHODOLOGY

We have developed a novel SS-nanopore assay[1] that is capable of selectively detecting short biotinylated dsDNA oligonucleotides. Here, monovalent streptavidin (MS, Howarth Group, Oxford U.) is used as a highly charged, high affinity tag for biotinylated DNA. Free MS is translocated through the pore too rapidly to be detected by our electronics. However, when attached to a DNA molecule, the additional viscous drag reduces the speed to a resolvable level (drag-regulated nanopore detection). Since translocation events occur almost exclusively due to DNA-MS binding, we can accurately quantify biotinylated DNA within a mixed sample.

RESULTS

By converting or tagging specific epigenetic modifications with a biotin, we can use our assay to selectively detect and quantify those target modifications. Our initial measurements utilize an enzymatic approach[2] in which DNA glucosyltransferase attaches an azide glucose moiety to 5hmC selectively. Click chemistry can then be used to covalently link biotin to this glucose, enabling SS- nanopore detection to be performed (Fig. 1).

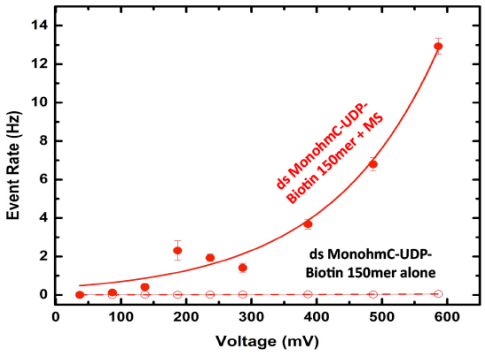

Figure 1: Event rate vs voltage for dsDNA with a single 5hmC nucleotide selectively labeled with biotin and measured alone (dashed red line) and with MS (solid red line). Significant events are caused only by MS binding.

CONCLUSIONS

A biotin labeling approach enables highly selective detection of 5hmC DNA. Expansion to 5mC, U, and oxoG is currently under way via a new, flexible labeling protocol.

ACKNOWLEDGMENTS

We thank J. Ruzicka and E. W. Taylor at UNCG for contributions.

REFERENCES

1. Carlsen, A., doi: 10.1021/nl501340d, 2014
2. Song, C.-X., doi:10.1038/nbt.1732, 2010

Virginia Tech
Wake Forest University
School of Biomedical Engineering and Sciences
14th Annual Graduate Student Research Symposium, May 13, 2015

SELECTIVITY OF 3'SH-T10-SA43 WITH S. AUREUS AND S. INTERMEDIUS

Huaning Zhao[1], Virginia R. Breazeal[2], Vaishnavi Srinivasaraghavan[3], Amy J. Pruden[2], Peter J. Vikesland[2] and Masoud Agah[3]
1. School of Biomedical Engineering and Science, Virginia Tech
2. Department of Civil and Environmental Engineering, Virginia Tech
3. Department of Electrical and Computer Engineering, Virginia Tech
Corresponding Author: Huaning Zhao, Email: huaning@vt.edu

INTRODUCTION

Staphylococcus aureus is one of the most important human pathogens because it can cause severe skin infections, food poisoning, and a range of other illnesses, which may become invasive and life threatening. In the experiment described herein, 3' thiol-functionalized aptamer specific to *S. aureus* were attached onto gold ECIS electrodes and used to detect *S. aureus* via dynamic monitoring of bioimpedance. The 3' SH-T10-Sa43 aptamer is a single-stranded DNA molecule previously isolated, which can specifically bind to *S. aureus*. Selective attachment of *S. aureus* to the aptamer-functionalized electrode was expected to result in an impedance increase. Staphylococcus intermedius, a close relative of *S. aureus*, was used as negative control.

METHODOLOGY

The 3'SH-T10-Sa43 aptamer was functionalized onto the surface of gold electrodes. Mercaptoundecanol (MCU) was then applied with the purpose of increasing the steric availability of the aptamer to the bacteria, and to prevent nonspecific binding of bacteria to the gold surface. A baseline impedance measurement was collected before bioimpedance measurements in the presence of bacteria for 2 hours. A final impedance measurement was collected after washing away loosely or nonspecifically bound bacteria.

RESULTS

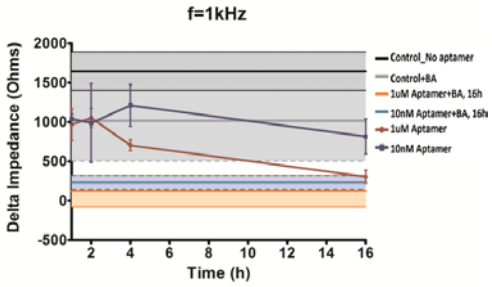

Figure 1: Impedance difference.

Figure 1 shows the impedance difference between baseline and measurement after addition of bacteria (*S. intermidius*). Also it shows the difference in impedance among different aptamer functionalization times at two concentrations. We find that the longer functionalization time of 3'SH-T10-Sa43 results in less *S. intermedius* attachment on the gold electrodes surface, as reflected by the decreasing impedance difference. These results suggest that surface saturation with aptamer and blocking agent can be achieved within the tested concentrations.

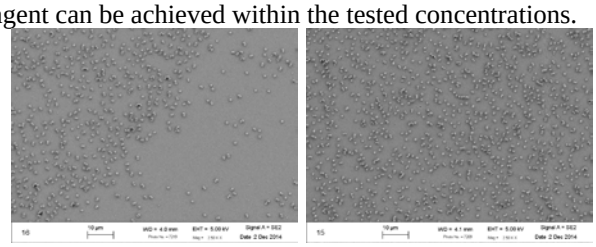

Figure 2: The SEM image for aptamer with S. intermidius (left); 3'SH-T10-Sa43 with S.aureus (right)

CONCLUSIONS

The density of *S. aureus* attachment to aptamer-modified electrodes is not significantly different than that of *S. intermidius*. A consistent result was observed from impedance measurements.

ACKNOWLEDGMENTS

We thank Dr. Pruden, Dr.Vikesland and Dr.Agah for their guide for this project.

REFERENCES

Cao X, Li S, Chen L, et al. Nucleic Acids Research. 2009;37(14):4621-4628.
Srinivasaraghavan V, et al. Biomedical Microdevices, vol. 16, no. 5, October 2014, pp. 689-696.